Investigating the role of mitochondria in regulating cell health and ageing

Nathan Dennis

MSc Biochemistry

School of Biosciences

University of Kent

I. Abstract

Reactive oxygen species (ROS) are highly reactive oxygen-containing compounds which are thought to have detrimental effects on cell health and ageing. Mitochondrial dysfunction is generally considered to elevate ROS production due to respiratory enzymes in the electron transport chain (ETC) engaging in side reactions with oxygen. However, countless attempts to alleviate mitochondrial ROS accumulation in model organisms have failed to yield improvements in cellular health or ageing. In addition, respiratory-incompetent *Saccharomyces cerevisiae* cells lacking the ETC CIV subunit Cox4p accumulate high levels of ROS not via the ETC, but via an ER-bound NADPH oxidase named Yno1p. The loss of Cox4p causes Ras2p to associate with the mitochondrial outer membrane, repressing the degradation of Yno1p by the endoplasmic reticulum-associated degradation pathway (ERAD). This process is in turn dependent on the bromodomain-containing transcription factor, Bdf1p, which, in Δ*cox4* cells, appears to dissociate from acetyl-lysine residues in histone tails and localise to the mitochondria alongside Ras2p. Here I propose that by impairing mitochondrial function, the loss of Cox4p downregulates cytosolic acetyl-CoA biosynthesis, resulting in histone hypoacetylation, and that by dissociating from hypoacetylated histones, Bdf1p serves to tether the histone acetylation state to ROS accumulation in Δ*cox4* cells. I demonstrate that the loss of Cox4p elevates ROS levels approximately 37-fold relative to WT cells and is associated with the downregulation of many genes involved in acetyl-CoA biosynthesis. Further, I show that the loss of Cox4p is associated with the downregulation of genes enriched for acetylated histone lysine residues. Lastly, I demonstrate that increasing the levels of acetyl-CoA, either by overexpressing the cytosolic acetyl-CoA synthetase *ACS2* or by supplementing cultures with potassium acetate, is sufficient to decrease ROS accumulation in Δ*cox4* cells and, in the case of the latter intervention, virtually eliminate it. These results indicate that defective acetyl-CoA metabolism is crucial for the accumulation of ROS in Δ*cox4* cells, and ought to spur further research into the links between metabolism and ROS accumulation in other organisms and under different conditions of respiratory deficiency.

II. Acknowledgements

First of all, I'd like to thank my supervisor, Dr. Campbell Gourlay, for providing me with the opportunity to begin this project, and for all the advice and encouragement which allowed me to see it through to the end. Previous research conducted by himself, Dr. Jane Leadsham and others laid the foundations for this work, so special thanks must go to them for opening such a fascinating area of research.

I would also like to thank all the members of the Gourlay lab for their generous help and support, especially Kevin Doyle, Jack Davis, and Daniel Pentland, who were always there to lend a helping hand.

Lastly, I would like to thank my family for the continuous emotional and financial support. Without their help this project would have been impossible to undertake.

III. Declaration

No part of this thesis has been submitted in support of an application for any degree or qualification of the University of Kent or any other University or institute of learning.

Nathan Dennis.

IV. Contents

V. List of figures

VI. List of abbreviations

ACL	ATP-Citrate Lyase
ACS	Acetyl-Coenzyme A Synthetase
AUC	Area Under the Curve
CI	Complex I (NADH:ubiquinone oxidoreductase)
CII	Complex II (succinate:ubiquinone oxidoreductase)
CIII	Complex III (ubiquinol:cytochrome c oxidoreductase)
CIV	Complex IV (cytochrome *c* oxidase)
DHAP	Dihydroxyacetone phosphate
DR	Downregulated
ER	Endoplasmic Reticulum
ERAD	Endoplasmic Reticulum Associated Degradation pathway
ETC	Electron Transport Chain
G3P	Glycerol-3-phosphate
GEO	Gene Expression Omnibus
GO	Gene Ontology
HHAAG	Histone Hypoacetylation-Activated Gene
IGR	Intergenic Region
IM	Inner Membrane
IMS	Intermembrane Space
KAc	Potassium Acetate
KAT	Lysine Acetyltransferase
KDAC	Lysine Deacetylase
LiAc	Lithium Acetate
MFRTA	Mitochondrial Free Radical Theory of Ageing
ORF	Open Reading Frame
PDH	Pyruvate Dehydrogenase

PEG	Polyethylene Glycol
PI	Propidium Iodide
PQQ	Plastoquinone
PTM	Post-Translational Modification
Q	Ubiquinone
$QH^{\bullet}$	Ubisemiquinone
QH2	Ubiquinol
ROS	Reactive Oxygen Species
RTG	Retrograde
SD	Synthetic Defined
SDL	Synthetic Dosage Lethal
SEM	Standard Error on the Mean
SOD	Superoxide Dismutase
SP	Stationary Phase
TCA	Tricarboxylic Acid
TPP	Triphenylphosphonium
UR	Upregulated
YHMI	Yeast Histone Modification Identifier
YNB	Yeast Nitrogen Base
YPD	Yeast Extract-Peptone-Dextrose
YPG	Yeast Extract-Peptone-Glycerol

1.1 Introduction

Mitochondria are perhaps the most versatile of the cellular organelles. Present in the vast majority of all eukaryotes, they are responsible for energy transduction, numerous biosynthetic reactions, and a play a large part in intracellular signalling (Guaragnella et al., 2018). Because of their diverse functionality, mitochondrial dysfunction can be particularly detrimental to cellular health, as illustrated by the many serious human diseases caused by or related to mutations in genes encoding mitochondrial proteins. Mitochondrial diseases can afflict virtually any organ or tissue and often affect multiple systems at once, particularly those most heavily reliant on oxidative phosphorylation such as the nervous system. To make matters worse, these diseases are also often highly degenerative, and are usually accompanied by high morbidity and mortality (Gorman et al., 2016). Furthermore, mitochondrial dysfunction has been implicated in the pathogenesis of much more widespread neurodegenerative diseases such as Parkinson's disease, Huntington's disease, and Alzheimer's disease (Carmo et al., 2018; Chen et al., 2019; Picone et al., 2014).

The role of mitochondrial dysfunction in the ageing process has also received considerable attention, as mitochondrial function declines with advancing age (Abrahám et al., 2010). Indeed, the longest-standing and arguably most influential theory of ageing, the Mitochondrial Free Radical Theory of Ageing (MFRTA) posits that dysfunctional mitochondria are the direct cause of the ageing process itself, as a result of their production of reactive oxygen species (ROS) such as superoxide ($O_2^{\bullet -}$) and hydrogen peroxide (H_2O_2; Harman, 1972; Sun et al., 2016; see section 1.1.2).

Most research concerning how mitochondria influence cellular health, including the ageing process, has focused on mitochondrial ROS production. The impacts of metabolic alterations caused by mitochondrial dysfunction, however, have been less thoroughly investigated. This is surprising considering the growing appreciation of the importance of chromatin modifications (particularly acetylation) in ageing, and the crucial role of mitochondria in providing the metabolic cofactors for these modifications (Yu et al., 2019). As such, the research presented here aims to further our knowledge regarding how mitochondrial dysfunction influences cellular health, with a focus on how broader metabolic changes, rather than simply changes in the mechanisms of energy transduction

(outlined in the proceeding section), influence the accumulation of ROS. Hopefully, this research will prove useful in the treatment of age-related decline and the numerous pathologies associated with mitochondrial dysfunction in humans.

1.2 The Mitochondrial electron transport chain

Mitochondria produce energy in the form of ATP via the electron transport chain (ETC; Fig. 1) in the inner mitochondrial membrane. The ETC is composed of a number of protein complexes, termed respiratory complexes, which together couple the oxidation of fuel molecules to the generation of ATP (Lasserre et al., 2015). The mitochondrial ETC is, to a large extent, conserved between animals, plants and fungi (Baile and Claypool, 2013). However, the ETC *Saccharomyces cerevisiae* differs from that of humans and many other organisms in that one of the major respiratory complexes, Complex I (CI; NADH:ubiquinone oxidoreductase), is absent. Instead, *S. cerevisiae* possesses a number of dehydrogenases embedded in the mitochondrial inner membrane (IM) including the glycerol-3-phosphate dehydrogenase Gut2p, the D-lactate dehydrogenase Dld1p, and the flavin-containing NADH dehydrogenases Nde1/2p and Ndi1p (Aßkamp et al., 2019; Bouchez and Devin, 2019; Feng et al., 2012; Rojo et al., 1998). Bar these differences and the presence of Var1p, a component of the small subunit of the *S. cerevisiae* mitochondrial ribosome (Fiori et al., 2003), all mitochondrially-encoded genes are conserved between *S. cerevisiae* and humans, which makes *S. cerevisiae* an ideal model organism for the investigation of mitochondrial function (Baile and Claypool, 2013).

The function of the ETC of *S. cerevisiae* can be summarised as follows (see Fig. 1 for a schematic representation): electrons from succinate, NADH or glycerol-3-phosphate are transferred to the hydrophobic electron carrier ubiquinone via Complex II (CII; succinate:ubiquinone oxidoreductase), the various NADH dehydrogenases (Nde1/2p or Ndi1p), or Gut2p (glycerol-3-phosphate dehydrogenase; see Fig. 1), respectively. Ubiquinol (the reduced form of ubiquinone) then reduces Complex III (CIII; ubiquinol:cytochrome c oxidoreductase). CIII and Dld1p (D-lactate dehydrogenase) reduce the soluble electron carrier cytochrome *c* and, finally, Complex IV (CIV; cytochrome *c* oxidase), couples the oxidation of reduced cytochrome *c* to the reduction of molecular oxygen, producing water.

CIII and CIV couple their redox reactions to the net movement of protons from the matrix to the intermembrane space (IMS). The process generates a large pH gradient and transmembrane electric potential, which combined constitute the proton-motive force (Δp). Complex V (F_1F_0 ATPase) utilises the proton-motive force to catalyse the phosphorylation of ADP to ATP (Lasserre et al., 2015).

This process of electron transport is not perfect, however. Not all electrons liberated from fuel molecules are used by CIV to catalyse the full reduction of molecular oxygen to water. A small proportion of molecular oxygen will instead undergo partial reduction by one of the many redox-active enzymes in mitochondria, producing $O_2^{\bullet-}$ and its dismutation product H_2O_2 (formed spontaneously or via the antioxidant enzyme superoxide dismutase [SOD]). In the presence of reduced iron, H_2O_2 and $O_2^{\bullet-}$ can in turn generate the highly reactive hydroxyl radical ($OH^{\bullet-}$) through the Haber-Weiss reaction (Halliwell and Gutteridge, 2015). Regardless of the importance of these mechanisms in determining the cellular levels of ROS (discussed in detail in section 1.4), it is clear that these reactive molecules can be highly damaging to cellular components, including DNA, and have been implicated in mitochondrial diseases, neurodegenerative diseases, and, as mentioned above, the ageing process (Harman, 1972; Kausar et al., 2018).

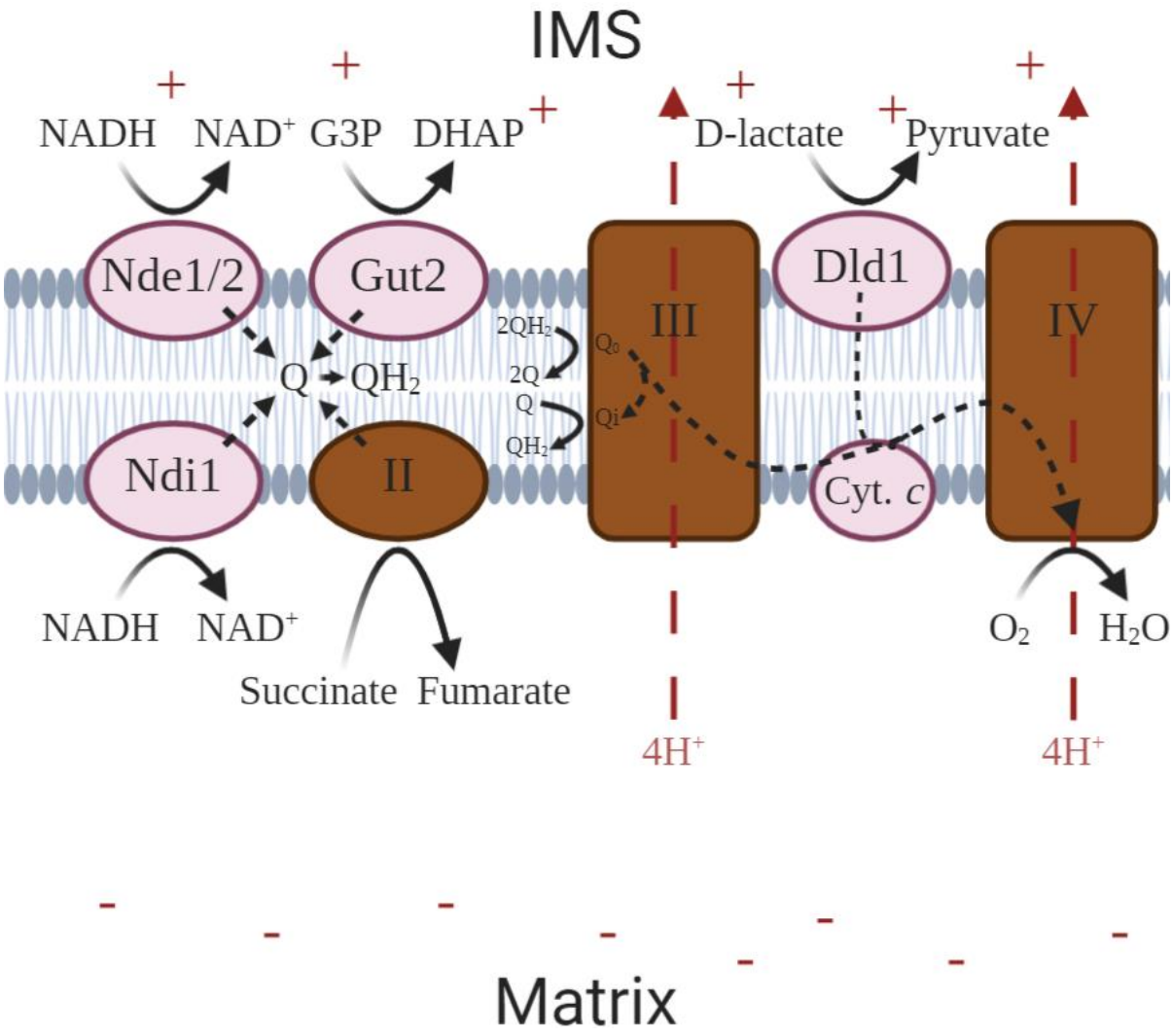

Fig. 1.1 Simplified schematic of the mitochondrial electron transport chain (ETC) in *Saccharomyces cerevisiae*. The net movement of protons from the matrix to the IMS is indicated in red. The three major respiratory complexes of the yeast ETC are coloured brown, other components of the ETC are coloured pink. II, Complex II (succinate: ubiquinone oxidoreductase); III, Complex III (ubiquinol: cytochrome c oxidoreductase); Dld1, D-lactate dehydrogenase; Cyt. c, cytochrome c; IV, Complex IV (cytochrome c oxidase). Nde1/2, IMS-facing NADH dehydrogenases; Gut2, glycerol-3-phosphate dehydrogenase; Ndi1, matrix-facing NADH dehydrogenase. G3P, glycerol-3-phosphate; DHAP, dihydroxyacetone phosphate; IMS, intermembrane space.

1.3 The mitochondrial free radical theory of ageing

ROS were initially postulated as causative agents of the ageing process by Denham Harman in 1956 (Harman, 1956). Harman recognised similarities between the damages caused by irradiation (ageing, cancer, etc.) and those arising spontaneously in nature, and proposed that these damages have a common cause – the oxygen-containing free radicals $OH^{\bullet}$ and HO_2. Harman went on to refine his Free Radical Theory of Ageing in 1972, focusing attention on the mitochondria as the major source of free radicals

in the cell (Harman, 1972). It was from here that our current conception of the Mitochondrial Free Radical Theory of Ageing (MFRTA) developed.

The MFRTA proposes that ROS, which are produced by mitochondria during respiration, leak out of the organelle to damage DNA, proteins, and lipid membranes; moreover, the MFRTA proposes that ROS also damage mitochondrial DNA, causing further mitochondrial dysfunction which in turn exacerbates ROS production and ROS-mediated damage to cellular components (Balaban et al., 2005). This offers a plausible explanation of the ageing process, as both mitochondrial dysfunction and cellular ROS levels correlate with ageing in humans and are commonly observed in age-related neurodegenerative diseases (Kausar et al., 2018; Ojaimi et al., 1999). Additionally, links between ROS production, oxidative damage and longevity have been established in a range of organisms including *S. cerevisiae*, the nematode worm *Caenorhabditis elegans*, *Drosophila* spp., and various mammalian species (Balaban et al., 2005).

Nevertheless, there are many issues with the MFRTA. The most prominent one being that attempts to increase longevity by genetically altering mitochondrial ROS production, or mitochondrial antioxidant activity, have yielded mixed results. Some studies have shown that the overexpression of mitochondrial antioxidants leads to increased longevity, reductions in damage to mtDNA, and reductions in cellular ROS levels. For example, Schriner et al. (2005) found that the overexpression of mitochondria-targeted catalase in mice brought about a 4.5-5.5 month extension of median lifespan and a 4.5 month extension of maximal lifespan, relative to their WT littermates. The mice were also less severely affected by the age-related cardiac pathologies arteriosclerosis and cardiomyopathy. Additionally, mitochondrial catalase-overexpressing mice showed less H_2O_2 production in isolated cardiac mitochondria and showed a lower degree of mtDNA damage in skeletal muscle, relative to WT mice. However, while this study and many others lend support to the MFRTA, just as many seem to contradict it. For example, in another study using mice, Pérez et al. (2009) overexpressed both CuZnSOD and the mitochondria-localised MnSOD (Halliwell and Gutteridge, 2015), yet found no difference in longevity in the CuZnSOD- and MnSOD-overexpressing transgenic strain relative to their WT counterparts. To complicate matters further, some studies demonstrate that increasing mitochondrial ROS production

may *increase* lifespan. Elevation of mitochondrial ROS production in *C. elegans*, brought about by deletion of the CoQ biosynthetic gene *clk-1* in combination with the mitochondrial SOD gene *sod-2*, resulted in an extension of lifespan relative to WT worms, directly contradicting the predictions of the MFRTA (Schaar et al., 2015).

Attempts to increase longevity using mitochondrial-targeted antioxidants have also been largely unsuccessful. Work on MitoQ, a ubiquinone derivative conjugated to the hydrophobic molecule triphenylphosphonium (TPP; Kelso et al., 2001) and arguably the most intensely studied mitochondrially-targeted antioxidant, has failed to show consistent longevity-promoting effects (Magwere et al., 2006; Sakellariou et al., 2016). However, some molecules have achieved some success in enhancing longevity. The plastoquinone- (PQQ) based antioxidant SkQ1 (10-[6′-plastoquinonyl] decyltriphenylphosphonium), for example, has been shown to have great potential in enhancing longevity. Anisimov et al. (2008) showed that SkQ1 elicits lifespan extension in the fungus *Podospora anserina*, the crustacean *Ceriodaphnia affinis*¸ *D. melanogaster*, and mice – in which it elicited a 100% increase in median lifespan. However, in addition to providing some compelling evidence for SkQ1's efficacy, Anisimov et al. illustrated the difficulty of interpreting such evidence within the framework of the MFRTA. Firstly, while SkQ1 did elicit a very large increase in the median lifespan of mice, it did not bring about any change in maximum lifespan. This finding was likely the result of rearing the mice in a non-sterile environment, as a further study using the same strain of mice (SHR mice) kept under pathogen-free conditions found no effect of SkQ1 on longevity (Anisimov et al., 2011). Also, in many cases SkQ1 only needed to be administered early in life to enhance longevity. Such an effect seems to suggest that SkQ1 may elicit part of its longevity-enhancing effects through the initiation of a life-extending genetic program early in development, rather than through the continuous prevention of ROS-mediated damages. Finally, a similar compound wherein PQQ was replaced by two methylene groups (C_{12}TPP), also elicited lifespan extension despite having no antioxidant activity (Anisimov et al., 2008). This is a common issue with many mitochondria-targeted antioxidants, as the hydrophobic TPP moiety which is the backbone of SkQ1, MitoQ and many other mitochondria-targeted antioxidants, can have an uncoupling effect which itself may enhance longevity (Gruber et al., 2013). Such issues

highlight the difficulty of disentangling the amelioration of ROS-mediated damages from other effects of molecules such as SkQ1. Overall, in light of the failure of molecules such as MitoQ to enhance longevity and the issues associated with the apparent longevity-enhancing effects of SkQ1, there is no clear picture of the efficacy of mitochondria-targeted antioxidants to slow ageing (Gruber et al., 2013).

1.4 Cellular sources of ROS

The findings outlined in section 1.3 have led many to reject the MFRTA or even declare it "dead" (Gladyshev, 2014). It is interesting to note, however, that while many have rejected the idea that ROS are the major cause of ageing, comparatively few have questioned the first link in the MFRTA chain – the notion that ROS are produced in a vicious cycle *by* dysfunctional mitochondria. Mitochondria are very frequently cited as the major source of ROS under normal conditions and under conditions of mitochondrial dysfunction (Balaban et al., 2005; Kausar et al., 2018; Sanz, 2016), but, as shown in the proceeding section, the evidence for this is obscure. Cellular ROS levels reflect all prooxidant and antioxidant activities within the cell, which includes ROS production by the ETC but also includes non-mitochondrial enzymatic ROS production, involving proteins such as xanthine oxidase and the NADPH oxidases, fatty acid β oxidation, and the ER protein disulphide resolution system (Rinnerthaler et al., 2012). Furthermore, the relative contributions of these pro-oxidant processes may be different for different ROS (e.g. $O_2^{\bullet-}$ or H_2O_2), different species (and within species, different cell types), and different physiological or pathophysiological conditions (Brown and Borutaite, 2012).

1.4.1 ROS production by the ETC

The mechanisms of ROS production from the ETC have been thoroughly studied for many years, mostly using isolated mitochondria, sub-mitochondrial particles, or isolated respiratory complexes from numerous organisms. This work has aimed to dissect the precise manner in which the respiratory complexes produce ROS and the conditions under which ROS production from the ETC may reach harmful levels (Kausar et al., 2018; Michael P. Murphy, 2009).

A large proportion of this work has focused on the mechanisms of ROS production by CI, which is thought to be the biggest producer of $O_2^{\bullet-}$ in mammalian mitochondria (Kausar et al., 2018; Michael P

Murphy, 2009; Treberg et al., 2011). While CI is absent in *S. cerevisiae* (see section 1.1), the mechanisms uncovered for the production of ROS by CI illustrate quite well the conditions required for the production of ROS by the ETC as a whole. CI produces ROS via both forward electron transport (NADH-oxidising) and reverse electron transport (NAD^+-reducing). These two modes of ROS production occur at two different sites within the complex and occur under distinct conditions. ROS production in the forward direction occurs when the flavin at the NADH-binding site (site I_F) is reduced. Oxygen can react with the reduced flavin at the NADH-binding site and produce superoxide. The likelihood of this occurring is greatly increased when the NADH/NAD^+ pool is highly reduced, as the proportion of reduced flavin is set by the NADH/NAD^+ ratio (Kausar et al., 2018; Treberg et al., 2011). Consequently, any condition which increases the NADH/NAD^+ ratio, such as damage to the downstream complexes including CIV, will lead to an increase in ROS production by CI (Murphy, 2009). Conversely, ROS production in the reverse direction is not dependent on the redox state of the NAD^+/NADH pool but instead requires a highly reduced ubiquinone pool and a high Δp (most importantly ΔpH; Lambert and Brand, 2004). ROS production in this manner is extremely sensitive to any changes in the Δp, as the addition of an uncoupler steeply reduces ROS production (Lambert and Brand, 2004). The site at which $O_2^{\bullet-}$ is produced via reverse electron transport (site I_Q) is located somewhere between the NAD-binding site and the Q-binding site, though its precise location is unknown (Kausar et al., 2018; Treberg et al., 2011). Interestingly, reverse electron transport to CI may achieve the highest rate of ROS production possible within mitochondria (Kausar et al., 2018; Michael P Murphy, 2009; Treberg et al., 2011).

Comparatively little information exists regarding ROS production by CII. For many years it was thought that CII was unimportant in determining mitochondrial ROS production until mutated, as previous studies demonstrated that mammalian CII produces only low levels of ROS under normal incubation conditions (Quinlan et al., 2012, 2011). However, recent research has shown that it could potentially act as a major producer of ROS under certain circumstances. Quinlan et al. 2012 demonstrated that in isolated rat muscle mitochondria, CII can produce high levels of ROS when both CI and CIII are inhibited and the succinate concentration is low. Like CI, CII can produce ROS in both the forward

(from succinate) and reverse (from reduced ubiquinone) directions. Furthermore, Quinlan et al. demonstrated that under these conditions, the rate of ROS production from CII may reach or exceed that of CI or CIII (Quinlan et al., 2012). The site of ROS production by CII is probably the reduced flavin (Quinlan et al., 2012; Siebels and Dröse, 2013), but this location is still controversial and Grivennikova et al. (2017) suggest that ROS are produced at the ubiquinone binding site instead. Interestingly, and in support of the former location, defects in the SDH-C subunit of CII (analogous to Sdh3p in *S. cerevisiae*) in *C. elegans* leads to ROS accumulation and premature ageing (Adachi et al., 1998; Senoo-Matsuda et al., 2001). A defective SDH-C subunit would allow for SDH-A (analogous to Sdh1p in *S. cerevisiae*) to accept an electron but bar its passage to ubiquinone, resulting in a highly reduced flavin and, consequently, greatly increasing the probability of ROS production by CII.

CIII is considered to be the second most prominent site of ROS production in the ETC of mammalian mitochondria after CI, and the biggest source of ROS in the ETC of *S. cerevisiae* (Zhao et al., 2019). CIII produces ROS via its Q-cycle mechanism. Put simply, in the Q cycle ubiquinol (QH_2) is oxidised to the ubisemiquinone radical ($QH^{\bullet}$) at the Q_0 site located on the IMS side of the mitochondrial IM, and the liberated electron is passed through CIII onto cytochrome *c*. Ubisemiquinone is then oxidised at the Q_0 site, passing an electron onto another molecule of ubiquinone bound to the Q_i site located on the matrix side of the mitochondrial IM. The ubisemiquinone thus formed is then reduced to ubiquinol at the Q_i site in another round of ubiquinol oxidation at the Q_0 site. ROS are produced at the Q_0 site only, when the ubisemiquinone intermediate nonenzymatically reacts with O_2 to produce $O_2^{\bullet-}$ (Zhao et al., 2019). $O_2^{\bullet-}$ can diffuse into the IMS or matrix despite the location of the Q_0 site on the IMS-side of the mitochondrial IM. The rate of ROS production by CIII is minimal under normal conditions, but is substantially increased by the Q_i site inhibitor antimycin A, as blockage of electron transport at the Q_i site stalls electrons at the Q_0 site, increasing the probability of $QH^{\bullet}$ interacting with O_2. This can, in turn, be reversed by treatment with Q_0 site inhibitors such as stigmatellin (Bleier and Dröse, 2013; Zhao et al., 2019). Most of the research into how CIII produces ROS has utilised antimycin A – far fewer studies have investigated how CIII might produce ROS under physiologically relevant conditions. Those that have suggest that CIII produces high levels of ROS when the membrane potential is high,

which effectively stops the transmembrane electrogenic steps of the Q-cycle, halting electrons at Q_0, and when the redox state of the Q pool is relatively balanced. However, even the latter condition is derived from studies using antimycin A (Bleier and Dröse, 2013).

In addition to the major respiratory complexes, previous research has demonstrated that the matrix- and IMS-facing NADH dehydrogenases are also sources of ROS in *S. cerevisiae*. Isolated mitochondria supplied with NADH produced less ROS when flavin-containing proteins, which include Nde1p, Nde2p and Ndi1p, were inhibited by diphenyleiodonium. Additionally, the deletion of Nde1p has been shown to decrease the rate of ROS formation in isolated mitochondria under resting conditions and in whole cells subjected to acute heat shock (Fedoseeva et al., 2017; Gomes et al., 2013). Corroborating this, the overexpression of *NDI1* and *NDE1* also elevates cellular ROS production in *S. cerevisiae* (Li et al., 2006).

Drawing from all this work, one can generalise that the ETC produces ROS when a blockage, caused by an inhibitor, hypoxia, or other disruption, allows for the acceptance of an electron upstream of the block but bars its passage downstream of the block, effectively heightening the probability of side reactions with oxygen. However, despite the evidence accrued in these studies, it is difficult to find convincing evidence that the ETC is the major source of ROS *in vivo*. Virtually all the studies cited above were conducted using isolated mitochondria or sub-mitochondrial particles, often using non-physiological conditions (most often using highly reducing conditions), and often using inhibitors such as antimycin A, the effects of which are unlikely to be reproduced *in vivo*. To highlight the issues associated with such studies, it is worth noting that one piece of research ubiquitously reported in the literature – the finding that approximately 1-2% of oxygen consumption results in the production of ROS by mitochondria – is highly misinterpreted. This figure is taken from Boveris et al. (1972), in which isolated rat liver mitochondria were found to produce 0.5 nmol H_2O_2 min^{-1} mg^{-1} protein, corresponding to approximately 1-2% of total oxygen consumption by the isolated mitochondria. However, this figure was obtained under highly reducing conditions (5 mM succinate) and during state 4 respiration. H_2O_2 production dropped significantly after the state 4 – state 3 transition and was also significantly lower with other substrates such as glutamate and malate. Furthermore, Boveris et al. also

measured the contributions of different subcellular fractions to total H_2O_2 accumulation in rat liver cells, and found the highest rates of H_2O_2 production in the microsomal fraction (42 nmol min^{-1} g^{-1} liver tissue), followed by the peroxisomes (30 nmol min^{-1} g^{-1} liver tissue) and the mitochondria (12 nmol min^{-1} g^{-1} liver tissue). These figures actually suggest that mitochondria are an important, but not predominant, source of ROS, a finding which tends to be ignored whenever the 1-2% figure is reported (Boveris et al., 1972; Brown and Borutaite, 2012).

1.4.2 ROS production by Yno1p

Aside from the issues associated with interpreting studies on isolated mitochondria, recent experimental evidence has demonstrated that in some instances of mitochondrial dysfunction, the ETC may not be a significant source of ROS. New research has shown that extra-mitochondrial ROS production by the ER-bound NADPH oxidase Yno1p supersedes that of the ETC in respiratory mutant strains of *S. cerevisiae* (Leadsham et al., 2013; Rinnerthaler et al., 2012; Yi et al., 2018). Leadsham et al. (2013) uncovered that the loss of Cox4p, an ETC subunit critical for CIV assembly and respiratory capacity, heightened ROS accumulation in *S. cerevisiae*, and found that treatment of Δ*cox4* cells with antimycin A to inhibit CIII did not exacerbate ROS production, indicating that the ETC is not the major source of ROS in these cells. Instead, the loss of Cox4p induced the Bdf1p-dependent translocation of Ras2p to the mitochondrial outer membrane, which in turn inhibited the degradation of Yno1p via the endoplasmic-reticulum associated degradation pathway (ERAD) during stationary phase (SP), resulting in greatly elevated ROS production from this enzyme. Yi et al. (2018) presented similar findings in Rho^0 cells, which lack mtDNA altogether, which suggests that this process is not specific to Δ*cox4* cells. Figure 1.2A presents in schematic form the process of Yno1p-mediated ROS accumulation in Δ*cox4* cells, in contrast to the standard view of how mitochondrial dysfunction induces ROS production from the ETC as presented in simplified form in Fig. 1.2B.

Not only is Yno1p-mediated ROS production in Δ*cox4* cells dependent on Bdf1p, but in these cells Bdf1p appears to localise, along with Ras2p, to the mitochondrial outer membrane (Leadsham and Gourlay, unpublished data). Bdf1p and its homolog Bdf2p, are members of the BET family of proteins expressed in *S. cerevisiae*. BET family proteins contain two bromodomains at their N-terminus which

bind acetylated lysine residues in histones and non-histone proteins, with those of the BET family preferentially binding acetylated lysine residues in the core histones H3 and H4 (García-Oliver et al., 2017). As such, it is fascinating that in Δ*cox4* cells, Bdf1p is found to associate with the mitochondria, which could imply its dissociation from acetylated lysine residues in histones H3 and H4. It is well known that mitochondria are crucial in the regulation of histone modifications, as discussed in the proceeding section, so in this instance it is possible that mitochondrial dysfunction is triggering the translocation of Bdf1p, and the resulting ROS production by Yno1p, in part by eliciting changes in chromatin structure.

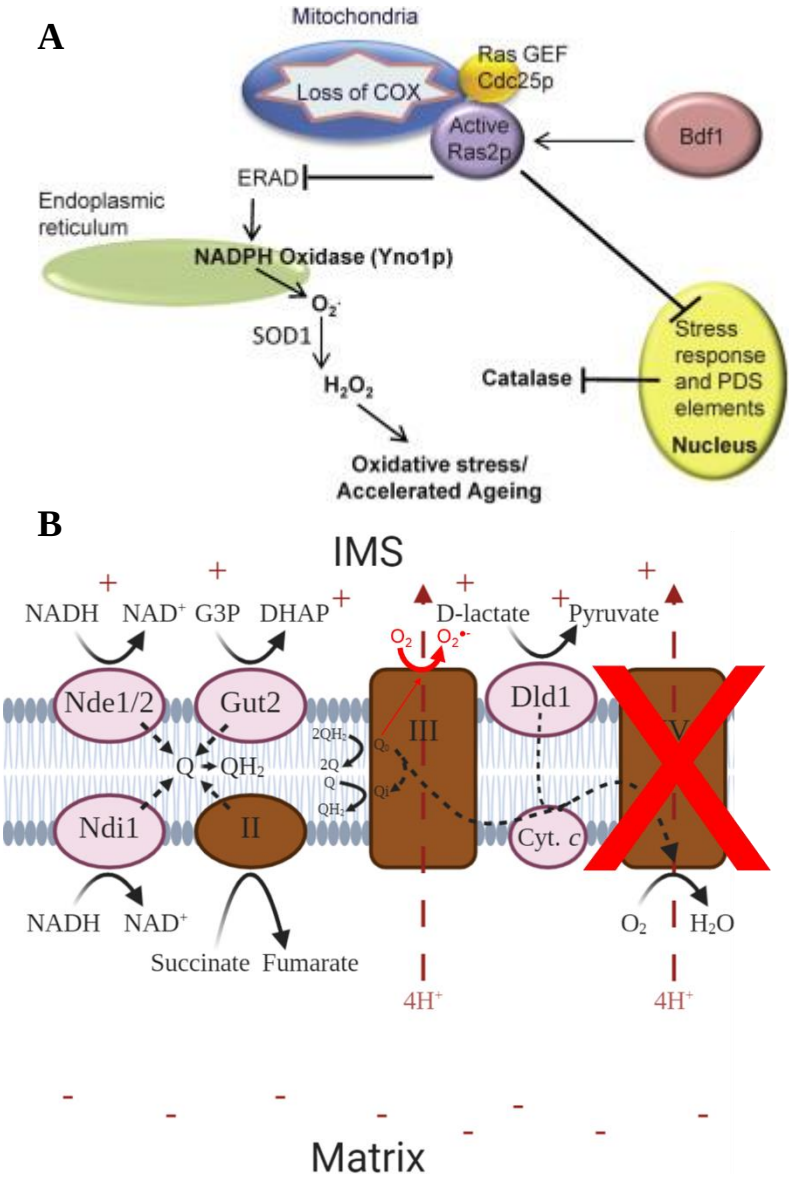

Fig. 1.2. The process of Yno1p-mediated ROS production in Δcox4 and Rho^0 cells (**A**; taken from Leadsham et al. 2013). In this process, the loss of Cox4p (or other components of the ETC in Rho^0 cells) triggers the Bdf1p-dependent translocation of Ras2p to the mitochondrial outer membrane, suppressing the degradation of Yno1p by the endoplasmic reticulum-associated degradation pathway (ERAD) and thereby significantly enhancing ROS production by this enzyme. Contrast this to the standard view of ETC-mediated ROS production presented in **B** (reproduced from Fig. 1.1 – c.f. figure legend for abbreviations), in which a disruption to the ETC, such as the inhibition of Complex IV (indicated here by the red cross) increases the likelihood of the other respiratory complexes participating in side reactions with oxygen. In this case, the Q_0 site of Complex III is shown to catalyse the partial reduction of O_2 to the superoxide radical ($O_2^{\bullet-}$; see the text for details regarding how this occurs).

1.5 Mitochondrial regulation of the epigenome

To fit within the limited space available in the nucleus, DNA must be efficiently compressed. But this must occur in a manner that allows for regulated access to the genetic material. This is accomplished by the compaction of DNA with histones to form nucleosomes, which in turn associate with one another to form chromatin (Fig. 1.3). Despite its compaction, chromatin is a highly dynamic structure capable of responding to various cellular cues – chiefly the physical displacement of nucleosomes (i.e. remodelling, carried out by ATP-dependent chromatin remodelling complexes), and the covalent modification of histones (Wiese and Bannister, 2020). These chromatin modifications are commonly termed "epigenetic" modifications.

All four of the core histones in yeast (H3, H4, H2A and H2B) undergo a multitude of reversible covalent modifications. Histone modifications regulate gene expression by altering chromatin accessibility (by changing the degree of compaction) or by providing binding sites for other regulatory proteins (e.g. bromodomain-containing proteins). Over 100 such post-translational modifications (PTMs) have been identified thus far, but only a fraction of these occur in *S. cerevisiae* (Wiese and Bannister, 2020). Yeast histones can undergo phosphorylation, methylation, ubiquitination and a range of acylations including succinylation, crotonylation, propionylation, butyrylation, malonylation, 2-hydroxyisobutyrylation and, by far the most well-studied and prevalent sub-type, acetylation (Barnes et al., 2019; Jaiswal et al., 2017). These modifications are dynamically regulated by the activities of various "writer" and "eraser" enzyme complexes, and by the availability of various metabolic cofactors.

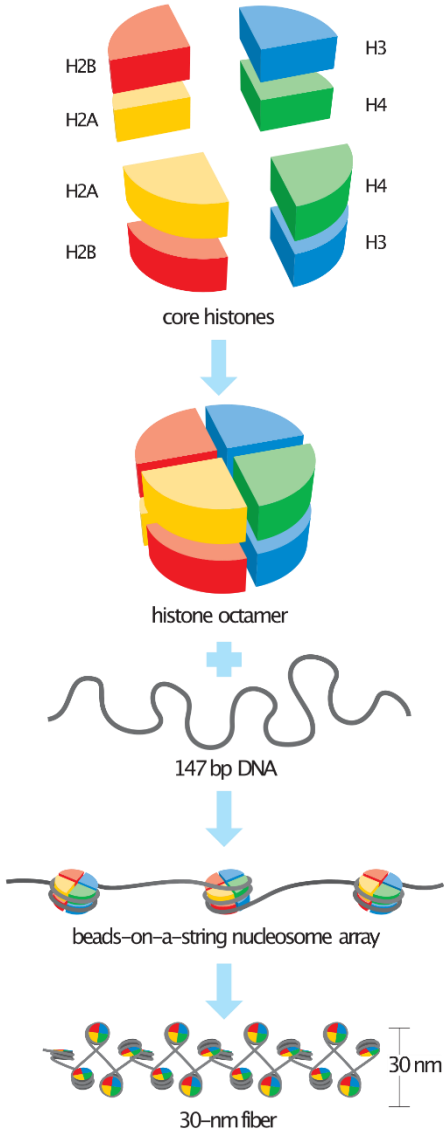

Fig. 1.3. The basic structure of eukaryotic chromatin. The nucleosome core particle is made up of 147bp of DNA wrapped around the histone octamer, formed by the interaction of two H3-H4 dimers with two H2A-H2B dimers. Nucleosomes can be arranged in the "beads-on-a-string" form as seen in the third panel, but are generally found in more compact forms, such as the 30 nm fibre shown in the final panel. The formation of higher-order structures like the 30 nm fibre are facilitated by histone tails (not shown here; see section 1.7.1) in combination with other proteins. Figure taken from Morgan (2007).

The reliance of histone modifications on metabolic cofactors tethers chromatin function to the cell's metabolic state, which is to a large extent underpinned by mitochondrial function. Thus, any change in mitochondrial function is likely to have large knock-on effects on chromatin structure, and consequently elicit large effects on all DNA-based processes. A defect in the electron transport chain which depletes cellular ATP pools would, for example, deplete kinases of their substrate for phosphorylation, and

would result in a lower flux through the ATP-dependent cytosolic acetyl-Coenzyme A (acetyl-CoA) biosynthetic pathway in yeast (described in the proceeding section). Consequently, a lower flux through the cytosolic acetyl-CoA biosynthetic pathway could, thanks to the compartmentalisation of acetyl-CoA metabolism in yeast, deplete the acetylation "writer" enzymes (lysine acetyltransferases [KATs]), of their cofactor, resulting in a downregulation of lysine acetylation. This has been demonstrated to occur in p^0 cells (cells lacking mtDNA), which show ATP depletion, histone hypoacetylation and drastically altered metabolite profiles during SP when compared to p^+ cells (Friis et al., 2014).

The influence of mitochondrial metabolism extends further than the epigenome, however. For example, the acetylation of non-histone proteins, including numerous mitochondrial proteins, is an enormously widespread process which affects virtually every aspect of cell physiology. In the case of bacteria and mammals this includes the synthesis of its metabolic cofactor, acetyl-CoA (see proceeding section; Baeza et al., 2016). As time goes on, the scope of metabolite-mediated regulation of cellular processes seems to ever increase. Recently, mitochondrial biosynthesis was shown to be yet another process regulated in part by mitochondrial metabolism. Bouchez et al. (2020) recently demonstrated that "labile" heme (meaning heme not incorporated as a prosthetic group into proteins) may regulate mitochondrial biogenesis, and hence cell growth on non-fermentable carbon sources, by stabilising Hap4p. Hap4p is the transcriptional co-activator of the HAP complex, which regulates the expression of many mitochondrial proteins involved in the TCA cycle, the OXPHOS machinery, etc. The first step of heme biosynthesis occurs in the mitochondrial matrix, in which Hem1p catalyses the condensation of glycine with succinyl-CoA to generate delta-aminolevulinate. Succinyl-CoA is in turn produced from the oxidation of alpha-ketoglutarate during the TCA cycle, so it is evident that alterations in mitochondrial metabolism could feed-back into the regulation of mitochondrial biogenesis (Baccolo et al., 2018; Bouchez and Devin, 2019; Bouchez et al., 2020).

The mitochondria-PTM network is highly relevant to ageing research, as some of the most robust pro-longevity phenotypes have been produced by altering acetylation patterns. Sirtuins, phylogenetically conserved NAD^+-dependent lysine deacetylases (KDACs – examples of the "eraser" complexes) are well-known for mediating the lifespan-extending effects of caloric restriction and elevating lifespan in

a range of organisms. In yeast, overexpression of the sirtuin gene *SIR2* suppresses the formation of extra-chromosomal rDNA circles (markers of cellular senescence), and extends replicative lifespan (Wierman and Smith, 2014). In *C. elegans*, SIR-2.1 interacts with 14-3-3 proteins to activate the transcription factor DAF-16, which induces a transcriptional program to enhance longevity and stress resistance (Berdichevsky et al., 2006).

Altering the activity of the "writer" and "eraser" complexes produces similar effects to modulating the availability of their metabolic cofactors. With regards to the lifespan extension caused by enhanced sirtuin activity, for example, such an extension can also be elicited via alterations in acetyl-CoA biosynthesis. In a study using *S. cerevisiae*, Eisenberg et al. (2014) demonstrated that a reduction in the activity of the nucleocytosolic acetyl-CoA synthetase (ACS) ACS2 conferred enhanced autophagic activity and prolonged lifespan. Conversely, knockdown of *MPC1* and *ACH1*, genes encoding proteins involved in mitochondrial acetyl-CoA metabolism, resulted in the accumulation of extracellular acetate, the hyperactivation of ACS2 concomitant with an increase in H3 acetylation, and a substantial decrease in lifespan. In light of these facts and the reliance of Yno1p-mediated ROS accumulation on Bdf1p, it is clear that the influence of mitochondrial function on acetyl-CoA metabolism, and the knock-on effects this has on cellular processes, must be studied further.

1.6 Acetyl-CoA biosynthesis in yeast

Acetyl-CoA is a crucial metabolite in all known life forms (van Rossum et al., 2016). Acetyl-CoA is utilised in the TCA cycle to produce ATP and precursors to amino acids, nucleotides, and porphyrins, and also participates in a multitude of other biosynthetic pathways, such as those involved in the production of fatty acids and sterols, glutathione, N-acetylglucosamine and S-adenosyl-methionine (Krivoruchko et al., 2015; Shi and Tu, 2015; Takahashi et al., 2006; van Rossum et al., 2016).

In yeast, the biosynthesis of acetyl-CoA is highly compartmentalised, with distinct pathways operating in the mitochondria, cytosol, and peroxisomes (Fig. 1.4), and limited transport between these compartments. The cytosol and the nucleus share the same pool of acetyl-CoA (henceforth termed the nucleocytosolic pool) due to the permeability of the nuclear envelope to small molecules. However, the

inner mitochondrial membrane and that of the peroxisomes are impermeable to acetyl-CoA (van Rossum et al., 2016). This is crucial, as it means that any acetyl-CoA produced within the mitochondria, which are highly concentrated for acetyl-CoA relative to the nucleus and cytoplasm, cannot directly influence the acetylation state of nucleocytosolic proteins (Galdieri et al., 2014; Takahashi et al., 2006; Weinert et al., 2014).

Mitochondrial acetyl-CoA production is conducted by the pyruvate dehydrogenase (PDH) complex, though the acetyl-CoA hydrolase/transferase Ach1p, which is localised to the mitochondrial matrix, is also involved. Whereas in the peroxisomes, acetyl-CoA is produced by the β-oxidation of fatty acids (Galdieri et al., 2014). In contrast, nucleocytosolic acetyl-CoA is produced by the acetyl-CoA synthetase enzymes Acs1p and Acs2p, which, due to the compartmentalisation of acetyl-CoA metabolism in *S. cerevisiae*, are solely responsible for the provision of nucleocytosolic acetyl-CoA – however some evidence suggests that Acs1p may also contribute to mitochondrial and peroxisomal acetyl-CoA biosynthesis (Takahashi et al., 2006; van Rossum et al., 2016).

As mentioned above, the isolation of subcellular acetyl-CoA pools in yeast results from membrane impermeability combined with the difficulty of intercompartmental acetyl-CoA transport. Only two mechanisms of intercompartmental acetyl-CoA transport exist in *S. cerevisiae*. Acetyl-CoA produced in the cytosol and the peroxisomes can be converted to acetyl-carnitine by the carnitine acetyltransferases Yat2p and Cat2p, respectively, and transported to the mitochondria via the acetyl-carnitine transporter Crc1p (Galdieri et al., 2014; van Roermund et al., 1995). However, *S. cerevisiae* lacks the capacity for the *de novo* carnitine synthesis, and as such this mechanism only operates in the presence of exogenous carnitine (e.g. in complex media). Cells growing without exogenous carnitine instead rely on the production of TCA cycle intermediates, via the glyoxylate cycle, to transport acetyl-CoA. TCA cycle intermediates can be transported into the mitochondria where they can serve as precursors for the formation of pyruvate and, consequently, acetyl-CoA in reactions catalysed by the PDH complex or possibly Acs1p as outlined below (Y. Chen et al., 2012). Conversely, whether mitochondria-cytosol acetyl-CoA transport occurs is unclear. However, Takahashi et al. (2006) demonstrated that reducing *ACS2* expression during fermentative growth results in histone

hypoacetylation, an effect which can be reversed by targeting *Salmonella enterica* ACS to the cytosol, but cannot be reversed by targeting ACS to the mitochondria – which clearly suggests that under these conditions, acetyl-CoA cannot be transported from the mitochondria to the cytosol.

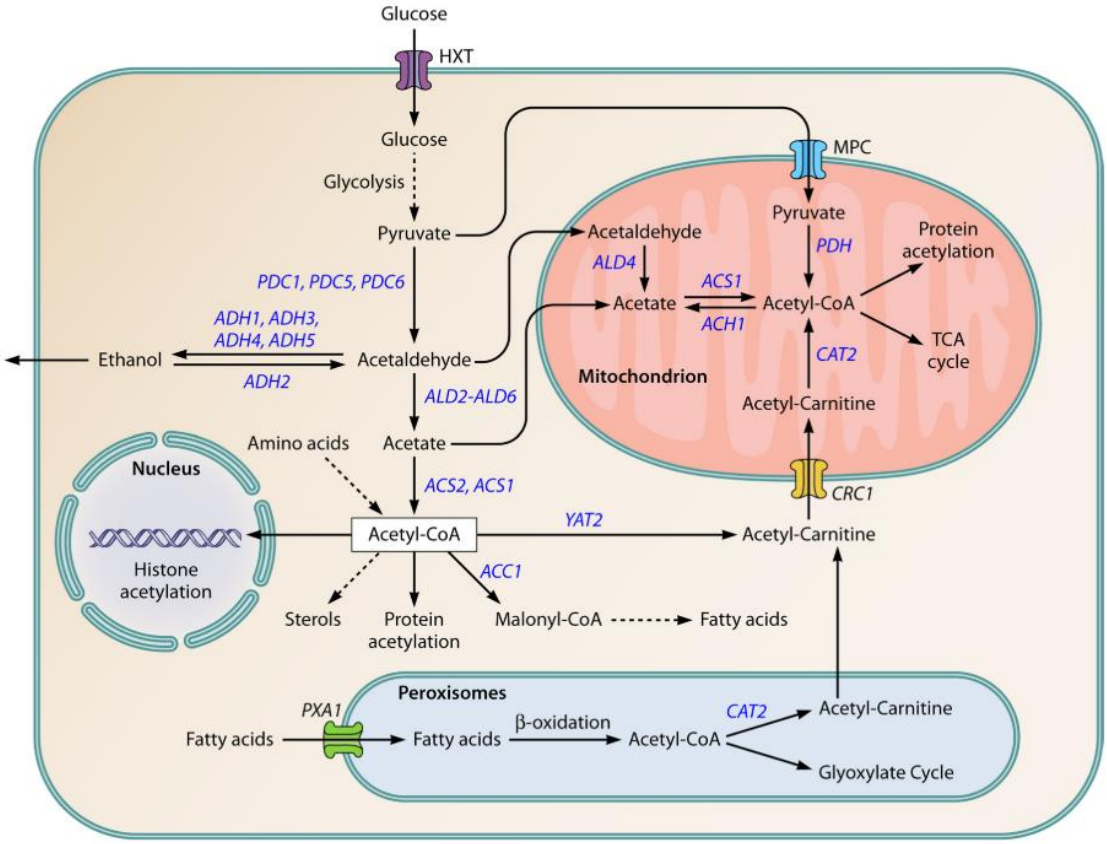

Fig. 1.4. An overview of acetyl-CoA metabolism in *S. cerevisiae*. Dashed arrows represent multi-step metabolic pathways. PDC1, 5, 6, pyruvate decarboxylase 5, 6; ADH1, 3, 4, 5, alcohol dehydrogenase 1, 3, 4, 5; ADL2-6, acetaldehyde dehydrogenase 2-6; ACS1, acetyl-CoA synthetase 1; ACS2, acetyl-CoA synthetase 2; YAT2, carnitine acetyltransferase; ACC1, acetyl-CoA carboxylase; PXA1, peroxisomal ABC transporter; CAT2, mitochondrial carnitine acetyltransferase; PDH, pyruvate dehydrogenase complex; ACH1, acetyl-CoA hydrolase/transferase; CRC1, mitochondrial acetyl-carnitine transporter. Figure taken from Galdieri et al. (2014).

1.6.1 Nucleocytosolic acetyl-CoA biosynthesis: the PDH bypass

In plants, animals, algae, and many species of fungi, nucleocytosolic acetyl-CoA is produced from citrate by ATP-citrate lyase (ACL). In contrast, *S. cerevisiae* and most other members of the subphylum *Saccharomycotina* produce nucleocytosolic acetyl-CoA via the PDH bypass (Galdieri et al., 2014). In this pathway, pyruvate produced during glycolysis is converted to acetaldehyde by pyruvate decarboxylase (PDC), which then engages in an NAD^+- or $NADP^+$-dependent reaction catalysed

acetaldehyde dehydrogenase (ADH) and is converted to acetate. Acetate then participates in an ATP-dependent reaction, catalysed Acs1p/Acs2p, in which it is ligated to Coenzyme A to produce acetyl-CoA (Fig. 1.5; van Rossum et al., 2016).

While Acs1p and Acs2p catalyse the same reaction, they differ substantially in their affinity for acetyl-CoA, their activity patterns during growth, and their subcellular localisation. Acs2p is constitutively active and is the critical enzyme for acetyl-CoA metabolism during growth on glucose, under which conditions Acs1p is strongly repressed (Galdieri et al., 2014). Acs1p is induced upon glucose exhaustion by the transcription factors Cat8p and Adr1p and appears to be critical for growth on non-fermentable carbon sources in cells growing in synthetic minimal media (Chen et al., 2012). However it is important to stress the media used here, as the evidence regarding the growth phenotype of *ACS1* deletion strains is rather contradictory, possibly due to the presence of exogenous carnitine in complex media (Chen et al., 2012). The importance of Acs1p for growth on non-fermentable carbon sources suggests that during respiratory growth, Acs2p produces inadequate quantities of acetyl-CoA for biosynthetic reactions, perhaps because of its ~30-fold lower affinity for acetate relative to Acs1p (Chen et al., 2012). Acs2p is primarily nuclear in its localisation, though it can also exhibit a cytosolic distribution depending on the nutritional environment. Takahashi et al. (2006) uncovered an almost complete nuclear localisation (>95% of total cellular Acs2p) when cells were grown on rich media with 2% glucose (YPD), but also found that in cells growing in media with 2% each glycerol and ethanol (YPGE), Acs2p was distributed between the nucleus (87%) and the cytosol (13%). The subcellular localisation of Acs1p is not entirely clear, but it seems to be present in the nucleus, cytosol, mitochondria, and potentially the peroxisomes, though evidence for a peroxisomal localisation is indirect and comes from a consideration of the amino acid sequence and activity patterns of the enzyme (Chen et al., 2012; Galdieri et al., 2014; Huh et al., 2003; Takahashi et al., 2006; Van Den Berg and Steensma, 1995). Acs1p contains a C-terminal SVKL sequence, similar to the SKL peroxisomal targeting sequence (Van Den Berg and Steensma, 1995). Additionally, like Acs1p, several enzymes of the glyoxylate cycle, which are partially peroxisomal, are also induced under conditions of glucose-limitation. Considering this, Acs1p could potentially serve as

a second peroxisomal source of acetyl-CoA under conditions in which the glyoxylate cycle is operative (Chen et al., 2012; Krivoruchko et al., 2015; Van Den Berg and Steensma, 1995).

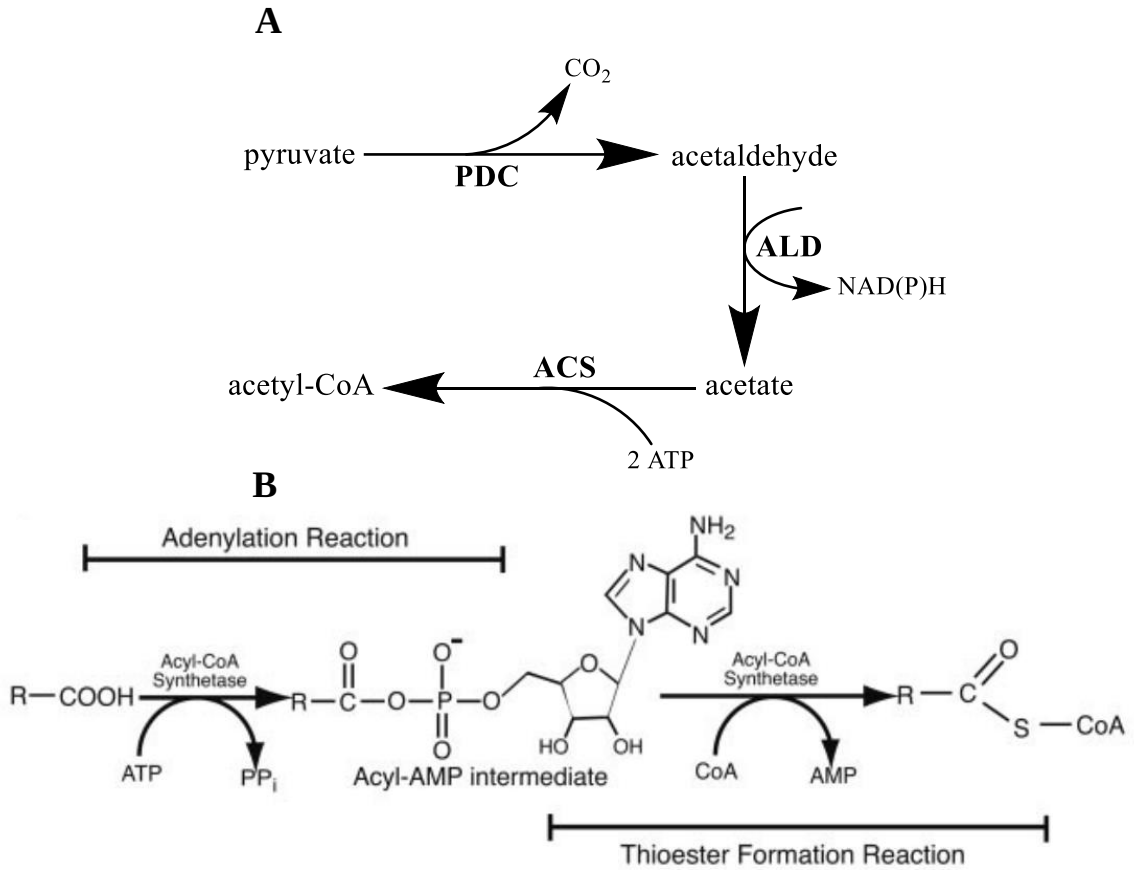

Fig. 1.5. (A) The PDH-bypass route of acetyl acetyl coenzyme A (acetyl-CoA) biosynthesis in *Saccharmoyces cerevisiae*. **(B)** Acetyl-CoA synthetase catalyses the production of acetyl-CoA via a two-step reaction involving an adenylation step and a ligation step. PDC, pyruvate decarboxylase; ALD, acetaldehyde dehydrogenase; ACS, acetyl coenzyme A synthetase. A is adapted from van Rossum et al. (2016); B is taken from Starai et al. (2002).

1.6.2 Mitochondrial acetyl-CoA biosynthesis

Mitochondrial acetyl-CoA is produced by the oxidative decarboxylation of pyruvate, catalysed by the pyruvate dehydrogenase (PDH) complex:

$$\text{Pyruvate} + NAD^+ + \text{CoA} \rightarrow \text{acetyl-CoA} + CO_2 + \text{NADH} + H^+$$

The pyruvate utilised in this process can be derived either from sugars, via glycolysis, or from the oxidation of malate by malate dehydrogenase within mitochondria (Krivoruchko et al., 2015; van Rossum et al., 2016). The PDH complex is a ~10 MDa protein complex made up of three major catalytic

subunits termed E1 (pyruvate dehydrogenase), E2 (dihydrolipoamide acetyltransferase) and E3 (dihydrolipoamide dehydrogenase), and one additional component termed protein X (involved in binding and positioning E2 and E3; Krivoruchko et al., 2015). Acetyl-CoA produced by the PDH complex then enters the TCA cycle in a step catalysed by citrate synthase. Because glucose represses respiratory function and the TCA cycle in *S. cerevisiae*, during fermentative growth little glycolytically-produced pyruvate is transported to mitochondria and converted to acetyl-CoA by the PDH complex (Galdieri et al., 2014). Additionally, in many organisms, the E3 subunit is inhibited by high [NADH]/[NAD^+] ratios, and as a result is only active during respiratory growth (van Rossum et al., 2016). Nevertheless, despite taking up approximately 1-2% of cellular volume the mitochondria contain ~33% of cellular acetyl-CoA during exponential growth with glucose as a carbon source. Meaning that under these conditions, the acetyl-CoA concentration in the mitochondria is approximately 20-30 times higher than that of the cytoplasm or nucleus (Weinert et al., 2014).

Mitochondrial acetyl-CoA levels are also influenced by the acetyl-CoA hydrolase/transferase Ach1p. Ach1p. Initially, Ach1p was assumed to act only as an acetyl-CoA hydrolase, perhaps to reduce acetyl-CoA accumulation during growth on acetate. However, recent research has uncovered an important role for Ach1p as an acetyl-CoA transferase, catalysing the transfer of CoA from succinyl-CoA onto acetate, thus producing acetyl-CoA while also protecting against the toxic effects of acetate accumulation (Orlandi et al., 2012). Ach1p has also been proposed to facilitate acetyl-CoA transport from the mitochondria to the cytosol. Chen et al. (2015) demonstrated that in PDC-deficient cells, Ach1p may convert mitochondrial acetyl-CoA to acetate, which can cross the mitochondrial membrane and be converted back into acetyl-CoA by Acs1p/Acs2p. This is also corroborated by Eisenberg et al. (2014) who found that the absence of Ach1p or Mpc1p caused a build-up of extracellular acetate and the upregulation of ACS enzyme activity. However, it is unclear whether this mechanism of acetyl-CoA transport occurs when the PDH bypass is intact.

1.7 Acetyl-CoA as a fuel gauge: linking metabolism and gene expression

Alongside its role in central metabolism, one of the major functions of acetyl-CoA is to act as an acetyl group donor for acetylation reactions (Cai and Tu, 2011). Acetylation reactions are very extensive, with approximately 50% of *S. cerevisiae* proteins undergoing irreversible N-α acetylation during translation. Similarly, reversible acetylation of lysine residues is a ubiquitous and ancient PTM, conserved from prokaryotes to humans, which targets histones and multitudes of non-histone proteins, thereby modulating gene expression, DNA repair, cell cycle progression, and many other processes. (Cai and Tu, 2011; Choudhary et al., 2009; Galdieri et al., 2014). The reversible nature of these modifications means that they can be altered dynamically according to the cellular levels of acetyl-CoA, which is in turn determined by the cellular metabolic state. In fact, the half-life of the acetyl-lysine modification is typically only 30 min – 2 h, making it unclear whether lysine acetylations are truly "epigenetic" at all as regards their heritability (Barnes et al., 2019). However, it is just this – the short-term, reversible nature of lysine acetylation – which renders acetyl-CoA capable of acting as a kind of fuel gauge, allowing cells to determine whether their metabolic state is appropriate to conduct a given process.

1.7.1 The extent and effects of acetylation reactions

The acetylation of histones can elicit changes in all DNA-based processes. Each of the core histones (H2A, H2B, H3 and H4) contain a globular core domain and a N-terminal tail which projects outward from the nucleosomes, both of which contain numerous lysine residues. Being positively charged, these lysine residues interact with the negatively charged sugar-phosphate backbone of DNA, thereby facilitating chromatin compaction (Barnes et al., 2019; Peng et al., 2008). However, acetylation neutralises their positive charge, lessening the degree of compaction and facilitating the access of the transcriptional machinery to DNA while also providing binding sites to proteins, such as bromodomain-containing proteins, which can further alter chromatin structure. Consequently, on the genome-scale, lysine acetylation of promoter histones is correlated with active transcription (Pokholok et al., 2005) – though a subset of genes, the histone hypoacetylation-activated genes (HHAAGs), deviate from this

general pattern. The HHAAGs, which include *ACS1* (see section 1.6.1), are expressed only when the levels of acetyl-CoA are low, and histones are generally hypoacetylated. Accordingly, these genes are expressed during the diauxic shift and throughout SP, when the levels of acetyl-CoA and histone acetylation decline (Cai et al., 2011; Mehrotra et al., 2014; Sandmeier et al., 2002).

Acetylation is not restricted to histones, however. Studies utilising high resolution mass spectrometry have identified thousands of non-histone proteins with acetylated lysine residues. These proteins participate in diverse cellular processes such as DNA repair, cell cycle progression, nuclear transport, and, interestingly, other PTMs. Choudhary et al. (2009) identified acetylation sites on many KATs, methyltransferases and nuclear ubiquitin-modifying enzymes (the "writers" of methylation and ubiquitination, respectively), and on many chromatin remodelling complexes including the SWI/SNF complex. Thus, lysine acetylation is involved both in the regulation of itself, and in the crosstalk between different types of PTM. This is logical as PTMs acting on lysine residues can compete with one another (Barnes et al., 2019), i.e. a given lysine residue cannot both be acetylated and methylated, for example, and as such altered acetylation patterns could signal an opportunity, or lack thereof, for another PTM to take place.

1.7.2 The regulation of lysine acetylation

Lysine acetylation is controlled enzymatically by KATs and KDACs, the "writers" and "erasers" (see section 1.5), respectively, of lysine acetylation. KATs catalyse the transfer of the acetyl group of acetyl-CoA onto the ε-amino group of lysine residues, and KDACs catalyse the hydrolysis of the amide linkage connecting the ε-amino group to the acetyl group, yielding acetate (Galdieri et al., 2014). The majority of KATs and KDACs function as multi-subunit complexes, though there are exceptions and some KATs, such as Gcn5p, can function alone and as a part of multi-subunit complexes (Galdieri et al., 2014; Gaupel et al., 2015; Sternglanz and Schindelin, 1999). These complexes, numbering approximately 20 in *S. cerevisiae*, have partially overlapping substrate specificity. For example, Gcn5p acetylates H3 lysine (K) 4, K9, K18 and K23, as does the KAT subunit Rpd3p; however, Rpd3p can acetylate several lysine residues on histone H4, whereas Gcn5p cannot. In large part due to their overlapping substrate specificity, KATs and KDACs tend to be dispensable for cellular viability, with

the exception of Esa1p (Galdieri et al., 2014; Smith et al., 1998). However, while they are rarely essential, KATs and KDACs can be crucial for maintaining optimal cellular health. The tetrameric KDAC Hda1C, for example, which is made up of two heterodimeric structural subunits, Hda2p and Hda3p, and a catalytic homodimer of Hda1p, preferentially deacetylates histones H2B and H3 and interacts with the transcriptional repressor Tup1p, affecting diverse cellular pathways such as mating, osmotic stress, oxygen consumption and glucose utilisation (Ha et al., 2019; Wu et al., 2001).

Mention the RTG here.

As mentioned in section 1.5, an additional layer of acetylation regulation is provided by the availability of its metabolic cofactor, acetyl-CoA. While the compartmentalisation of acetyl-CoA metabolism and the specificity of certain KATs and KDACs complicates the matter significantly, disruptions to acetyl-CoA metabolism are highly likely to elicit changes in overall lysine acetylation. For example, previous research has demonstrated that reducing Acs2p activity leads to severe histone hypoacetylation at H2B K16, H3 K9, H4 K5, and H4 K16, in yeast cells exponentially growing on glucose (Takahashi et al., 2006). Conversely, the aforementioned research of Eisenberg et al. (2014) demonstrated that impairing mitochondrial acetyl-CoA biosynthesis by deleting *MPC1* or *ACH1* resulted in the accumulation of extracellular acetate, the hyperactivation of ACS activity and an increase in overall lysine acetylation. The plasticity of lysine acetylation to cellular acetyl-CoA levels is even more strongly illustrated in the case of mitochondrial proteins, which are acetylated at high frequency. In humans, the acetylation of mitochondrial proteins is regulated in part by the sirtuin-class deacetylase 3 (SIRT3), but so far, no mitochondrially-active KAT complex has been identified. There is strong evidence, however, that in mitochondria there exists widespread nonenzymatic acetylation, facilitated by the high concentration of acetyl-CoA (see section 1.6.2) and the highly alkaline conditions of the mitochondrial matrix (Weinert et al., 2014).

From this it follows that broad changes in lysine acetylation can be induced by fluctuations in the levels of acetyl-CoA. However, the influence of KATs and KDACs mean that such fluctuations do not always influence lysine acetylation uniformly. For example, while Eisenberg et al. 2014 found an increase in overall lysine acetylation, and elevated H3 acetylation in Δ*mpc1* and Δ*ach1* cells, the level of acetylated

H4 was unchanged relative to WT cells. To complicate matters further, the interrelationships between acetylated lysine residues are quite complex. Within a given genomic locus, the acetylation state of lysine residues can be both positively and negatively correlated with one another. For instance, Kurdistani et al. (2004) found that H4 K18ac and K12ac are strongly positively correlated, but H4 K16ac and H3 K18ac are strongly negatively correlated. In addition, Kurdistani et al. (2004) discovered that correlations between individual acetylated lysine residues differ between open-reading frames (ORFs) and intergenic regions (IGRs). Therefore, lysine acetylation appears to be at least partially regulated by the acetylation state of other lysine residues.

Despite these particularities, there is strong evidence that lysine acetylation is regulated by mitochondrial function. The mitochondria can regulate lysine acetylation directly via the retrograde response (RTG) pathway, a cytoplasmic mitochondria-to-nucleus signalling pathway responsible for inducing a transcriptional program to adapt metabolism to compromised respiratory capacity (Andréasson et al., 2019). The retrograde response pathway is controlled primarily by three proteins, a heterodimeric complex of Rtg1p and Rtg3p, and Rtg2p, a sensor of mitochondrial dysfunction. Rtg2p induces the translocation of Rtg1p-Rtg3p to the nucleus by sequestering Mks1p, the major negative regulator of the RTG pathway. While the dynamics of their association are still under investigation, Rtg2p binds exclusively to hypophosphorylated Mks1p, thereby allowing their association to be governed in part by the cellular levels of ATP. Outside of its role as a positive regulator of Rtg1p-Rtg3p, Rtg2p forms part of the SAGA-like (SLIK) KAT complex, and is necessary for its full catalytic activity (Guaragnella et al., 2018; Liu and Butow, 2006; Pray-Grant et al., 2002; Trendeleva and Zvyagilskaya, 2018). SLIK binds to the promoters of RTG-target genes, thus linking mitochondrial dysfunction directly with transcriptional activation via the promotion of histone acetylation at specific target genes. In contrast, mitochondrial function also indirectly influences broad-scale lysine acetylation via its roles in the provision of acetyl-CoA. During growth in glucose-rich media, oxidative phosphorylation is repressed, and cells maintain similar levels of acetyl-CoA and histone acetylation regardless of their respiratory competence. Conversely, in SP, the level of acetylated H4 is significantly lower in p^0 cells (cells lacking mtDNA) when compared to that of p^+ cells. This is accompanied in p^0 cells by a large

drop in the cellular concentrations of ATP, acetyl-CoA and the carbohydrate storage molecules trehalose and glycogen (Enjalbert et al., 2000; Friis et al., 2014). Friis *et al.* (2014) demonstrated that H4 acetylation in p^0 cells could be rescued by glucose alone – moreover, glucose was shown to restore H4 acetylation by rectifying the energetic deficit of p^0 cells and not by any uptake-dependent signalling, as supplementation with 2-deoxyglucose, a glucose analogue which cannot be fully metabolised, did not restore H4 acetylation.

1.8 Study objectives

This study aimed to deepen our knowledge of the relationship between mitochondrial dysfunction and the epigenetic status of chromatin, and to explore the knock-on effects this relationship has on cellular health. Scientists are only beginning to explore these areas, and the research outlined here will contribute to this new and ongoing project. This study has the potential to significantly boost our understanding of how mitochondrial dysfunction impacts cellular health, and why similar perturbations of mitochondrial function are associated with ageing, neurodegenerative diseases, and other serious illnesses. Previous models have proved ineffective at explaining these associations (see sections 1.3-1.4), so perhaps a new model, as explored in this study, will prove more useful in understanding, and eventually treating, these conditions.

Specifically, the aims of this study were to further investigate the mechanism of Yno1p-mediated ROS production in Δ*cox4* cells. The research presented here is focused on investigating the relationship between the loss of Cox4p, acetyl-CoA metabolism, and ROS accumulation. The findings of Friis et al. (2014; see the preceding section) were used to adapt a working model for the relationship between the loss of Cox4p and Yno1p-medaited ROS production. In this model, it was assumed that CIV dysfunction could impair acetyl-CoA synthesis in many ways, but perhaps the simplest mechanism through which it could accomplish this would be an ATP deficit commencing at SP. An ATP deficit would likely result in decreased flux through the PDH-bypass (see section 1.6.1), resulting in a smaller pool of nucleocytosolic acetyl-CoA. Since histone acetylation is governed by the availability of acetyl-CoA (see sections 1.7.2 and 1.7.3), a reduction in the levels of acetyl-CoA would likely cause histone

hypoacetylation. Consequently, histone hypoacetylation was hypothesised to cause the dissociation of Bdf1p from said hypoacetylated histones, inducing its association with the mitochondria and thereby eliciting Ras2p-dependent ROS accumulation via Yno1p.

These aims were investigated by focusing on the following areas:

1. Analysis of the levels of acetyl-CoA in stationary-phase Δ*cox4* cells
2. Analysis of ROS accumulation in acetyl-CoA, KAT and KDAC mutants
3. Analysis of the relationship between loss of Cox4p, gene expression and histone acetylation sites
4. Examination of the effect of *ACS2* overexpression on ROS accumulation in Δ*cox4* cells
5. Examination of the effect of exogenous acetate on ROS accumulation in Δ*cox4* cells

2. Materials and Methods

2. 1 Yeast strains and growth conditions

Unless stated otherwise, all experiments were carried out in *S. cerevisiae* strain BY4741 and respective mutant strains as listed in Table 2.1. Overnight cultures were grown in YPD medium (1% yeast extract [Difco], 2% bactopeptone [Difco], 2% glucose [Fisher Scientific]) in a 30ºC rotary incubator set to rotate at 180 RPM. All strains used in this study were maintained on YPD plates (as above with 20% Oxoid Technical Agar No. 3). pAG306 transformants were initially maintained on SD-URA plates (0.675% Yeast Nitrogen Base w/o Amino Acids [Formedium], 0.193% synthetic dropout Kaiser media w/o uracil [Formedium], 2% glucose [Fisher Scientific], 20% Oxoid Technical Agar No. 3) before being transferred to YPD plates (see section 2.3.1).

Table 2.1 Origin and genotype of *S. cerevisiae* strains used in this study.

Strain	Genotype	Origin
WT (BY4741)	Mata *his3*Δ1 *leu2*Δ *met15*Δ *ura3*Δ	Horizon Discovery™ Yeast Knockout Collection
Δ*cox4*	BY4741 Δ*cox4*::*KanMX*	Leadsham and Gourlay, 2010
Tet-WT	URA3::CMV-tTA MATa his3-1 leu2-0 met15-0	Horizon Discovery™ Yeast Tet-Promoters Hughes
Tet-ACS2	pACS2::kanR-tet07-TATA URA3::CMV-tTA MATa his3-1 leu2-0 met15-0	Horizon Discovery™ Yeast Tet-Promoters Hughes
Δ*hda2*	BY4741 Δ*hda2*::*KanMX*	Horizon Discovery™ Yeast Knockout Collection
Δ*acs1*	BY4741 Δ*acs1*::*KanMX*	Horizon Discovery™ Yeast Knockout Collection
Δ*ngg1*	BY4741 Δ*ngg1*:: *KanMX*	Horizon Discovery™ Yeast Knockout Collection

Δ*hda2*	BY4741 Δ*hda2*:: *KanMX*	Horizon Discovery™ Yeast Knockout Collection
Δ*hos1*	BY4741 Δ*hos1*:: *KanMX*	Horizon Discovery™ Yeast Knockout Collection
Δ*hda3*	BY4741 Δ*hda3*:: *KanMX*	Horizon Discovery™ Yeast Knockout Collection
Δ*hda1*	BY4741 Δ*hda1*::*KanMX*	Horizon Discovery™ Yeast Knockout Collection
Δ*hos3*	BY4741 Δ*hos3*::*KanMX*	Horizon Discovery™ Yeast Knockout Collection
Δ*sap30*	BY4741 Δ*sap30*::*KanMX*	Horizon Discovery™ Yeast Knockout Collection
Δ*rpd3*	BY4741 Δ*rpd3*::*KanMX*	Horizon Discovery™ Yeast Knockout Collection
Δ*hos2*	BY4741 Δ*hos2*::*KanMX*	Horizon Discovery™ Yeast Knockout Collection
Δ*sin3*	BY4741 Δ*sin3*::*KanMX*	Horizon Discovery™ Yeast Knockout Collection
Δ*dep1*	BY4741 Δ*dep1*::*KanMX*	Horizon Discovery™ Yeast Knockout Collection
Δ*sds3*	BY4741 Δ*sds3*::*KanMX*	Horizon Discovery™ Yeast Knockout Collection
Δ*rxt2*	BY4741 Δ*rxt2*::*KanMX*	Horizon Discovery™ Yeast Knockout Collection
Δ*hat1*	BY4741 Δ*hat1*::*KanMX*	Horizon Discovery™ Yeast Knockout Collection
Δ*hat2*	BY4741 Δ*hat2*::*KanMX*	Horizon Discovery™ Yeast Knockout Collection
Δ*hpa2*	BY4741 Δ*hpa2*::*KanMX*	Horizon Discovery™ Yeast Knockout Collection

Δ*sas2*	BY4741 Δ*sas2*::*KanMX*	Horizon Discovery™ Yeast Knockout Collection
Δ*sas3*	BY4741 Δ*sas3*::*KanMX*	Horizon Discovery™ Yeast Knockout Collection
Δ*gcn5*	BY4741 Δ*gcn5*::*KanMX*	Horizon Discovery™ Yeast Knockout Collection
Δ*yng1*	BY4741 Δ*yng1*::*KanMX*	Horizon Discovery™ Yeast Knockout Collection
Δ*rtt109*	BY4741 Δ*rtt109*: *KanMX*	Horizon Discovery™ Yeast Knockout Collection
Δ*ahc1*	BY4741 Δ *ahc1*::*KanMX*	Horizon Discovery™ Yeast Knockout Collection
Δ*hpa3*	BY4741 Δ*hpa3*::*KanMX*	Horizon Discovery™ Yeast Knockout Collection
Δ*sas5*	BY4741 Δ*hfi1*::*KanMX*	Horizon Discovery™ Yeast Knockout Collection
Δ*hfi1*	BY4741 Δ*hfi1*::*KanMX*	Horizon Discovery™ Yeast Knockout Collection
Δ*fun19*	BY4741 Δ*fun19*::*KanMX*	Horizon Discovery™ Yeast Knockout Collection
Δ*nat4*	BY4741 Δ*nat4*::*KanMX*	Horizon Discovery™ Yeast Knockout Collection
Δ*yor338w*	BY4741 Δ*yor338w*::*KanMX*	Horizon Discovery™ Yeast Knockout Collection
Δ*sgf73*	BY4741 Δ*sgf73*::*KanMX*	Horizon Discovery™ Yeast Knockout Collection
Δ*elp3*	BY4741 Δ*elp3*::*KanMX*	Horizon Discovery™ Yeast Knockout Collection
Δ*ada2*	BY4741 Δ*ada2*::*KanMX*	Horizon Discovery™ Yeast Knockout Collection

Δ*rtg2*	BY4741 Δ*rtg2*::*KanMX*	Horizon Discovery™ Yeast Knockout Collection
Δ*mks1*	BY4741 Δ*mks1*::*KanMX*	Horizon Discovery™ Yeast Knockout Collection
Δ*tup1*	BY4741 Δ*tup1*::*KanMX*	Horizon Discovery™ Yeast Knockout Collection
Δ*ach1*	BY4741 Δ*ach1*::*KanMX*	Horizon Discovery™ Yeast Knockout Collection
Δ*mpc1*	BY4741 Δ*mpc1*::*KanMX*	Horizon Discovery™ Yeast Knockout Collection

2.2 Plasmids

2.2.1 Plasmid growth and extraction

DH5-α (F$^-$ φ80*lac*ZΔM15 Δ(*lac*ZYA-*arg*F)U169 *rec*A1 *end*A1 *hsd*R17(r_K^-, m_K^+) *pho*A *sup*E44 λ$^-$ *thi*-1 *gyr*A96 *rel*A1) or DB3.1 (F$^-$*mcr*A Δ(*mrr*-*hsd*RMS-*mcr*BC) Φ80*lac*ZΔM15 Δ*lac*X74 *rec*A1 *ara*Δ139 Δ(*ara*-*leu*)7697 *gal*U *gal*K *rps*L (Str^R) *end*A1 *nup*G *fhu*A::*IS2*) *Escherichia coli* were grown to obtain all plasmids used in this study as listed in Table 2.2. Cells were inoculated with plasmid and incubated in 3 ml LB media with appropriate antibiotic for 24 h in a 37^{o}C rotary incubator set to rotate at 180 RPM. Plasmids were then isolated using a QIAPrep Spin Miniprep kit according to the manufacturer's instructions. All expression vectors contained the *URA3* selection marker for growth in *S. cerevisiae*.

Table 2.2 Details of plasmids used in this study

Plasmid	Summary	Antibiotic for growth in *E. coli*	Source
pAG306	Destination vector with *ccdB* site and GPD promoter. Can integrate into *S. cerevisiae* chromosome 1 following NotI digestion.	Ampicillin (1 mg/ml)	pAG306-GPD-ccdB chr I was a gift from Dan Gottschling (Addgene plasmid # 41894 ; http://n2t.net/addgene:41894 ; RRID:Addgene_41894)
pDONR221-*ACS2*	Entry vector containing *ACS2*. Lacks a *ccdB* site. Grown in DH5-α *E. coli*.	Kanamycin (50 µg/ml)	Purchased from DNASU plasmid repository
pAG306-*ACS2*	Expression vector containing *ACS2* and a GPD promoter. Lacks *ccdB* site. Can integrate into *S. cerevisiae* chromosome 1 following NotI digestion. Grown in DH5-α *E. coli*.	Ampicillin (1 mg/ml)	This study.

2.2.2 pAG306-*ACS2* overexpression plasmid construction

Overexpression of *ACS2* was accomplished using the pAG306 expression vector (Table 2.2), which can integrate into a region of *S. cerevisiae* chromosome 1 after NotI digestion. pAG306-*ACS2* was constructed using ThermoFisher's gateway cloning system according to their instructions (ThermoFisher, n.d.). Briefly, pAG306-*ACS2* was prepared by integrating *ACS2* into the pAG306 integration vector from a pDONR221-*ACS2* entry clone via an LR reaction.

Proper integration of *ACS2* into the pAG306 vector backbone was confirmed using the restriction enzyme NotI (Promega). The reaction was set up according to the manufacturer's guidelines and

incubated at 37°C for 4 h. NotI-digest products were analysed using agarose gel electrophoresis as outlined in section 2.4.

2.3 Strain transformation

2.3.1 pAG306- transformations

All plasmid transformations were performed using a modified version of a previous protocol (Gietz and Woods, 2002). pAG306-*ACS2* transformations were conducted using the linear DNA fragments produced by NotI digestion (see section 2.2.2). 3 ml overnight cultures were inoculated in 20 ml fresh YPD. Cells were grown to log-phase (4-5 h), harvested by centrifugation at 4000 RPM for 5 min, and resuspended in 400 µl sterile MQ water. 100 µl aliquots were centrifuged at 10000 RPM for 30 sec, before being resuspended in 360 µl of transformation master mixture (Table 2.3). The reaction mixtures were incubated at 42°C for 40 min. After 40 min of incubation, the reaction mixtures were centrifuged at 10000 RPM, resuspended in 200 µl sterile MQ water, and pipetted onto SD-URA plates. The plates were incubated at 30°C for three days, and any colonies were streaked out on to fresh SD-URA plates. Colony PCR was used to confirm successful transformants (see section 2.3.2), and any successful transformants were streaked out and maintained on YPD plates thereafter.

Table 2.3 Components of the transformation master mix

Component	Volume (µL)
Polyethylene glycol (PEG; 50% w/v)	240
LiAc (1 M)	36
ssDNA (10 mg ml^{-1}; boiled)	10
Sterile MQ water	70
Plasmid (150 ng/µl)	4

2.3.2 Colony PCR to confirm genomic integration of pAG306 plasmids

Successful pAG306- transformations were confirmed using colony PCR. DNA extracts were prepared by first resuspending a small amount of each transformant colony in 40 µl 20 mM H_2O_2. The

resuspended cells were then boiled at 95ºC for 10 min, cooled on ice for 10 min, and centrifuged at 4000 RPM for 5 min. 1 µL supernatant was then added to PCR reactions set up according to Table 2.4. PCR reactions were incubated in a Biorad C1000 thermal cycler according to Table 2.5. PCR products were analysed via agarose gel electrophoresis as outlined in section 2.4. Alongside transformant colonies, PCR reactions were set up and analysed as above using pAG306-empty vector WT transformants, and with untransformed WT or Δ*cox4* cells, which acted as positive and negative controls, respectively.

Table 2.4 PCR reactions for confirming successful pAG306-*ACS2* transformants. Reagent quantities for 20 µl reactions are shown.

Component	Volume (µl)
PCRBio 2X TaqMix Red	10
10 µM forward primer (ATAATACCGCGCCACATAGC)	2
10 µM reverse primer (GAAGGATAGTTCGAAGCTCGC)	2
Extracted DNA (100 ng/µl)	1
Sterile MQ H_2O	5

Table 2.5 Thermal cycler settings for confirming successful pAG306-*ACS2* transformants. Denature to extend steps were repeated for 30 cycles.

	pAG306-*ACS2* (PCRBio 2X TaqMix Red)	
Step	Temperature (ºC)	Time (s)
Initial denature	95	60
Denature	95	15
Anneal	60	15
Extend	72	15
Final extend	72	600

2.4 Agarose gel electrophoresis

DNA samples were analysed using 0.8% w/v agarose gels (with 1X TAE [1 mM EDTA, 0.114 % [v/v] acetic acid, 40 mM Tris-base] as solvent) containing 0.4 µg/ml ethidium bromide. Gels were immersed in 1 X TAE in a 50 ml gel tank, and additional ethidium bromide was added to the anode-end of the tank to a final concentration of 1 µg/ml. Each sample well was filled with 5 µl sample DNA (150 ng/µl) and 1 µl 6X orange G (NEB). Each ladder well contained 1 µl 1kb+ DNA ladder (Invitrogen), 4 µl MQ H_2O and 1 µl 6X orange G. Gels were run at 90-120V for 30 min and were visualised using a SynGene GBox XX6 imaging system and captured using GeneSys imaging software.

2.5 Measurement of acetyl-CoA levels in *S. cerevisiae* cells

Acetyl-CoA was extracted from cells in accordance with a modified version of a previous protocol (Liu et al., 2017). 5 ml overnight cultures were inoculated to $A_{600} \approx 0.1$ in 50 ml YPD and incubated in a 30°C rotary incubator set to rotate at 180 RPM. Cells were harvested after 24h of growth by centrifugation at 4000 RPM for 15 min, weighed, and resuspended in 10 ml -80°C methanol to quench cellular metabolism. Subsequently, cells were centrifuged at 4000 RPM for 15 min, resuspended in 2 ml boiling ethanol, and vortexed with glass beads for 5 min to release intracellular metabolites. 1ml supernatant was vacuum dried after centrifugation at 4000 RPM for 1 min, and the resulting lyophilised powder was stored at -20°C until use.

Acetyl-CoA extracts were resuspended in 100 µl sterile MQ water and analysed using the PicoProbe™ acetyl-CoA fluorometric assay kit (abcam®) according to the manufacturer's instructions. Fluorescence was measured using the low concentration (0-100 pmol acetyl-CoA) standards. Fluorescence readings were standardised by the wet weight of harvested cell pellets. Acetyl-CoA levels were analysed using at least three biological replicates per sample.

2.6 Cellular H_2O_2 accumulation

Cellular H_2O_2 levels were measured using the cell-permeant fluorescent indicator dye H_2DCF-DA, which is converted to the highly fluorescent 2',7'-dichlorofluorescein following cleavage by intracellular esterases and subsequent oxidation. This fluorescent signal can then be detected in individual cells using flow cytometry.

Overnight cultures were inoculated to $A_{600} \approx 0.1$ in YPD and incubated with H_2DCF-DA (final concentration 5 µg ml^{-1}) for 24h in a BMG LabTech SPECTROstar nano plate reader according to section 2.7. WT and Δ*cox4* strains were included with each experiment to normalise the data. Growth assays were conducted simultaneously to ensure all strains were in SP during ROS measurements. ROS accumulation was analysed in triplicate, with an additional culture per strain acting as a negative control lacking the ROS dye H_2DCF-DA. After 24h of growth, 2.5 µl of each culture was suspended in 500 µl PBS (pH 7.4), supplemented with the necrosis indicator dye propidium iodide (PI; final concentration 1 µg/ml), and assessed for ROS accumulation and necrosis using a BD Accuri™ C6 Plus flow cytometer. The use of both H_2DCF-DA and PI simultaneously allows for the measurement of H_2O_2 accumulation in live cells, which display low PI fluorescence, as opposed to dead or dying cells, which display high PI fluorescence. Unless stated otherwise, 10000 cells per sample were analysed. Cells were classified into one of four groups with reference to a highly PI-fluorescent positive control, made by heating a PI-stained WT sample at 80°C for 5 min (see Fig. 2.1 for details). The proportion of high ROS cells reported in this study corresponds to the proportion of cells in the lower right quadrant of Fig. 2.1.

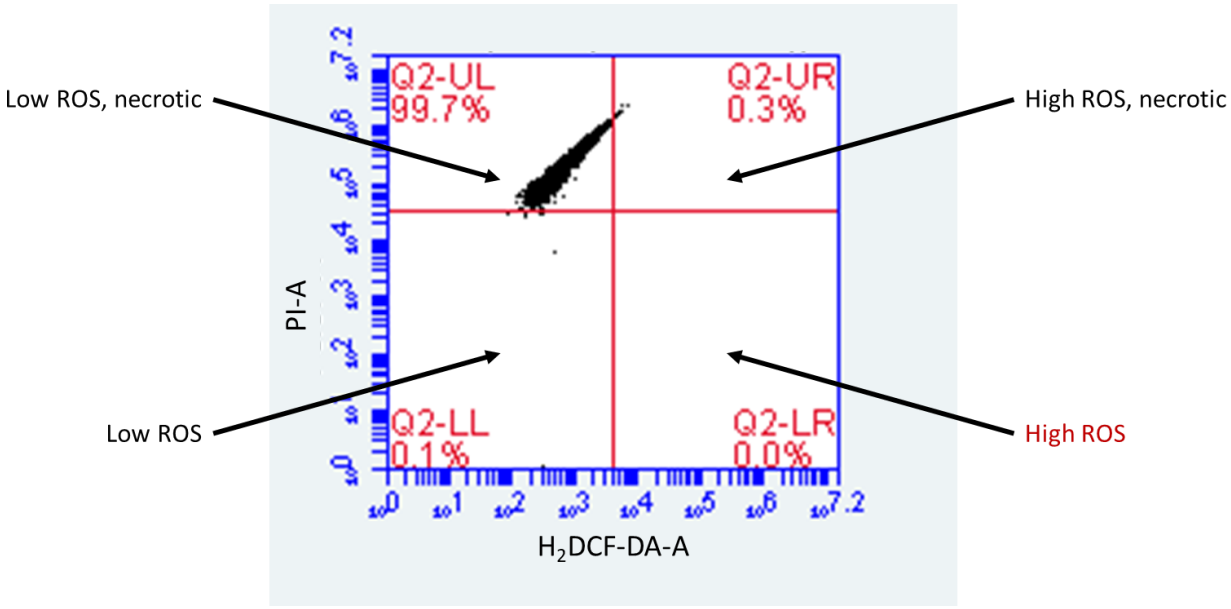

Fig. 2.1. Classification of cell types according to H_2DCF-DA and PI signal characteristics. Cells were classified using a quadrant placed around a positive control group of WT cells dyed with PI and heated at 80°C as outlined in section 2.6. Cells falling above the boundary of the PI signal threshold were classified as necrotic, and those falling above the boundary of the H_2DCF-DA signal were classified as high ROS. As such, ROS accumulation in live cells was measured as the proportion of cells occupying the lower (non-necrotic) right (high ROS) quadrant.

2.7 Yeast growth assays

Overnight cultures were inoculated to a starting A_{600} of 0.1 in fresh YPD prior to analysis. Growth assays were conducted in sterile Greiner 24-well plates, with at least three biological replicates per sample, in a BMG LabTech SPECTROstar nano plate reader. The instrument was set to shake the plate in a linear and double-orbital fashion according to Table 2.6 and measure the A_{600} every 360 seconds for at least 24h.

Table 2.6 BMG LabTech SPECTROstar nano instrument settings used in growth assays.

Setting	Value
Cycle time	360 sec
Shaking mode	8-minute orbital shake proceeded by double-orbital shaking
Shaking frequency	400 RPM
Temperature	30°C
Positioning delay	0.5 sec

2.8 Analysis of histone acetylation in *S. cerevisiae* genes

Gene expression data obtained from Leadsham and Gourlay (2010) or Ladurner et al. (2003) were used to identify genes showing differential expression in the absence of Cox4p or Bdf1p, respectively. These gene lists were split by cellular compartment using SGD GO-SLIM (https://www.yeastgenome.org/goSlimMapper) into genes encoding mitochondrial or non-mitochondrial proteins, and analysed using the Yeast Histone Modification Identifier (YHMI; http://cosbi4.ee.ncku.edu.tw/YHMI/; Fig. 2.2). The YHMI uses ChIP-chip/ChIP-seq datasets of 32 histone modifications (acetylation, methylation, phosphorylation, ubiquitination, and histone variants) and 83 chromatin regulators, all downloaded from the SGD (see supplementary Table 2 of Wu et al. 2018 for information about strain backgrounds and original data sources). The YHMI determines which genes from the *S. cerevisiae* genome contain a given histone modification, for example H3 K14ac, by extracting the maximum log_2-fold enrichment of that modification (log_2 (H3 K14ac/H3 here) from the corresponding ChIP-chip/ChIP-seq dataset. Subsequently, a gene is assumed to contain H3K14ac (or any other histone modification included in the YHMI) if log_2 (H3 K14ac/H3) ≥ *threshold*, which can be set manually by the user but in this study was left at the default value of 1 for all modifications. In contrast, the YHMI determines which genes contain binding sites for histone/chromatin regulators using the data of Venters et al. (2011), who identified interactions between chromatin regulators and genomic DNA under normal (25°C) and acute heat-shock (37°C) conditions using ChIP-chip. Using its lists of

S. cerevisiae genes which contain specific histone modifications and chromatin regulator binding sites, the YHMI examines the relative enrichment of modified histones in the promoters and coding regions of a user-defined list of input genes. In the text, if a list of genes is said to be enriched for a specific lysine modification, this means that said list contains a greater proportion of genes containing that lysine modification than occurs in the *S. cerevisiae* genome, as determined by the YHMI. This applies also for binding sites for histone/chromatin regulators. Put simply, a list of genes is said to be enriched for a particular lysine modification if:

$$\frac{[T]}{[R]} > \frac{[S]}{[F]}$$

Where [T] is the number of genes within a user-defined list of length [R] which contain that lysine modification, and [S] is the number of genes with that lysine modification within the list of all genes in the *S. cerevisiae* genome [F]. For more information see Wu et al. (2018).

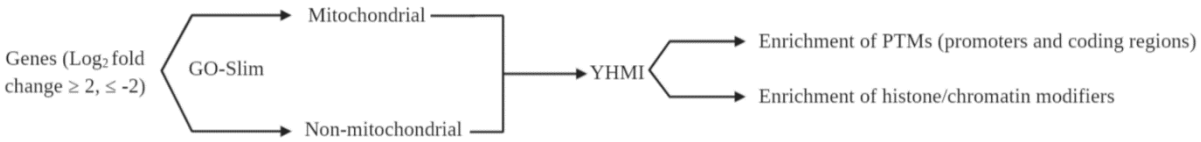

Fig. 2.2. Workflow for the analysis of histone lysine modifications in lists of genes showing differential expression in response to the loss of Cox4p or Bdf1p.

2.9 Peroxide sensitivity plating

Overnight cultures were diluted to $OD_{600} \approx 0.1$ in sterile MQ H_2O and 200 µl of the diluted cultures were pipetted into the left-most wells of a 32-well spotting plate according to Fig. 2.3. Five 10-fold dilutions of each culture were prepared by sequentially transferring 20 µl culture into 180 µl sterile MQ water. The cultures were then spotted using a 32-pin spotter in biological and technical duplicate onto YPD agar plates containing 2 mM H_2O_2. The plates were incubated for 72 h in a 30°C stationary incubator and peroxide sensitivity was checked visually by imaging each plate with a Samsung Galaxy A70 Smart Phone.

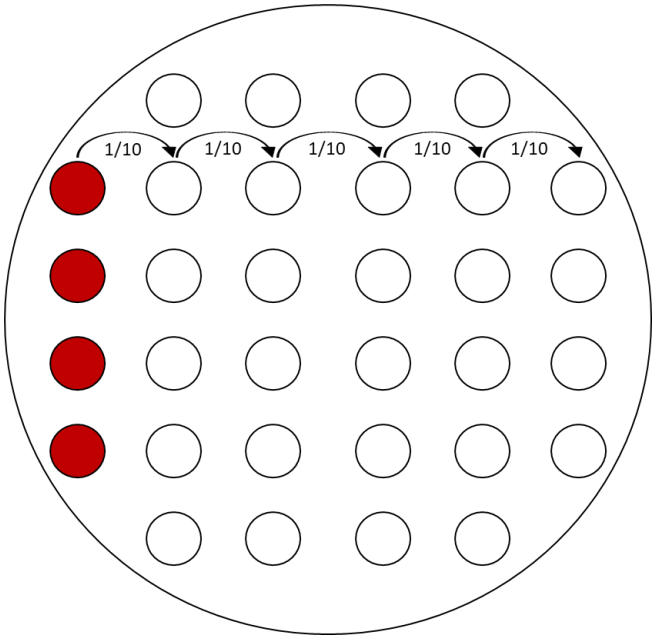

Fig. 2.3. Layout of the 32-well spotting plate used for assessing the sensitivity of *S. cerevisiae* strains to hydrogen peroxide. Cultures were diluted to $OD_{600} \approx 0.1$ in sterile MQ water and 200 µl of each diluted culture was transferred into the left-most wells of the plate (shown in red). Five ten-fold dilutions of each culture were prepared by sequentially diluting 20 µl culture in 180 µl sterile MQ water as shown by the arrows.

2.10 Statistical analysis

All data were analysed in R v. 3.6.2. All growth data were analysed using the *Summarizegrowth*() function of the *growthcurver* package for R V. 3.6.2. All area-under-the-curve (AUC) values reported in the text correspond to the auc_e (empirical AUC) parameter of the *growthcurver* package, a parameter calculated by summing the areas of trapeziums constructed using consecutive A_{600} values from time 0 to time *t* (Sprouffske and Wagner, 2016). Unless otherwise stated, all data were analysed using a one-way ANOVA. All figures were produced using the *ggplot2* package for R v. 3.6.2. All data presented in the text are means ± SEM.

3 Results

3.1 Δ*cox4* cells are depleted of acetyl-CoA and produce high levels of ROS

Previous research by Leadsham et al. (2013) demonstrated that Δ*cox4* cells accumulate very high levels of ROS during SP as a result of the activity of the NADPH oxidase Yno1p. Elevated ROS production by Yno1p is dependent on the association of Ras2p with the mitochondrial outer membrane, which is in turn dependent on the presence of the BET family protein Bdf1p (Fig. 1.2A). Interestingly, Bdf1p, like other BET family proteins, is usually bound to acetylated lysine residues in the tails of histones H3 and H4 (García-Oliver et al., 2017) but appears to relocate to the mitochondria in response to the loss of Cox4p (Leadsham and Gourlay, unpublished data). This points to a possible role of acetyl-CoA metabolism and histone hypoacetylation in Yno1p-mediated ROS accumulation in cells lacking CIV activity.

Considering this, I sought to determine whether ROS accumulation was related to perturbed acetyl-CoA metabolism in Δ*cox4* cells. To investigate this, I first examined the acetyl-CoA levels of WT and Δ*cox4* cells using the PicoProbe acetyl-CoA fluorometric assay kit, and measured ROS accumulation in live WT and Δ*cox4* cells via flow cytometry using the ROS dye H_2DCF-DA in conjunction with the necrosis-indicator dye PI. Interestingly, Δ*cox4* cells showed a moderate but non-significant reduction in acetyl-CoA levels when compared to WT cells (Fig. 3.1) and displayed greatly elevated levels of ROS (Fig. 3.2).

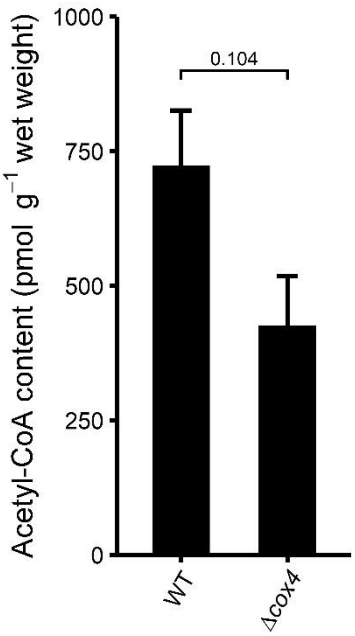

Fig. 3.1. Acetyl-CoA levels (standardised by the wet weight of pelleted cells; see section 2.6) in WT and Δ*cox4* cells. Acetyl-CoA was extracted from 50 mL YPD cultures and analysed using a PicoProbe™ fluorometric acetyl-CoA assay kit (abcam®) as described in section 2.6. Data are means ± SEM of at least three biological replicates. Annotations represent the results of a one-way ANOVA (P value).

A reduction in acetyl-CoA levels could be caused simply by an ATP deficit during SP but could also be influenced by changes in the expression of genes involved in acetyl-CoA metabolism. A search of the Gene Expression Omnibus (GEO) database uncovered unpublished time-course gene expression data from Δ*cox4* cells over 58 h of growth in YNB media (YNB + NH_4 + 2% glucose; cells grown in 50 ml cultures at 30ºC, 200 RPM; Gibney et al. 2019; https://www.ncbi.nlm.nih.gov/geo/query/acc.cgi?acc=GSE140353). My analysis of the Gibney et al. (2019) data clearly showed that *ACS2* underwent a marked downregulation in Δ*cox4* cells relative to their WT counterparts as they entered SP (Fig. 3.3; entry into SP was inferred from the de-repression of *ACS1* in WT and Δ*cox4* cells). Additionally, my analysis found that while *ACS1* and other targets of Cat8p, one of two transcription factors which control *ACS1* expression in *S. cerevisiae*, were de-repressed upon SP entry in Δ*cox4* cells, their expression did not seem to reach the same levels as they did in WT cells (Fig. 3.3). Considering the expression of *ACT1* did not appear to differ between WT and Δ*cox4* cells over the same time period (Fig. 3.3), these differences in the expression of *ACS2* and *ACS1* are unlikely to be due to a general transcriptional impairment in Δ*cox4* cells.

Taken together, the reductions in the levels of acetyl-CoA and the expression of *ACS1* and *ACS2* in Δ*cox4* cells warranted further investigation of the relationship between acetyl-CoA metabolism and ROS accumulation.

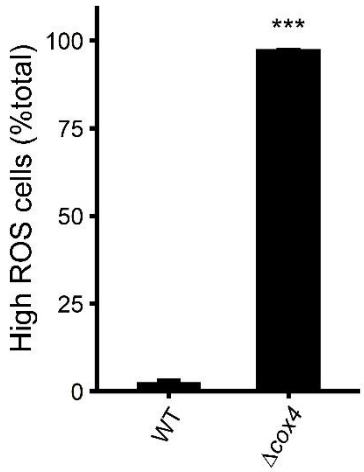

Fig. 3.2. ROS accumulation (proportion of total cells showing high ROS levels; calculated according to section 2.6 and Fig. 1) in WT and Δ*cox4* cells. ROS accumulation was measured in live cells using a BD Accuri™ C6 Plus flow cytometer with the ROS dye H_2DCF-DA in conjunction with the necrosis-indicator dye propidium iodide. 10000 cells per sample were analysed. The data are means ± SEM of three biological replicates. Annotations represent the results of a one-way ANOVA; ***, $P < 0.001$.

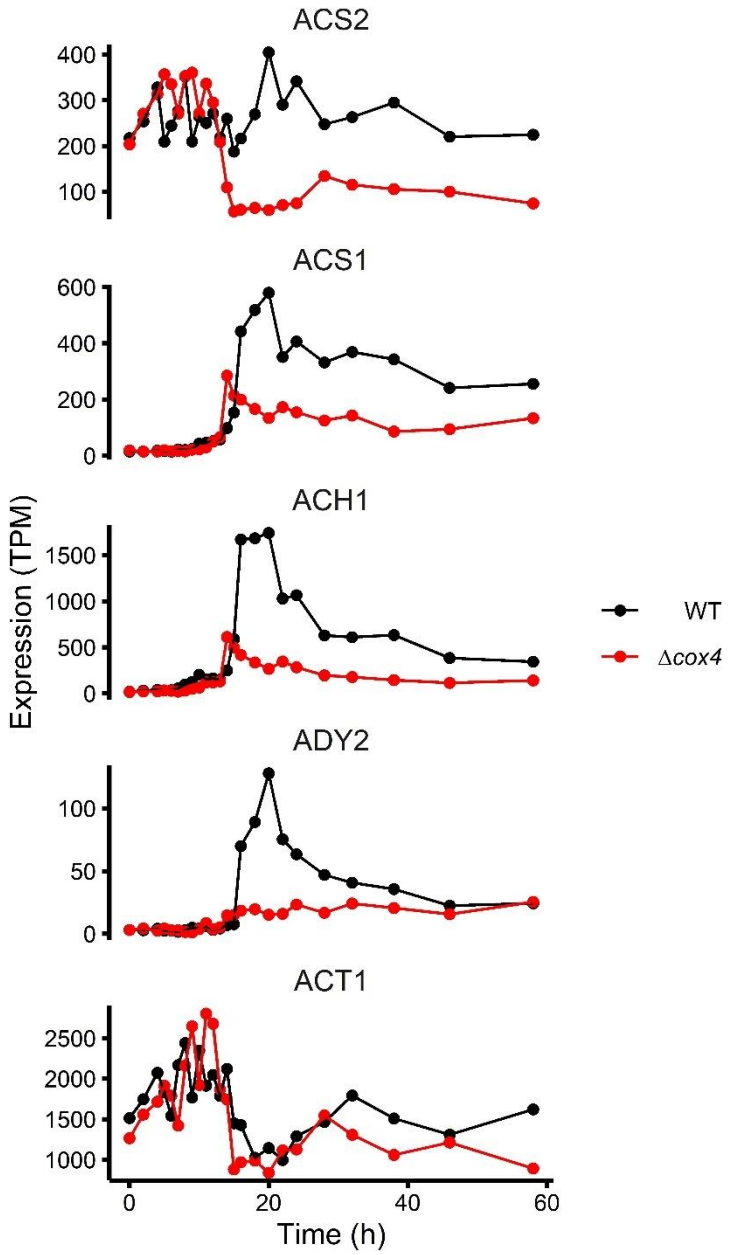

Fig. 3.3. Expression (transcripts per kilobase-million; TPM) of *ACS2*, *ACS1*, *ACH1*, *ADY2* and *ACT1* in WT (black lines) and Δcox4 (red lines) cells growing in YNB media (YNB + NH_4 + 2% glucose). *ACS2*, acetyl-CoA synthetase 2; *ACS1*, acetyl-CoA synthetase 1; *ACH1*, acetyl-CoA hydrolase/transferase; *ADY2*, acetate transporter. The data are single biological replicates.

3.2 ROS accumulation in acetyl-CoA, KAT and KDAC mutants

After observing that the absence of Cox4p leads to a reduction in the expression of *ACS1* and *ACS2* during SP, I sought to examine how perturbations to acetyl-CoA metabolism might impact ROS accumulation. As such, I examined how ROS accumulation was affected in cells lacking genes involved in acetyl-CoA metabolism, or genes encoding KAT or KDAC subunits (Table 3.1). ROS accumulation

was analysed via flow cytometry after 24h of growth in YPD media in a BMG LabTech SpectroStar Nano plate reader. The growth data collected from each strain were used to prepare growth curves which were then used to visually confirm each strain had entered SP. The AUC of each growth curve were compared using the *SummarizeGrowth()* function of the *growthcurver* package for R v. 3.6.2.

Table 3.1. Descriptions of the proteins absent in the acetyl-CoA, KAT, and KDAC mutants used in this study.

Protein	Description
Ach1p	Acetyl-CoA hydrolase/transferase. Localised to the mitochondria and cytosol (Galdieri et al., 2014).
Acs1p	Acetyl-CoA synthetase isoform. One of two active in *Saccharomyces cerevisiae*. Localised to the cytosol, mitochondria and possibly the peroxisomes (Chen et al., 2012; Galdieri et al., 2014; Huh et al., 2003; Takahashi et al., 2006; Van Den Berg and Steensma, 1995).
Ada2p	Chromatin-binding subunit of the SAGA, SLIK and ADA KAT complexes. Stimulates Gcn5p activity (Hoke et al., 2008).
Ahc1p	Subunit of the ADA KAT complex. Loss of Ahc1p disrupts the structural integrity of ADA (Eberharter et al., 1999). Not part of the closely related KAT complexes SAGA and SLIK (Lee et al., 2011).
Dep1p	Component of the Rpd3L KDAC complex (Carrozza et al., 2005).
Fun19p	Protein of unknown function and unknown cellular localisation
Gcn5p	Catalytic subunit of the SAGA, SLIK and ADA KAT complexes (Gaupel et al., 2015). Acting independently of KAT complexes, Gcn5p can acetylate free histones but not nucleosomes (Sternglanz and Schindelin, 1999).
Hat1p	Catalytic subunit of the HAT-B KAT complex (Poveda and Sendra, 2008).
Hat2p	Enzymatic activity stimulatory subunit of the HAT-B KAT complex (Poveda and Sendra, 2008).
Hda1p	Class II KDAC. Catalytic subunit of the Hda1C KAT complex (Ha et al., 2019).

Hda2p	Structural subunit of the Hda1C KAT complex. Structurally similar to Hda3p, with which it forms a dimer. Possesses an N-terminal DNA binding domain and a C-terminal coiled-coil domain. The latter domain is essential for the KDAC activity of Hda1C (Ha et al., 2019).
Hda3p	Structural subunit of the Hda1C KAT complex. Structurally similar to Hda2p, with which it forms a dimer. Possesses an N-terminal DNA binding domain and a C-terminal coiled-coil domain. The latter domain is essential for the KDAC activity of Hda1C (Ha et al., 2019).
Hfi1p	Component of the SAGA KAT complex. Involved in the maintenance of its structural integrity (Bhaumik and Green, 2002).
Hos1p	Class I KDAC. Has a specific role in regulating the anaphase-to-metaphase transition by deacetylating Smc3p, a subunit of the cohesin complex (Xiong et al., 2010).
Hos2p	Class I KDAC. Deacetylates histones in the coding regions of genes. Subunit of the Set3C complex and essential for its structural integrity (Mou et al., 2006).
Hos3p	Class I KDAC. Deletion results in little change in the global histone acetylation state. Insensitive to the KDAC inhibitor trichostatin A (Wang and Collins, 2014).
Hpa2p	KAT. Forms tetramer in the presence of acetyl-CoA. Acetylates both histones and non-histone proteins (Sampath et al., 2013).
Hpa3p	KAT. Acetylates histones and non-histone proteins (Sampath et al., 2013).
Mks1p	Negative regulator of the RTG pathway. Bound and sequestered by Rtg2p (Trendeleva and Zvyagilskaya, 2018).
Mpc1p	Subunit of mitochondrial pyruvate carrier (MPC), an inner-membrane-bound complex that facilitates pyruvate uptake into mitochondria (Galdieri et al., 2014).
Nat4p	Member of the N-terminal acetyltransferase family of enzymes. Acetylates the N-termini of histones H2A and H4 (Polevoda et al., 2009).

Ngg1p	Subunit of SAGA, SLIK and ADA KAT complexes. Facilitates nucleosome acetylation and expands the lysine specificity of Gcn5p (Balasubramanian et al., 2002).
Rpd3p	Subunit of the Rpd3L and Rpd3S KDAC complexes (Chen et al., 2012).
Rtg2p	Important component of the RTG pathway. Regulates the subcellular localisation of Rtg1p-Rtg2p by sequestering Mks1p. Subunit of SLIK KAT complex (Guaragnella et al., 2018; Jazwinski, 2013).
Rtt109p	KAT. Acetylates newly synthesised histone H3 (Cheng et al., 2016).
Rxt2p	Component of the Rpd3L KDAC complex (Carrozza et al., 2005).
Sap30p	Component of the Rpd3L KDAC complex (Carrozza et al., 2005).
Sas2p	Catalytic subunit of the SAS KAT complex (Pérez-Martínez et al., 2020).
Sas3p	Catalytic subunit of the NuA3 KAT complex (John et al., 2000).
Sas5p	Subunit of the SAS KAT complex. Required for the KAT activity of SAS. Stimulates activity of Sas2p (Pérez-Martínez et al., 2020; Sutton et al., 2003).
Sds3p	Component of the Rpd3L KDAC complex. Required for its structural integrity and catalytic activity (Lechner et al., 2000).
Sgf73p	Subunit of the deubiquitination module of the SAGA and SLIK KAT complexes (Lee et al., 2009).
Sin3p	Component of Rpd3L and Rpd3S KDAC complexes (Carrozza et al., 2005).
Tup1p	General repressor of transcription. When bound to its co-repressor Cyc8p, can recruit KDACs to regions of DNA and produce a repressive chromatin structure. Can recruit Hda1C to deacetylate histones H3/H2B in regions repressed by Tup1p-Cyc8p (Wu et al., 2001).
Yng1p	Subunit of the NuA3 KAT complex. Contains C-terminal plant homeodomain (PHD) finger domain which can interact with methylated H3 K4 (Howe et al., 2002; Martin et al., 2006).
Yor338w	Putative protein of unknown function. Paralog of Fun19p.

3.2.1 ROS production is not elevated in Δ*acs1*, Δ*mpc1* and Δ*ach1* cells

Interestingly, direct disruption of acetyl-CoA metabolism appeared to have little impact on ROS accumulation. Deletion of the mitochondrial pyruvate transporter *MPC1*, or deletion of the acetyl-CoA hydrolase/transferase *ACH1*, resulted in only small increases in ROS accumulation relative to WT cells (Fig. 3.4A), far lower than that observed in Δ*cox4* cells. Most unexpectedly, ROS accumulation in Δ*acs1* cells, which rely on the much lower affinity Acs2p for nucleocytosolic acetyl-CoA production, was not higher than that of WT cells (Fig. 3.4B).

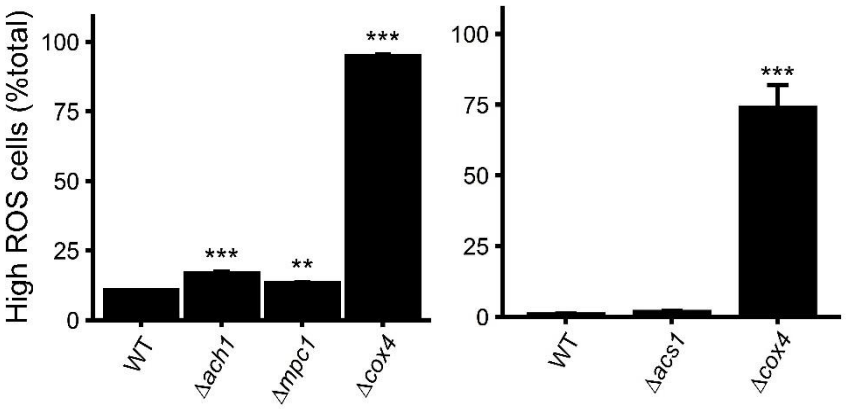

Fig. 3.4. ROS accumulation (proportion of total cells showing high ROS levels; calculated according to section 2.6 and Fig. 1) in WT and Δ*cox4* cells and in mutants with impaired mitochondrial (**A**) or cytosolic (**B**) acetyl-CoA metabolism. ROS accumulation was measured in live cells using a BD Accuri™ C6 Plus flow cytometer with the ROS dye H_2DCF-DA in conjunction with the necrosis-indicator dye propidium iodide. 10000 cells per sample were analysed. Data are means ± SEM of three biological replicates. Annotations represent the results of a one-way ANOVA relative to the WT strain; ***, $P < 0.001$; **, $P < 0.01$; *, $P < 0.05$.

3.2.2 Repression of *ACS2* induces necrosis but does not elevate ROS accumulation

Though the deletion of Acs1p elicited no increase in ROS accumulation, it was unclear whether a reduction in the activity of Acs2p, which as mentioned in section 1.6 differs in its localisation and activity patterns, would produce a similar outcome. Acs2p is required for growth on glucose, meaning ROS accumulation in an *ACS2* deletion strain could not be analysed. Instead, ROS accumulation was measured using cells with *ACS2* under the control of a doxycycline-repressible promoter (henceforth termed tet-*ACS2*, see Table 2.1 for genotypes of this strain and the tet-WT control). ROS levels in the tet-ACS2 strain were measured as in section 2.6 after 24h growth in YPD media supplemented with 1

ng/ml, 100 ng/ml, 1 µg/ml, or 10 µg/ml doxycycline. Only 1000 events were collected per sample due to low cell counts in cultures treated with high concentrations of doxycycline.

Doxycycline induced a concentration-dependent growth impairment in the tet-*ACS2* strain (Fig. 3.5B, C). In contrast, this did not occur in the tet-WT strain (Fig. 3.5A, C; strain x dose interaction, $F_{3, 24} = 208.56$, $P < 0.001$; two-way ANOVA with AUC data), indicating that the growth impairment was due to the concentration-dependent repression of *ACS2* by doxycycline and not by any direct toxic effects. Like the results obtained in Δ*acs1* cells, the repression of *ACS2* by doxycycline did not elicit any increase in ROS accumulation ($F_{3, 8} = 1.556$, $P = 0.274$; Table 3.2), with the 10 µg/ml doxycycline treatment only inducing high levels of ROS in 0.933 ± 0.133 % of tet-*ACS2*. However, doxycycline did induce necrosis in a concentration-dependent manner, with almost 80% of tet-*ACS2* cells treated with 10 µg/ml doxycycline staining PI-positive (Fig. 3.6). Again, this did not occur in tet-WT cells (strain x dose interaction, $F_{3, 16} = 182.92$, $P < 0.001$; two-way ANOVA), indicating that the repression of *ACS2* induces necrosis in glucose-rich media.

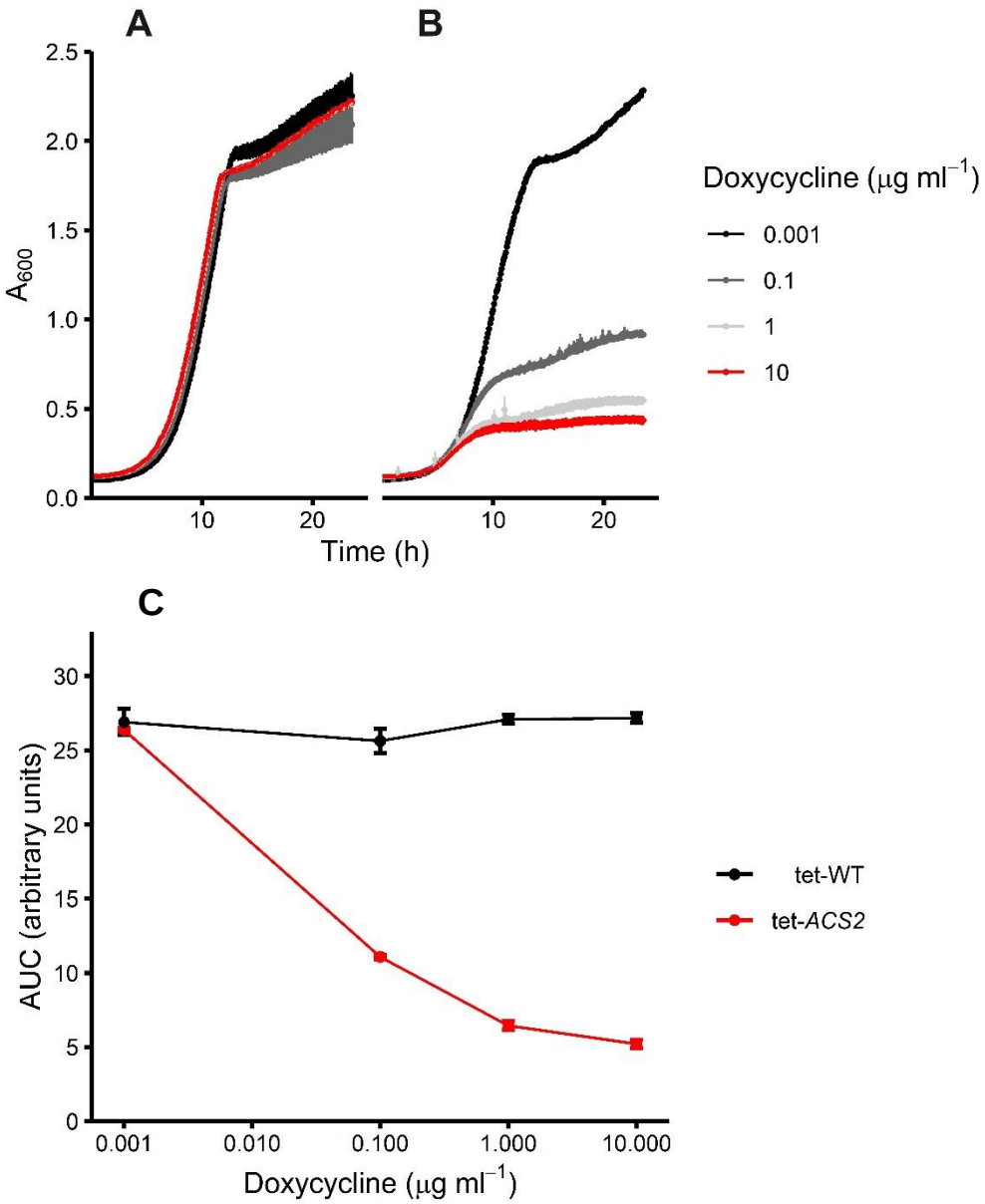

Fig. 3.5. Growth characteristics of tet-WT and tet-*ACS2* cells incubated with increasing concentrations of doxycycline. **A, B,** growth (absorbance at 600 nm) of tet-WT (**A**) and tet-*ACS2* (**B**) cultures incubated with either 1 ng/ml (black line), 100 ng/ml (dark grey line), 1 µg/ml (light grey line) or 10 µg/ml (red line) doxycycline. **C,** Area under the curve (AUC) for the growth data presented in **A** and **B** in the tet-WT (black line) and tet-*ACS2* (red line) cultures. All data are means ± SEM of at least three biological replicates.

Table 3.2. ROS accumulation in tet-WT and tet-*ACS2* cells incubated for 24h in YPD media supplemented with increasing concentrations of doxycycline. ROS accumulation was measured in live cells using a BD Accuri™ C6 Plus flow cytometer with the ROS dye H_2DCF-DA and the necrosis-indicator dye propidium iodide. 1000 cells per sample were analysed. Data are means ± SEM of three biological replicates.

Strain	[Doxycycline] (µg /ml)	High ROS cells (% total; mean ± SEM)
tet-WT	0.001	0.125 ± 0.025
	0.1	0.073 ± 0.073
	1	0.01 ± 0.006
	10	0.007 ± 0.003
tet-ACS2	0.001	0.487 ± 0.055
	0.1	1.8 ± 0.902
	1	0.69 ± 0.156
	10	0.933 ± 0.133

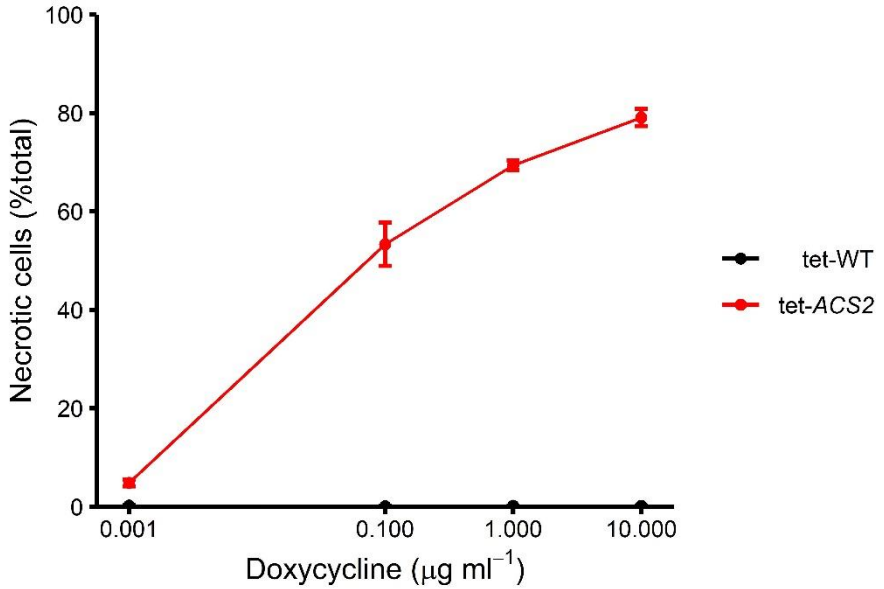

Fig. 3.6. Proportion of necrotic, low-ROS cells (% of total cells falling into the upper left quadrant of Fig. 2.1; see section 2.7) in tet-WT (black line) and tet-*ACS2* (red line) cultures incubated with increasing concentrations of doxycycline for 24h. Necrosis was measured using a BD Accuri™ C6 Plus flow cytometer with the necrosis-indicator dye propidium iodide. 1000 cells per sample were analysed. The data are means ± SEM of three biological replicates.

3.2.2 ROS accumulation in KAT and KDAC mutants

Most of the KAT and KDAC mutants examined in this study displayed only marginally elevated ROS levels, far lower than that elicited by the loss of Cox4p (Figs. 3.7-3.8; Table 2). However, strong increases in ROS accumulation relative to WT cells were observed in cells lacking the Hda1C KDAC subunit Hda2p (Fig. 3.7B), or the SAGA, SLIK and ADA subunits Gcn5p or Ngg1p (Fig. 3.7A, F; Table 2). Interestingly, Δ*hda2* was also the only strain tested that, like Δ*cox4*, appeared to exhibit an elevation of ROS levels across the entire population (Fig. 3.9). All other strains tested exhibited a major population of cells producing similar levels of ROS to the WT, and a subpopulation producing high levels of ROS (data not shown). Furthermore, Δ*hda2* was the only strain tested that, again similar to the Δ*cox4* strain, appeared respiratory-incompetent, showing no growth during SP in YPD (Fig. 3.10A) and no growth at all when incubated with YP + 2% glycerol (YPG; Fig. 3.10B).

Notably, while ROS accumulation was elevated by the deletion of either *NGG1* or *GCN5*, the deletion of *GCN5*, which encodes the catalytic subunit of the SAGA, SLIK and ADA complexes, elicited a much lower increase in ROS levels when compared to that caused by the deletion of *NGG1* (compare Fig. 3.7A, F; Table 2). Similarly, ROS accumulation was not elevated in cells lacking Hda1p, the catalytic subunit of the Hda1C KDAC complex, or the other structural subunit, Hda3p (compare Fig. 3.7B, 3.7D and 3.8D; Table 2). Additionally, ROS accumulation was not elevated in cells lacking Tup1p, which recruits Hda1p to specific chromosomal regions repressed by Tup1p-Cyc8p (Fig. 3.7D; Table 3.1; Wu et al., 2001).

3.2.3 ROS accumulation is elevated in both Δ*mks1* and Δ*rtg2* cells

Alongside acetyl-CoA, KAT and KDAC mutants, ROS accumulation was investigated in cells lacking Rtg2p and Mks1p, the positive and negative regulators of the retrograde (RTG) pathway, respectively. The RTG pathway is induced in response to impaired mitochondrial energy metabolism and involves a KAT complex, SLIK, in which Rtg2p is incorporated as a subunit. Moreover, the deletion of Rtg2 can impair the KAT activity of this complex (Pray-Grant et al., 2002). Therefore, it was worth investigating how ROS accumulation was affected by over-activation (via deletion of *MKS1*) or under-activation (via deletion of *RTG2*) of the RTG pathway. ROS accumulation was elevated in Δ*rtg2* cells and to an even

greater extent in Δ*mks1* cells, though again not to the same degree as it was Δ*cox4* cells (Fig. 3.11; Table 3.3). Thus, an elevation in ROS accumulation was elicited by both over-activation and under-activation of the RTG pathway.

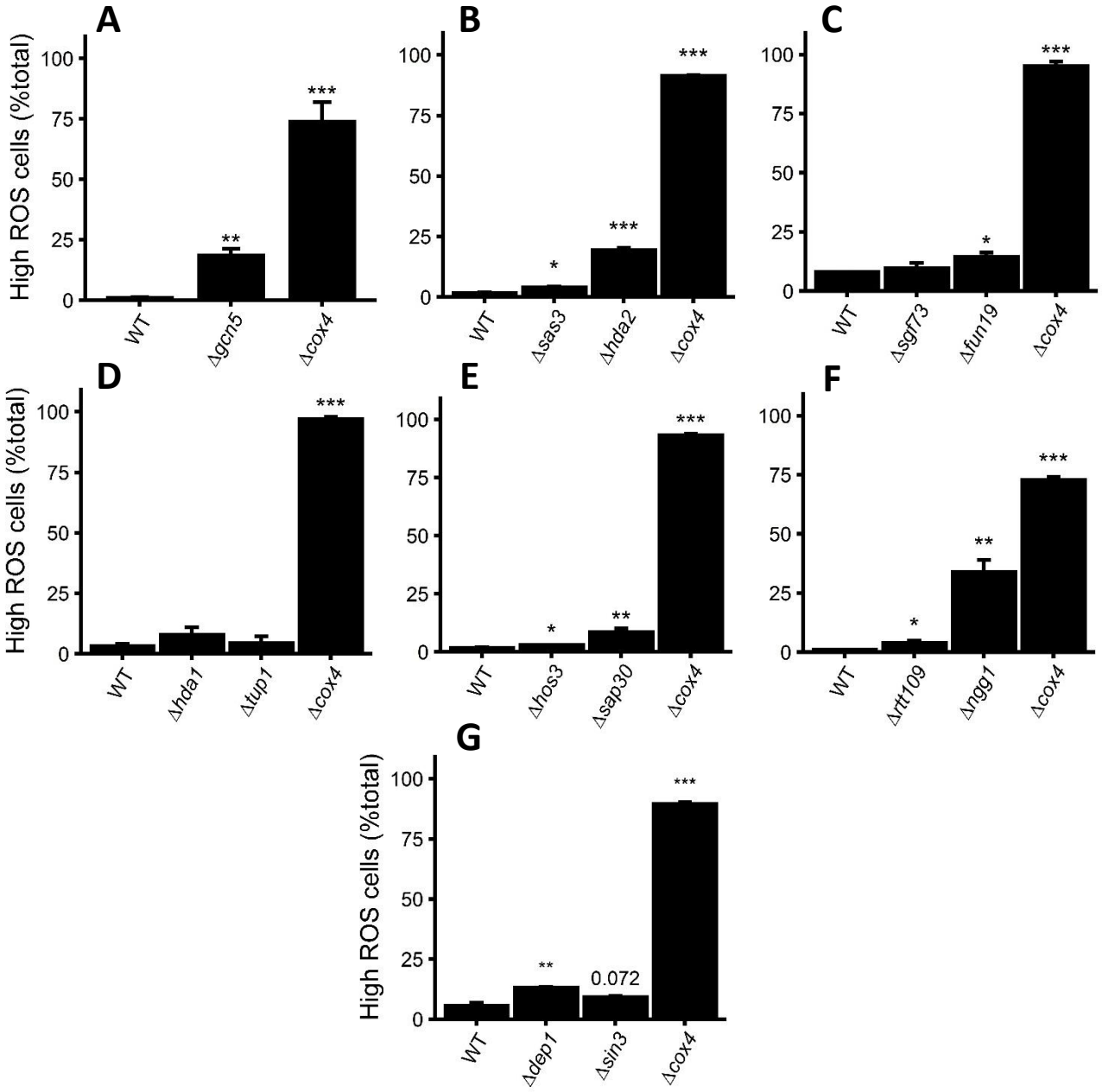

Fig. 3.7. ROS accumulation (proportion of total cells showing high ROS levels; calculated according to section 2.6 and Fig. 1) in WT and Δ*cox4* strains, and in acetyl-CoA, KAT, and KDAC mutants (see Table 1). ROS accumulation was measured in live cells using a BD Accuri™ C6 Plus flow cytometer with the ROS dye H_2DCF-DA in conjunction with the necrosis-indicator dye propidium iodide. 10000 cells per sample were analysed. Data are means ± SEM of three biological replicates. Annotations represent the results of a one-way ANOVA relative to the WT strain; ***, $P < 0.001$; **, $P < 0.01$; *, $P < 0.05$.

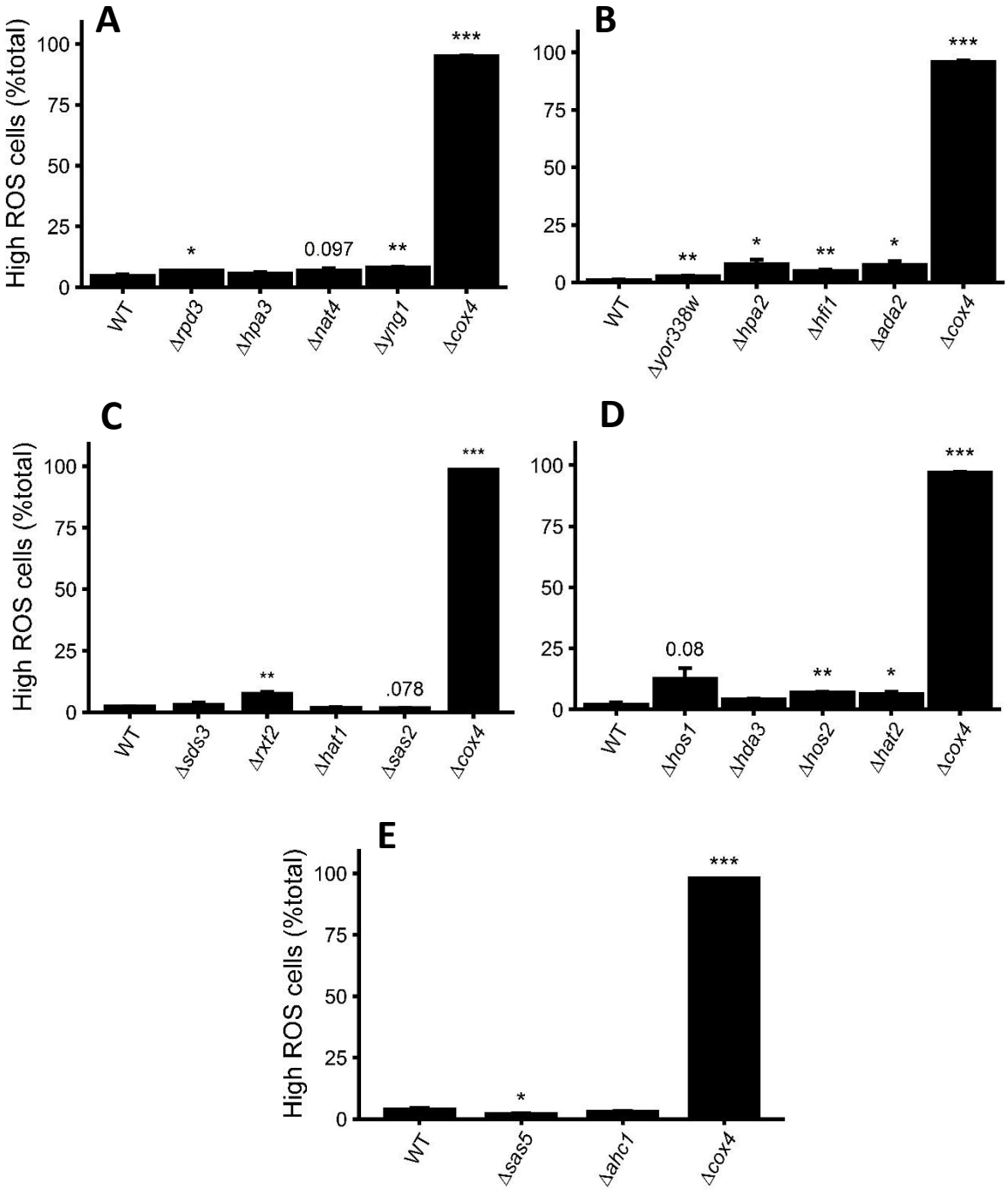

Fig. 3.8. ROS accumulation (proportion of total cells showing high ROS levels; calculated according to section 2.6 and Fig. 1) in WT and Δ*cox4* strains, and in acetyl-CoA, KAT, and KDAC mutants (see Table 1). ROS accumulation was measured in live cells using a BD Accuri™ C6 Plus flow cytometer with the ROS dye H_2DCF-DA in conjunction with the necrosis-indicator dye propidium iodide. 10000 cells per sample were analysed. The data are means ± SEM of three biological replicates. Annotations represent the results of a one-way ANOVA relative to the WT; ***, $P < 0.001$; **, $P < 0.01$; *, $P < 0.05$.

Table 3.3. ROS accumulation (fold-change relative to WT cells; see section 2.6 and Fig. 1) in Δ*cox4* cells and in acetyl-CoA, KAT, and KDAC mutants (see Table 1). Data are means ± SEM of at least three biological replicates. Data for Δ*cox4* cells represent the average fold-change in ROS accumulation across every experiment (N = 39).

Strain	ROS accumulation (fold-change)
Δ*cox4*	37.439 ± 3.747
Δ*ach1*	1.586 ± 0.046
Δ*acs1*	1.745 ± 0.361
Δ*ada2*	7.425 ± 1.686
Δ*ahc1*	0.761 ± 0.062
Δ*dep1*	2.405 ± 0.033
Δ*fun19*	1.810 ± 0.207
Δ*gcn5*	19.231 ± 2.747
Δ*hat1*	0.832 ± 0.071
Δ*hat2*	3.234 ± 0.515
Δ*hda1*	2.377 ± 1.006
Δ*hda2*	10.932 ± 0.636
Δ*hda3*	2.066 ± 0.185
Δ*hfi1*	4.810 ± 0.508
Δ*hos1*	6.355 ± 2.263
Δ*hos2*	3.514 ± 0.146
Δ*hos3*	1.810 ± 0.097
Δ*hpa2*	7.876 ± 1.679
Δ*hpa3*	1.193 ± 0.134
Δ*mks1*	4.618 ± 0.444
Δ*mpc1*	1.235 ± 0.030
Δ*nat4*	1.483 ± 0.193
Δ*ngg1*	33.333 ± 4.843
Δ*rpd3*	1.448 ± 0.011

Δ*rtg2*	3.442 ± 0.168
Δ*rtt109*	3.820 ± 0.904
Δ*rxt2*	3.270 ± 0.356
Δ*sap30*	5.329 ± 0.874
Δ*sas2*	0.728 ± 0.087
Δ*sas3*	2.260 ± 0.207
Δ*sas5*	0.544 ± 0.043
Δ*sds3*	1.312 ± 0.374
Δ*sgf73*	1.204 ± 0.293
Δ*sin3*	1.679 ± 0.100
Δ*tup1*	1.330 ± 0.881
Δ*yng1*	1.732 ± 0.065
Δ*yor338w*	2.683 ± 0.166

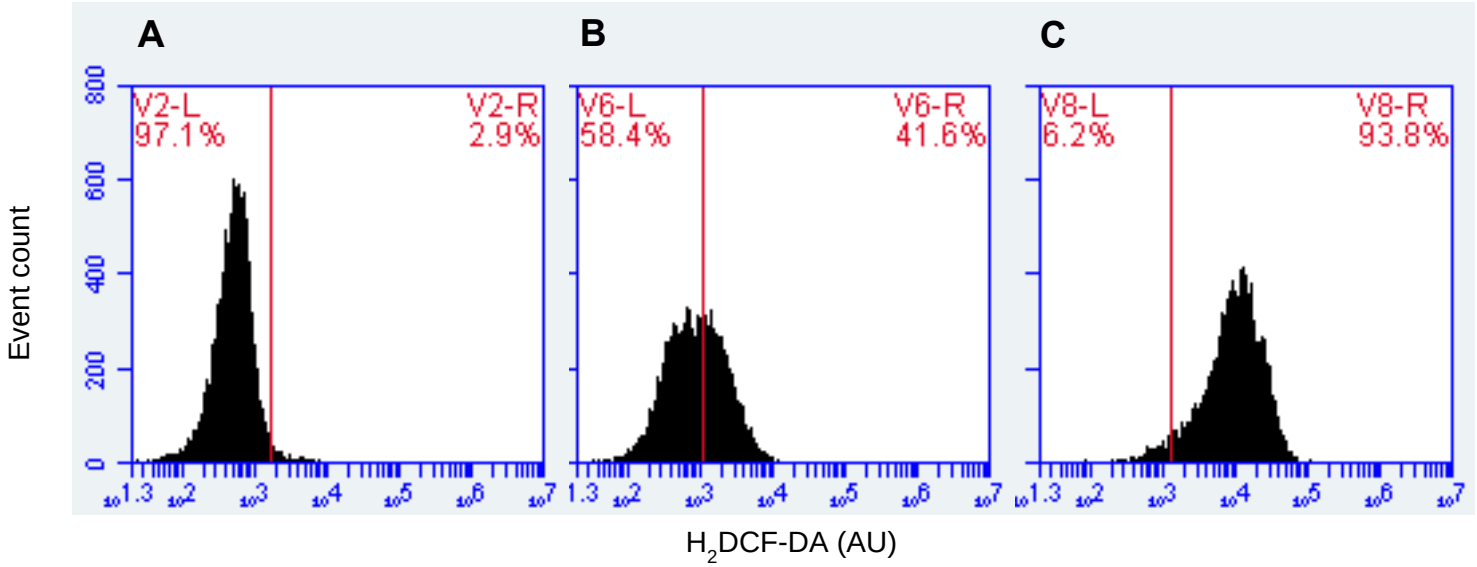

Fig. 3.9. Representative histograms of ROS accumulation (H_2DCF-DA signal; arbitrary units) in WT **(A)**, Δ*hda2* **(B)** and Δ*cox4* **(C)** strains. ROS levels were measured in live cells using a BD Accuri™ C6 Plus flow cytometer with the ROS dye H_2DCF-DA and the necrosis-indicator dye propidium iodide. 10000 cells per sample were analysed. The vertical line was placed after the maximum H_2DCF-DA signal observed in a WT sample stained with the necrosis indicator dye propidium iodide but not with the ROS dye H_2DCF-DA. The annotations to the left and right of the vertical line represent the percentage of cells falling in that area.

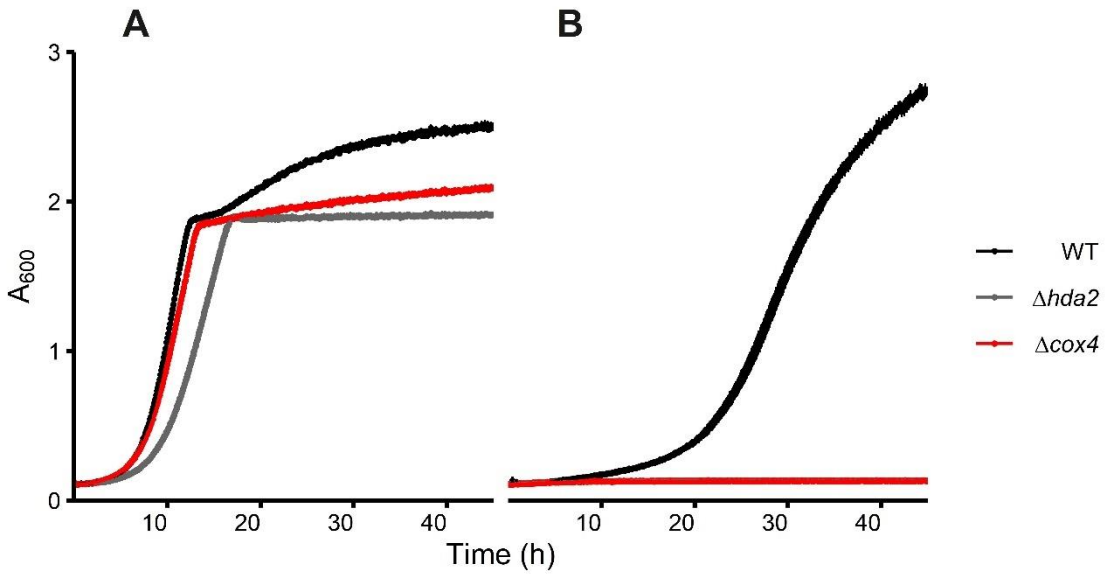

Fig. 3.10. Growth (absorbance at 600 nm) of WT (black line), Δ*hda2* (grey line) and Δ*cox4* (red line) strains in YPD (**A**; YP + 2% glucose) or YPG (**B**; YP + 2% glycerol) media. YPD O/Ns were inoculated to an A_{600} of 0.1 in either YPD or YPG and grown for 45h in a BMG LabTech Spectrostar Nano plate reader according to section 2.6. Data are means ± SEM of four biological replicates.

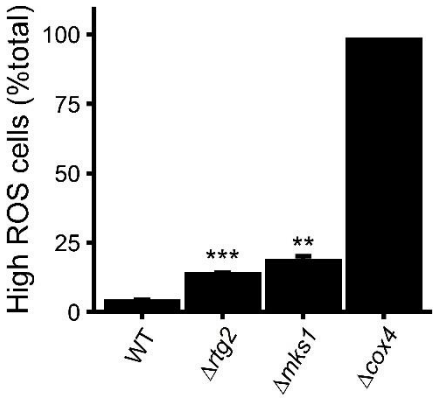

Fig. 3.11. ROS accumulation (proportion of total cells showing high ROS levels; calculated according to section 2.6 and Fig. 1) in WT, Δ*rtg2*, Δ*mks1* and Δ*cox4* strains. ROS accumulation was measured in live cells using a BD Accuri™ C6 Plus flow cytometer with the ROS dye H_2DCF-DA in conjunction with the necrosis-indicator dye propidium iodide. 10000 cells per sample were analysed. The data are means ± SEM of three biological replicates. Annotations represent the results of a one-way ANOVA relative to the WT; ***, $P < 0.001$; **, $P < 0.01$.

3.3 Abundance of histone acetylation sites in genes upregulated (UR) or downregulated (DR) by loss of Cox4p

Section 3.1 and 3.2 suggested that acetyl-CoA levels were inversely correlated with ROS levels in Δ*cox4* cells and that interfering with acetyl-CoA metabolism can affect ROS accumulation. However, it was still unclear if the loss of Cox4p caused a reduction in histone acetylation, and whether this reduction corresponded to acetylated residues usually bound by Bdf1p. Genes enriched for acetylated lysine residues are likely to be actively transcribed when acetylated, as this process is, in general, correlated with active transcription (Pokholok et al., 2005), and would therefore likely exhibit a decline in expression upon a drop in the cellular concentration of acetyl-CoA. Therefore, since the loss of Cox4p may result in acetyl-CoA depletion (see section 3.1), downregulated genes were hypothesised to be enriched for acetylated histone lysine residues. Additionally, due to the role of Bdf1p in Yno1p-mediated ROS accumulation, in which it moves from the nucleus to associate with the mitochondria (see section 1.7.3), genes showing differential expression in response to the loss of Cox4p were hypothesised to be enriched for Bdf1p binding sites in particular (H4 K5ac, K8ac, K12ac and K16ac, and H2A K5ac). I sought to investigate these hypotheses using microarray data produced by Leadsham and Gourlay (2010), in which cells lacking the phosphodiesterase Pde2p were grown for 24h in the presence of 4 mM cAMP. Under these conditions, cAMP accumulates and elicits a reduction in *COX4* transcript levels and an accumulation of ROS. Genes showing greater than two-fold up- or downregulation (UR and DR, respectively) by cAMP treatment were split into two groups according to their association with either the mitochondria or non-mitochondrial compartments (henceforth termed mitochondrial genes or non-mitochondrial genes, respectively), using GO-SLIM (see Fig. 3.12 for GO term enrichment of UR and DR genes) and analysed using the YHMI (Wu et al., 2018). The YHMI analyses the abundance of histone acetylation sites, along with many other PTMs, in both the promoter and coding regions of genes, relative to the entire *S. cerevisiae* genome (see section 2.8 for details). The YHMI also analyses the abundance of binding sites for histone/chromatin modifiers relative to data from Venters et al. (2011), who identified interactions between histone/chromatin modifiers and genomic DNA in *S. cerevisiae* under normal (25^{o}C) and acute heat-shock (37^{o}C) conditions (Wu et al.,

2018). Unless stated otherwise, all histone/chromatin modifier data presented here relate to the 25°C data of Venters et al. (2011).

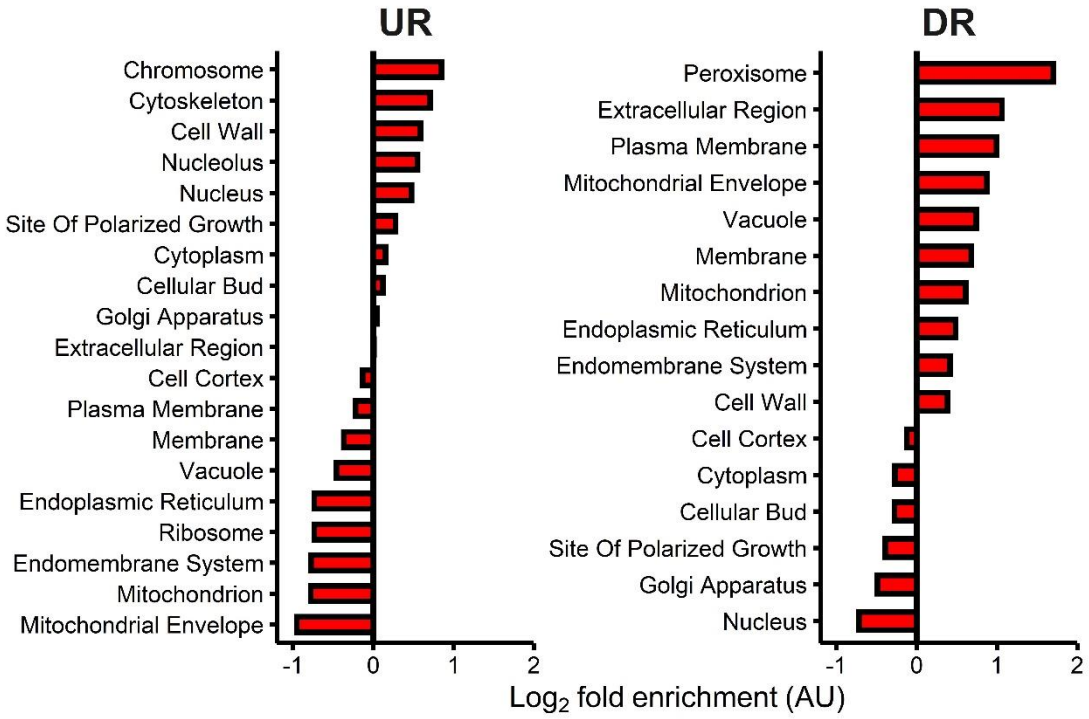

Fig. 3.12. GO-SLIM term enrichment (Log_2 fold enrichment relative to the proportion at which they are present in the *S. cerevisiae* genome) for genes significantly upregulated (**UR**; N = 668) or downregulated (**DR**; N = 465) in Δ*pde2* cells treated with 4 mM cAMP for 24h. The data presented here were generated using microarray data from Leadsham et al. (2010). Terms with fewer than 10 representative genes are not shown.

3.3.1 Non-mitochondrial DR genes are highly enriched for acetylated H4 and H2A in the coding regions

Unexpectedly, in the case of non-mitochondrial genes, neither DR nor UR genes were enriched for histone acetylation sites in the promoter regions, with DR genes showing no clear acetylation enrichment at all and UR genes showing slight enrichment in H4 K5ac and H4ac (Table 3.4). However, DR genes were highly enriched for numerous histone acetylation sites in the coding regions, in particular H4 K8ac, K12ac and K16ac, all of which are binding sites for Bdf1p bromodomains (Ladurner et al., 2003). DR genes were also highly enriched for acetylated H2A K5, another core histone with which Bdf1p interacts (García-Oliver et al., 2017). In contrast, none of these sites were enriched

in UR genes, and H4 K16ac was highly depleted (Table 3.4). Taken together, these results indicate that non-mitochondrial DR genes are usually hyperacetylated relative to the rest of the genome.

Aside from the enrichment of acetylated histone residues, there were also major differences in the enrichment of sites for histone/chromatin modifiers between non-mitochondrial DR and UR genes. On average, DR genes showed a slight but non-significant enrichment for histone/chromatin modifiers (Fig. 3.13), and were highly enriched for Tup1p, Hho1p, Hif1p, Rpt6p and Ioc4p in particular (Fig. 3.14). The large enrichment of Tup1p in DR genes is interesting due to its involvement with the Hda1C complex (see section 3.2 and Table 3.1), which as outlined in section 3.3 can elicit the accumulation of ROS when its structural subunit, Hda2p, is removed. Interestingly, when including the acute heat-shock data of Venters et al. (2011; see above), DR genes were also enriched for several subunits of the chromatin-remodelling RSC complex (Rsc1p, Rsc2p, Rsc8p and Rsc9p), whereas UR genes were enriched for none of these regulators.

Table 3.4. Significantly ($P < 0.05$) enriched/depleted histone acetylation sites in the promoter regions of non-mitochondrial Δ*pde2* genes downregulated (DR) or upregulated (UR) by treatment with 4 mM cAMP (see section 3.4). The data presented here were produced using microarray data from Leadsham and Gourlay (2010), analysed with the Yeast Histone Modification Identifier (YHMI; see section 3.4 and 2.8 for details; see also Wu et al. [2018]).

Dataset	Name	Trend	P-value	Fold Enrichment	Observed Ratio (A/B)	Expected Ratio (C/D)
DR	H3K14ac	Depleted	< 0.001	0.634	143/456 (31.36%)	3250/6572 (49.45%)
	H3K18ac	Depleted	< 0.001	0.668	140/456 (30.70%)	3022/6572 (45.98%)
	H4ac	Depleted	< 0.001	0.717	177/456 (38.82%)	3559/6572 (54.15%)
	H3K23ac	Depleted	< 0.001	0.533	42/456 (9.21%)	1135/6572 (17.27%)

	H3K9ac	Depleted	< 0.001	0.704	104/456 (22.81%)	2129/6572 (32.40%)
	H2AK5ac	Depleted	< 0.001	0.565	43/456 (9.43%)	1097/6572 (16.69%)
	H3K4ac	Depleted	0.003	0.783	90/456 (19.74%)	1656/6572 (25.20%)
	H4ac [H2O2]	Enriched	0.013	1.143	178/456 (39.04%)	2244/6572 (34.14%)
	H3K56ac	Depleted	0.014	0.701	32/456 (7.02%)	658/6572 (10.01%)
	H3K14ac [H2O2]	Enriched	0.017	1.092	263/456 (57.68%)	3470/6572 (52.80%)
UR	H4ac [H2O2]	Depleted	< 0.001	0.704	144/599 (24.04%)	2244/6572 (34.14%)
	H3K56ac	Depleted	< 0.001	0.600	36/599 (6.01%)	658/6572 (10.01%)
	H4ac	Enriched	0.023	1.073	348/599 (58.10%)	3559/6572 (54.15%)
	H3K14ac [H2O2]	Depleted	0.025	0.926	293/599 (48.91%)	3470/6572 (52.80%)
	H3K23ac	Depleted	0.033	0.841	87/599 (14.52%)	1135/6572 (17.27%)
	H4K5ac	Enriched	0.046	1.211	71/599 (11.85%)	643/6572 (9.78%)

Table 3.5. Significantly (P < 0.05) enriched/depleted histone acetylation sites in the coding regions of non-mitochonndrial Δ*pde2* genes downregulated (DR) or upregulated (UR) by treatment with 4 mM cAMP (see section 3.3). The data presented here were produced using microarray data from Leadsham and Gourlay (2010) analysed with the Yeast Histone Modification Identifier (YHMI; see section 3.3 and 2.8 for details; see also Wu et al. [2018]).

Dataset	Residue	Trend	P-value	Fold Enrichment	Observed Ratio (A/B)	Expected Ratio (C/D)
DR	H3K14ac	Depleted	< 0.001	0.637	114/456 (25.00%)	2578/6572 (39.23%)
	H4ac [H2O2]	Enriched	< 0.001	1.364	245/456 (53.73%)	2589/6572 (39.39%)
	H4K8ac	Enriched	< 0.001	1.919	84/456 (18.42%)	631/6572 (9.60%)
	H4ac	Depleted	< 0.001	0.826	200/456 (43.86%)	3491/6572 (53.12%)
	H4K16ac	Enriched	< 0.001	2.266	25/456 (5.48%)	159/6572 (2.42%)
	H3K18ac	Depleted	0.001	0.770	93/456 (20.39%)	1740/6572 (26.48%)
	H2AK5ac	Enriched	0.011	1.517	32/456 (7.02%)	304/6572 (4.63%)
	H4K12ac	Enriched	0.013	1.497	32/456 (7.02%)	308/6572 (4.69%)
	H3K14ac [H2O2]	Enriched	0.019	1.100	241/456 (52.85%)	3158/6572 (48.05%)
UR	H3K4ac	Depleted	< 0.001	0.651	58/599 (9.68%)	977/6572 (14.87%)
	H4ac [H2O2]	Depleted	< 0.001	0.848	200/599 (33.39%)	2589/6572 (39.39%)

H3K23ac	Depleted	0.001	0.681	48/599 (8.01%)	773/6572 (11.76%)
H4ac	Enriched	0.001	1.113	354/599 (59.10%)	3491/6572 (53.12%)
H4K16ac	Depleted	0.040	0.552	8/599 (1.34%)	159/6572 (2.42%)
H3K9ac	Depleted	0.043	0.886	140/599 (23.37%)	1734/6572 (26.38%)
H3K4ac	Depleted	< 0.001	0.651	58/599 (9.68%)	977/6572 (14.87%)

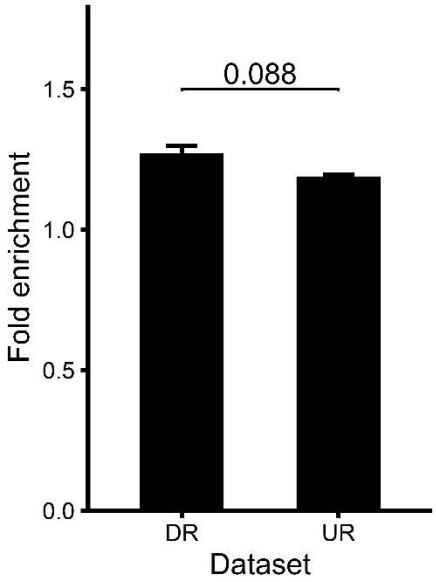

Fig. 3.13. Average fold enrichment (relative to the expected number of binding sites in the *S. cerevisiae* genome) of histone/chromatin regulators in non-mitochondrial genes from Δ*pde2* cells downregulated (DR) or upregulated (UR) by cAMP treatment (see section 3.3). Enrichment values were calculated using the Yeast Histone Modification Identifier according to section 3.3 and 2… (see also Wu et al. [2018]) The data are means ± SEM (N = 21 [DR]; N = 15 [UR]).

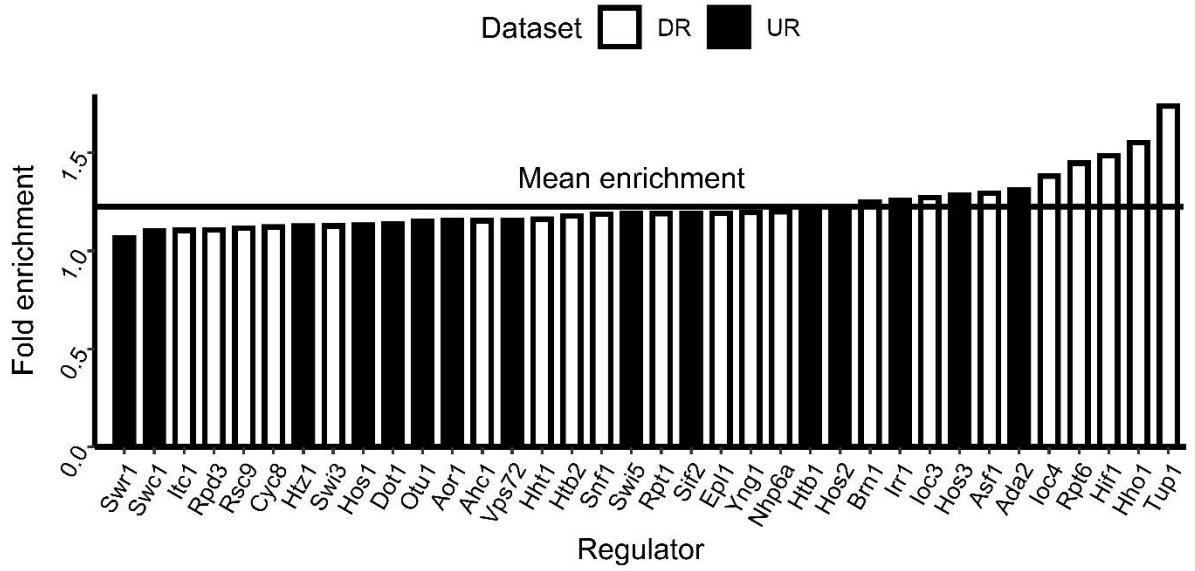

Fig. 3.14. Fold enrichment (relative to the expected number of binding sites in the *S. cerevisiae* genome) of histone/chromatin regulators in non-mitochondrial genes from Δ*pde2* cells downregulated (DR) or upregulated (UR) by cAMP treatment (see section 3.3). Enrichment values were calculated using the Yeast Histone Modification Identifier according to section 3.3 and 2… (see also Wu et al. [2018]). The horizontal line represents the mean enrichment of these regulators.

3.3.2 Mitochondrial DR genes are highly enriched for acetylated H4 and H2A in promoters and coding regions

Unlike non-mitochondrial genes, mitochondrial genes were enriched for various acetylated residues in the promoter regions. DR genes were particularly enriched for H4 K8ac and H4 K12ac but depleted for H3 K14ac, whereas UR genes were not enriched for H4 K8ac or K12ac but were moderately enriched for H3 K14ac (Table 3.6). In the coding regions, DR genes were highly enriched for H3 K14ac, H4 K8ac, H4 K16ac and H2A K5ac (Table 3.7). Additionally, in contrast to non-mitochondrial UR genes, mitochondrial UR genes were also highly enriched for H4 K5ac in the coding regions. As with the results outlined in the previous section, these results indicate that mitochondrial DR genes, and, to a lesser extent, UR genes, are hyperacetylated relative to the rest of the genome. Moreover, all the aforementioned acetylated residues are binding sites for Bdf1p (García-Oliver et al., 2017; Ladurner et al., 2003), which further implicates the activity of Bdf1p in cAMP-mediated ROS accumulation.

Mitochondrial DR and UR genes also differed in their enrichment for histone/chromatin regulators, though not in their average enrichment (1.411 ± 0.038 and 1.272 ± 0.098, respectively; $F_{1, 17} = 1.368$, P = 0.258, one-way ANOVA), with DR genes showing particularly high enrichment for Irr1p and Hho1p (Fig. 3.15). Similar to non-mitochondrial genes, when including the acute heat-shock data of Venters et al. (2011), mitochondrial DR genes were also enriched for multiple RSC complex subunits (Rsc1, Rsc8 and Rsc9), whereas UR genes were not enriched for any RSC complex subunit.

Table 3.6. Significantly (P < 0.05) enriched/depleted histone acetylation sites in the promoter regions of mitochondrial Δ*pde2* genes downregulated (DR) or upregulated (UR) by treatment with 4 mM cAMP (see section 3.3). The data presented here were produced using microarray data from Leadsham and Gourlay (2010) analysed with the Yeast Histone Modification Identifier (YHMI; see section 2…. for details).

Dataset	Residue	Trend	P-value	Fold Enrichment	Observed Ratio (A/B)	Expected Ratio (C/D)
DR	H3K14ac	Depleted	< 0.001	0.703	41/118 (34.75%)	3250/6572 (49.45%)
	H4ac [H2O2]	Enriched	0.005	1.340	54/118 (45.76%)	2244/6572 (34.14%)
	H3K18ac	Depleted	0.014	0.774	42/118 (35.59%)	3022/6572 (45.98%)
	H4K8ac	Enriched	0.023	1.621	19/118 (16.10%)	653/6572 (9.94%)
	H4K12ac	Enriched	0.043	1.850	10/118 (8.47%)	301/6572 (4.58%)
UR	H3K14ac	Enriched	0.018	1.257	46/74 (62.16%)	3250/6572 (49.45%)

Table 3.7. Significantly (P < 0.05) enriched/depleted histone acetylation sites in the coding regions of mitochondrial Δ*pde2* genes downregulated (DR) or upregulated (UR) by treatment with 4 mM cAMP (see section 3.3). The data presented here were produced using microarray data from Leadsham and Gourlay (2010) analysed with the Yeast Histone Modification Identifier (YHMI; see section 2…. for details).

Dataset	Residue	Trend	P-value	Fold Enrichment	Observed Ratio (A/B)	Expected Ratio (C/D)
DR	H4ac [H2O2]	Enriched	< 0.001	1.592	74/118 (62.71%)	2589/6572 (39.39%)
	H4K8ac	Enriched	< 0.001	2.295	26/118 (22.03%)	631/6572 (9.60%)
	H3K14ac	Depleted	0.004	0.691	32/118 (27.12%)	2578/6572 (39.23%)
	H4K16ac	Enriched	0.008	2.802	8/118 (6.78%)	159/6572 (2.42%)
	H3K14ac [H2O2]	Enriched	0.022	1.199	68/118 (57.63%)	3158/6572 (48.05%)
	H2AK5ac	Enriched	0.046	1.832	10/118 (8.47%)	304/6572 (4.63%)
UR	H4K5ac	Enriched	0.004	2.406	12/74 (16.22%)	443/6572 (6.74%)
	H4ac	Enriched	0.027	1.221	48/74 (64.86%)	3491/6572 (53.12%)

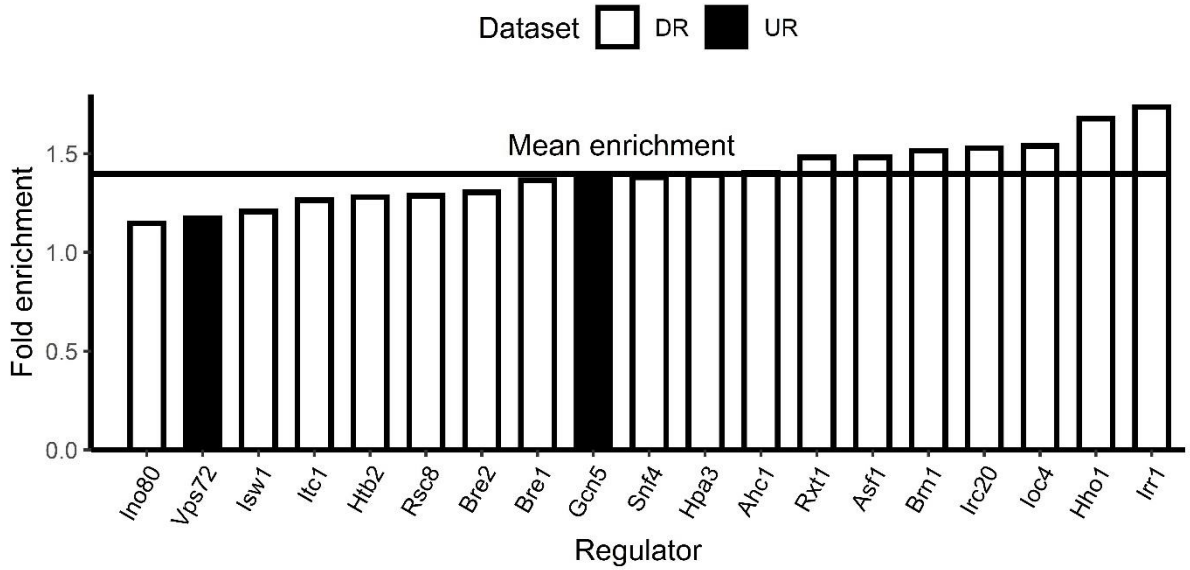

Fig. 3.15. Fold enrichment (relative to the expected number of binding sites in the *S. cerevisiae* genome) of histone/chromatin regulators in mitochondrial genes from Δ*pde2* cells downregulated (DR) or upregulated (UR) by cAMP treatment (see section 3.3). Enrichment values were calculated using the Yeast Histone Modification Identifier according to section 3.3 and 2… (see also Wu et al. [2018]). The horizontal line represents the mean enrichment of these regulators.

3.3.3 Δ*bdf1* cells and Mut-*bdf1* cells resemble Δ*pde2*-cAMP cells with respect to histone acetylation

After finding that genes downregulated by cAMP treatment in Δ*pde2* cells were generally enriched for acetylated histone lysine residues, I wondered if the loss of Bdf1p, which as mentioned above is pivotal for Yno1p-mediated ROS accumulation, would result in a similar phenotype with regards to the enrichment of acetylated lysine residues. I therefore examined the microarray data of Ladurner et al. (2003), which contains gene expression data from Δ*bdf1* cells and from Mut-*BDF1* cells – cells in which the acetyl-lysine binding activity of Bdf1p had been abolished by mutating two tyrosine residues (Tyr186 and Tyr353) into arginine residues.

As above, lists of significantly upregulated (UR) or downregulated (DR) genes were collected and split by subcellular compartment into mitochondrial or non-mitochondrial genes using GO-SLIM. As might be expected, there was a large degree of overlap between Δ*bdf1* and Mut-*BDF1* cells with regards to GO-SLIM term enrichment. However, this overlap was not complete, as, for example, Δ*bdf1* UR genes

were highly enriched for the terms “Cell Wall” and “Extracellular Region”, whereas Mut-*BDF1* UR genes were not (Fig. 3.16).

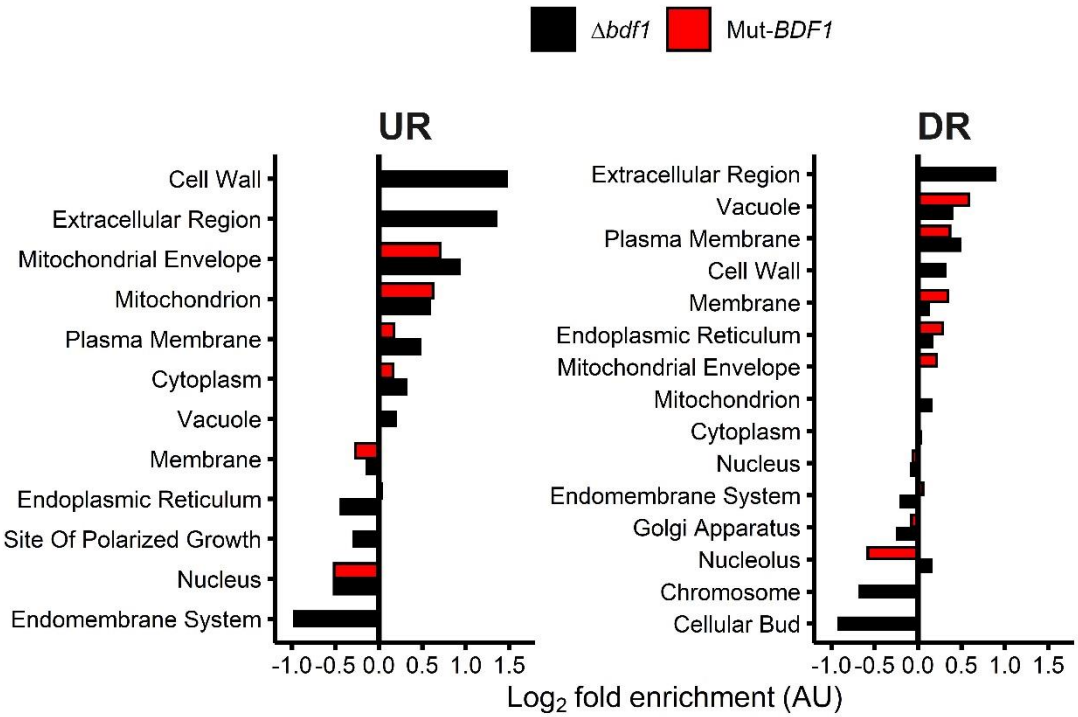

Fig. 3.16. GO-SLIM term enrichment (Log_2 fold enrichment relative to the proportion at which they are present in the *S. cerevisiae* genome) for genes significantly upregulated (**UR**) or downregulated (**DR**) in Δ*bdf1* cells (black bars; N = 197 UR genes, N = 332 DR genes) or Mut-*BDF1* cells (red bars; N = 106 UR genes, N = 249 DR genes). The data presented here were generated using microarray data from Ladurner et al. (2003). Terms with fewer than 8 representative genes are not shown.

Non-mitochondrial DR genes from Δ*bdf1* cells showed similar patterns of acetylation enrichment to Δ*pde2* cells. Mut-*BDF1* cells to a large extent also showed similar patterns of acetylation enrichment, though the data from these cells were complicated by the relatively low number of genes classified as “Mitochondrial” by GO-SLIM (results presented in Table A1-4). Apart from H4 K5ac in the DR gene set, non-mitochondrial genes differentially expressed in Δ*bdf1* cells were not enriched for acetylated lysine residues in the promoter regions (Table 3.8). However, as with Δ*pde2* cells treated with cAMP, the coding regions of non-mitochondrial DR genes were highly enriched for Bdf1p-binding sites (H4 K5ac, K8ac and K12ac, and H2A K5ac), as were UR genes in the case of H4 K8ac (Table 3.9). In the case of mitochondrial genes, there was little enrichment for acetylated lysine residues in the promoters of DR and UR genes (Table 3.10). However, mitochondrial DR genes were highly enriched for

numerous acetylated lysine residues in the coding regions (Table 3.11), in particular the Bdf1p-binding sites H4 K5ac, H4 K8ac, H4 K12ac, H3 K14ac and H2A K5ac. Put simply, Δ*bdf1* cells seem to phenocopy Δ*pde2* cells in the sense that both conditions (cAMP treatment in Δ*pde2* cells, and the loss of Bdf1p) cause a downregulation of genes enriched for acetylated histone lysine residues.

Table 3.8. Significantly ($P < 0.05$) enriched/depleted histone acetylation sites in the promoter regions of downregulated (DR) or upregulated (UR) non-mitochondrial genes in Δ*bdf1* cells. The data presented here were produced using microarray data from Ladurner et al. (2003), analysed with the Yeast Histone Modification Identifier (YHMI; see section 2.8 and Wu et al. [2018] for further information).

Cell	Dataset	Name	Trend	P-value	Fold Enrichment	Observed Ratio (A/B)	Expected Ratio (C/D)
Δ*bdf1*	DR	H3K14ac [H2O2]	Depleted	0.001	0.822	118/272 (43.38%)	3470/6572 (52.80%)
		H3K18ac	Depleted	0.014	0.855	107/272 (39.34%)	3022/6572 (45.98%)
		H4K5ac	Enriched	0.015	1.428	38/272 (13.97%)	643/6572 (9.78%)
		H4ac [H2O2]	Depleted	0.021	0.829	77/272 (28.31%)	2244/6572 (34.14%)
		H3K14ac	Depleted	0.024	0.877	118/272 (43.38%)	3250/6572 (49.45%)
	UR	H3K18ac	Depleted	< 0.001	0.519	37/155 (23.87%)	3022/6572 (45.98%)
		H4ac	Depleted	< 0.001	0.584	49/155 (31.61%)	3559/6572 (54.15%)
		H3K14ac	Depleted	< 0.001	0.561	43/155 (27.74%)	3250/6572 (49.45%)
		H3K23ac	Depleted	0.001	0.486	13/155 (8.39%)	1135/6572 (17.27%)

	H3K9ac	Depleted	0.004	0.697	35/155 (22.58%)	2129/6572 (32.40%)
	H4K5ac	Depleted	0.005	0.396	6/155 (3.87%)	643/6572 (9.78%)
	H3K14ac [H2O2]	Enriched	0.005	1.197	98/155 (63.23%)	3470/6572 (52.80%)
	H2AK5ac	Depleted	0.009	0.580	15/155 (9.68%)	1097/6572 (16.69%)

Table 3.9. Significantly ($P < 0.05$) enriched/depleted histone acetylation sites in the coding regions of downregulated (DR) or upregulated (UR) non-mitochondrial genes in Δ*bdf1* cells. The data presented here were produced using microarray data from Ladurner et al. (2003), analysed with the Yeast Histone Modification Identifier (YHMI; see section 2.8 and Wu et al. [2018] for further information).

Cell	Dataset	Name	Trend	P-value	Fold Enrichment	Observed Ratio (A/B)	Expected Ratio (C/D)
Δ*bdf1*	DR	H4K12ac	Enriched	< 0.001	2.039629	26/272 (9.56%)	308/6572 (4.69%)
		H4K5ac	Enriched	0.001	1.745319	32/272 (11.76%)	443/6572 (6.74%)
		H2AK5ac	Enriched	0.002	1.907508	24/272 (8.82%)	304/6572 (4.63%)
		H4K8ac	Enriched	0.004	1.531649	40/272 (14.71%)	631/6572 (9.60%)
		H4ac	Enriched	0.017	1.121228	162/272 (59.56%)	3491/6572 (53.12%)
	UR	H4ac	Depleted	< 0.001	0.607275852	50/155 (32.26%)	3491/6572 (53.12%)
		H3K14ac	Depleted	< 0.001	0.542746315	33/155 (21.29%)	2578/6572 (39.23%)

		H3K14ac [H2O2]	Enriched	< 0.001	1.315769474	98/155 (63.23%)	3158/6572 (48.05%)
		H4ac [H2O2]	Enriched	< 0.001	1.359289301	83/155 (53.55%)	2589/6572 (39.39%)
		H3K18ac	Depleted	0.001	0.584827586	24/155 (15.48%)	1740/6572 (26.48%)
		H3K9ac	Depleted	0.002	0.611303345	25/155 (16.13%)	1734/6572 (26.38%)
		H4K8ac	Enriched	0.039	1.478288431	22/155 (14.19%)	631/6572 (9.60%)

Table 3.10. Significantly (P < 0.05) enriched/depleted histone acetylation sites in the promoter regions of downregulated (DR) or upregulated (UR) mitochondrial genes in Δ*bdf1* cells. The data presented here were produced using microarray data from Ladurner et al. (2003), analysed with the Yeast Histone Modification Identifier (YHMI; see section 2.8 and Wu et al. [2018] for further information).

Cell	Dataset	Name	Trend	P-value	Fold Enrichment	Observed Ratio (A/B)	Expected Ratio (C/D)
Δ*bdf1*	DR	H4ac [H2O2]	Depleted	0.028	0.669	16/70 (22.86%)	2244/6572 (34.14%)
	UR	H4ac [H2O2]	Enriched	0.001	1.621	31/56 (55.36%)	2244/6572 (34.14%)
		H3K14ac [H2O2]	Enriched	0.001	1.387	41/56 (73.21%)	3470/6572 (52.80%)
		H3K14ac	Depleted	0.006	0.650	18/56 (32.14%)	3250/6572 (49.45%)
		H2AK5ac	Depleted	0.011	0.321	3/56 (5.36%)	1097/6572 (16.69%)

Table 3.11. Significantly (P < 0.05) enriched/depleted histone acetylation sites in the coding regions of downregulated (DR) or upregulated (UR) mitochondrial genes in Δ*bdf1* cells. The data presented here were produced using microarray data from Ladurner et al. (2003), analysed with the Yeast Histone Modification Identifier (YHMI; see section 2.8 and Wu et al. [2018] for further information)

Cell	Dataset	Name	Trend	P-value	Fold Enrichment	Observed Ratio (A/B)	Expected Ratio (C/D)
Δ*bdf1*	DR	H3K14ac	Enriched	0.002	1.457	40/70 (57.14%)	2578/6572 (39.23%)
		H4K8ac	Enriched	0.002	2.232	15/70 (21.43%)	631/6572 (9.60%)
		H3K23ac	Enriched	0.002	2.065	17/70 (24.29%)	773/6572 (11.76%)
		H2AK5ac	Enriched	0.005	2.780	9/70 (12.86%)	304/6572 (4.63%)
		H4K12ac	Enriched	0.005	2.743	9/70 (12.86%)	308/6572 (4.69%)
		H3K18ac	Enriched	0.032	1.403	26/70 (37.14%)	1740/6572 (26.48%)
		H4ac	Enriched	0.038	1.210	45/70 (64.29%)	3491/6572 (53.12%)
		H4K5ac	Enriched	0.044	1.907	9/70 (12.86%)	443/6572 (6.74%)
	UR	H4ac [H2O2]	Enriched	< 0.001	1.723	38/56 (67.86%)	2589/6572 (39.39%)
		H3K14ac [H2O2]	Enriched	0.000	1.561	42/56 (75.00%)	3158/6572 (48.05%)
		H3K14ac	Depleted	0.004	0.546	12/56 (21.43%)	2578/6572 (39.23%)

3.4 ROS accumulation in Δ*cox4* cells is reduced by *ACS2* overexpression

Investigating ROS accumulation in KAT and KDAC mutants demonstrated that ROS accumulation could be altered by various disruptions to acetyl-CoA metabolism. However, the nature of the relationship between acetyl-CoA levels and ROS accumulation in Δ*cox4* cells remained unclear. Therefore, I sought to examine how altering the levels of acetyl-CoA directly might impact ROS levels in Δ*cox4* cells. I accomplished this by measuring ROS accumulation in Δ*cox4* cells overexpressing the acetyl-CoA synthetase Acs2p (pAG306-*ACS2*; henceforth termed Δ*cox4-ACS2* cells; Table 2.2). All transformations of WT and Δ*cox4* cells with pAG306-*ACS2* were confirmed successful using colony PCR according to section 2.3 and Table 2.4 (results are presented in Fig. A1). Cells were grown in YPD media and ROS levels were analysed in live cells using the ROS dye H_2DCF-DA in conjunction with the necrosis-indicator dye PI as described in section 2.6.

The overexpression of *ACS2* in Δ*cox4* cells lead to a small but significant reduction in ROS accumulation after 24h of growth (Fig. 3.17). However, since ROS accumulation in Δ*cox4* cells commences at SP and subsequently increases over time (Leadsham and Gourlay, unpublished data), and an ATP deficit during SP could result in acetyl-CoA depletion regardless of the activity of Acs2p, it was worth investigating how ROS levels changed over time in Δ*cox4-ACS2* cells relative to Δ*cox4* cells. As such, ROS accumulation was also examined in Δ*cox4-ACS2* cells every 2.5h following entry of Δ*cox4* cells into SP. Δ*cox4-ACS2* cells appeared to show a significant lag in time-dependent ROS accumulation relative to non-transformed Δ*cox4* cells (3.18B; strain x time interaction: $F_{1, 56} = 10.298$, $P = 0.002$; two-way ANOVA), despite displaying no changes in growth characteristics (Fig. 3.18A). The overexpression of *ACS2* in Δ*cox4* cells lead to a significant reduction in ROS accumulation at all time points tested relative to non-transformed Δ*cox4* cells (all $F > 23.986$, $P < 0.001$), with the maximum difference observed after 16.5h of growth. Taken together, these results strongly indicated that ROS accumulation in Δ*cox4* cells is influenced by cellular acetyl-CoA levels and warrant further investigation into how *ACS2* overexpression ameliorates ROS accumulation in these cells.

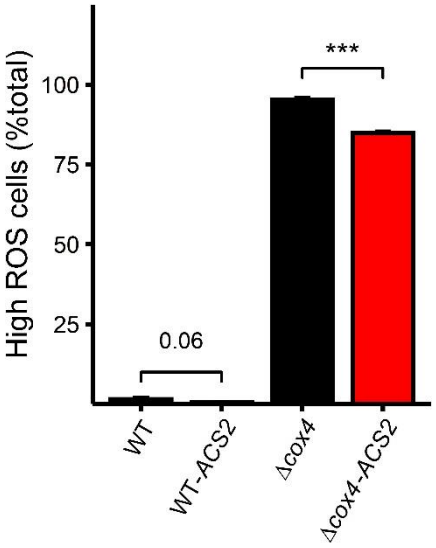

Fig. 3.17. ROS accumulation (proportion of total cells showing high ROS levels; calculated according to section 2.6 and Fig. 1) in WT and Δ*cox4* cells (black bars), and in WT and Δ*cox4* cells overexpressing the acetyl-CoA synthetase gene *ACS2* (red bars). ROS accumulation was measured in live cells using a BD Accuri™ C6 Plus flow cytometer with the ROS dye H_2DCF-DA and the necrosis-indicator dye propidium iodide. 10000 cells per sample were analysed. The data are means ± SEM of three biological replicates. Annotations represent the results of a one-way ANOVA; ***, P < 0.001

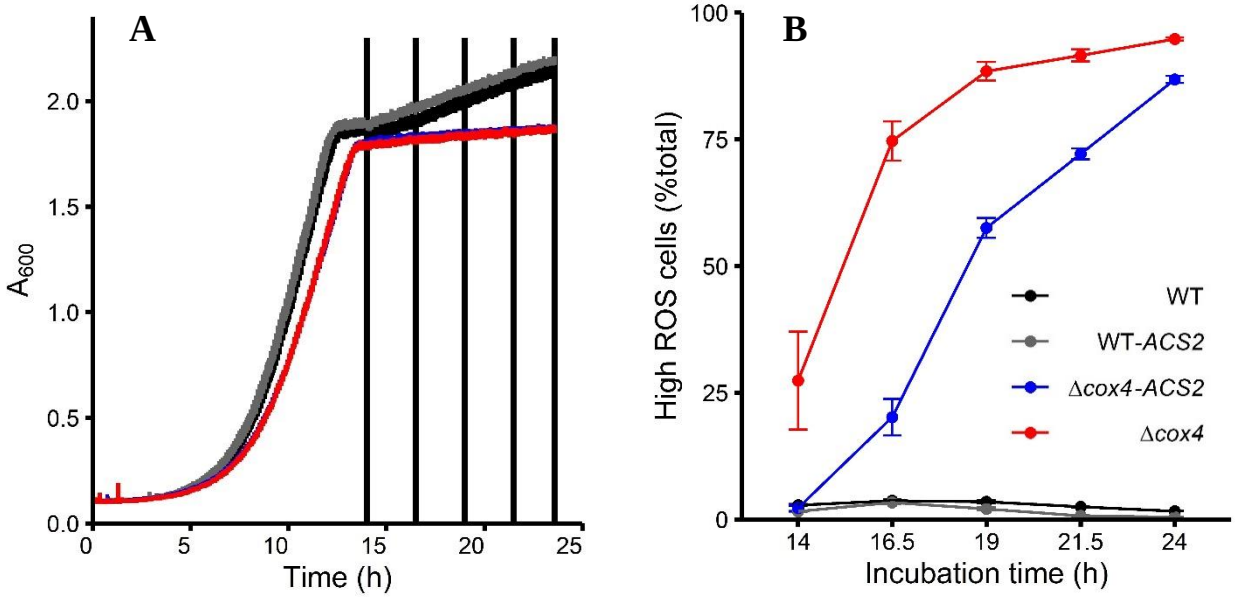

Fig. 3.18. Growth characteristics (**A**) and time-dependent ROS accumulation (**B**; measured at the time points indicated by the vertical lines in **A**) in WT cells (black lines), Δ*cox4* cells (red lines) and WT and Δ*cox4* cells overexpressing the acetyl-CoA synthetase gene *ACS2* (grey and blue lines, respectively. ROS accumulation was measured in live cells using a BD Accuri™ C6 Plus flow cytometer with the ROS dye H_2DCF-DA and the necrosis-indicator dye propidium iodide. 10000 cells per sample were analysed. Data are means ± SEM of three biological replicates.

3.5 Potassium acetate prevents ROS accumulation in Δ*cox4* cells

After finding that ROS accumulation could be ameliorated in Δ*cox4* cells by the overexpression of *ACS2*, I wished to see if direct supplementation with acetate, which has been previously shown to allow respiratory-incompetent cells to maintain WT levels of H4 acetylation (Friis et al., 2014), would also reduce ROS accumulation in these cells. To test this, I supplemented YPD cultures with potassium actetate (KAc; final concentration 1% w/v) directly after inoculation (time 0h), or after 14h of growth in non-supplemented YPD media, after which time both WT and Δ*cox4* cells had entered SP (Fig. 3.19). ROS levels were then measured every 2.5h for 7.5h, then again at 41h of growth, via flow cytometry as described in section 2.6. To account for variability in the exponential growth rate between samples, the data have been standardised using the times at which each strain was observed to have entered SP (henceforth termed time in SP).

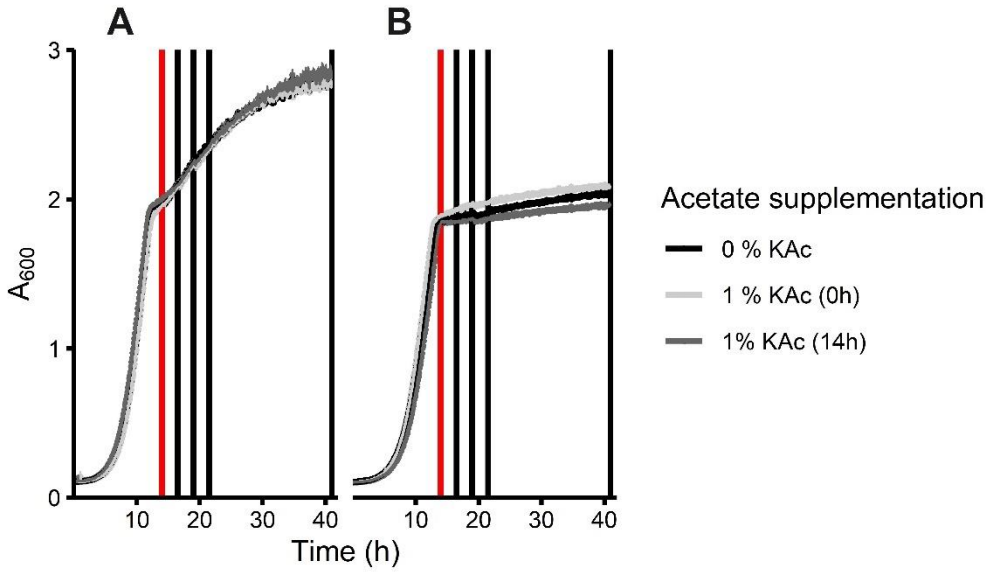

Fig. 3.19. Growth (absorbance at 600 nm) of WT (**A**) and Δ*cox4* (**B**) cultures in YPD (black lines) or YPD supplemented with potassium acetate (KAc; final concentration 1% w/v) either at the point of inoculation (light grey lines; 1% KAc [0h]) or after 14 h of growth in non-supplemented YPD (dark grey lines; 1% KAc [14h]). The red vertical line is placed at the time point of KAc supplementation (14h); the black vertical lines are placed at the time points at which ROS measurements were conducted. YPD O/Ns were inoculated to an A_{600} of 0.1 in YPD +/- KAc as described in the text. Data are means ± SEM of at least three biological replicates.

Acetate supplementation drastically reduced ROS accumulation in Δ*cox4* cells regardless of the time at which it was administered (Fig. 3.20; strain x KAc supplementation x time in SP interaction, $F_{2, 62} = 52.381$, $P < 0.001$; three-way ANOVA), though acetate supplementation at 14 h growth seemed to further delay ROS accumulation, as these cells showed reduced ROS accumulation over time relative to those supplemented with 1 % KAc at the point of inoculation (KAc supplementation x time in SP interaction, $F_{1, 20} = 21.364$, $P < 0.001$; two-way ANOVA using data from Δ*cox4* 1 % KAc [0 h] and [14 h] samples). Further, when untreated Δ*cox4* cells were supplemented with KAc (final concentration 1 % w/v) after 41 h of growth, and incubated for an additional two hours, ROS levels dropped approximately 2.6-fold (Fig. 3.21; $T_2 = 11.808$, $P < 0.001$; paired T-test). To test whether the acetate supplementation was simply interfering with the activation of H_2DCF-DA, WT cells were treated with antimycin A (final concentration 50 nM) after 41h of growth and re-analysed for ROS accumulation. ROS levels were elevated in the same manner regardless of acetate supplementation (Fig. 3.22), indicating that the acetate supplementation was not interfering with the activation of H_2DCF-DA. Nevertheless, to further investigate the affect of potassium acetate on ROS accumulation in Δ*cox4* cells, spotting assays were conducted to assess their sensitivity to exogenous peroxide when supplemented with potassium acetate. YPD O/Ns of the WT and Δ*cox4* strains were inoculated to $OD_{600} \approx 0.1$ in sterile MQ water and spotted in biological and technical duplicate onto YPD plates +/- 1 % Kac and +/- 2 mM hydrogen peroxide (see section 2.9 for further methodological details). The plates were then incubated at 30^{o}C for 72 h and imaged using a Samsung Galaxy A70 smart phone. As expected, Δ*cox4* cells were far more sensitive to exogenous peroxide than WT cells (Fig. 3.23A, B). However, KAc supplementation did not restore WT-levels of peroxide sensitivity in Δ*cox4* cells, as it apparently did with regards to ROS accumulation, and instead elicited only a partial recovery (Fig. 3.23B, D). Though, importantly, this recovery was not likely due to KAc simply promoting growth regardless of the strain background, as there appeared to be a slight growth impairment in cultures grown on YPD + 1% KAc plates relative those grown on YPD control plates (Fig. 3.23 A, C).

Overall, despite the slight discrepancy between ROS levels as measured using H_2DCF-DA and peroxide resistance, these data strongly suggest a link between ROS accumulation, acetyl-CoA metabolism, and histone acetylation in Δ*cox4* cells.

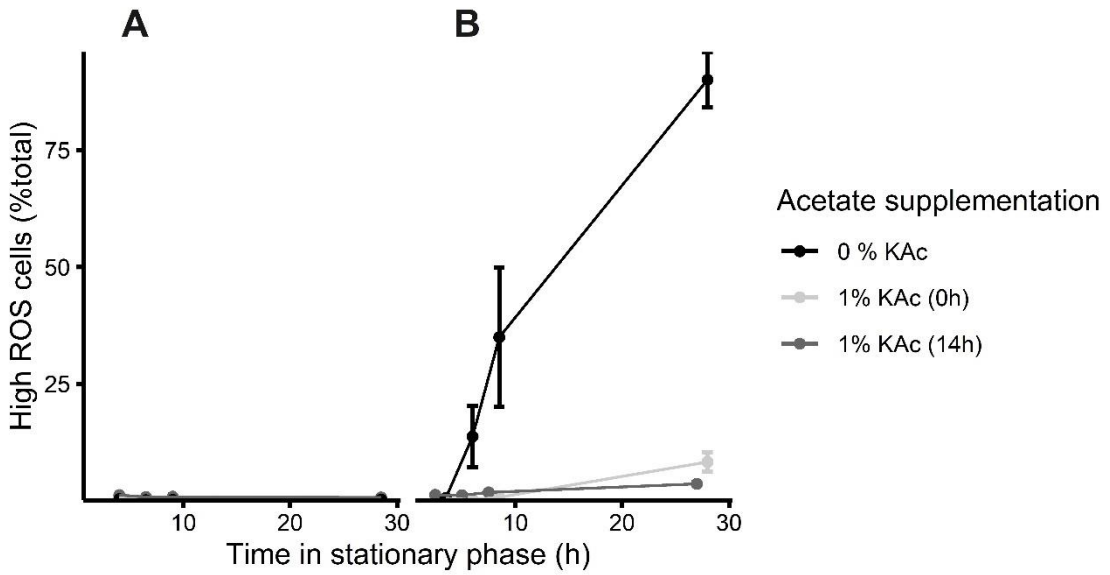

Fig. 3.20. ROS accumulation (proportion of total cells showing high ROS levels; calculated according to section 2.6 and Fig. 2.1) over time in WT (**A**) and Δ*cox4* (**B**) cells untreated with potassium acetate (0% KAc, black line), treated at the point of inoculation with potassium acetate (1% KAc [0h]; light grey line), or treated upon entry into SP with potassium acetate (1% KAc [14h]; dark grey line). To account for variability in the exponential growth rate between samples, the data have been standardised using the time at which each strain was observed to enter SP. ROS accumulation was measured in live cells using a BD Accuri™ C6 Plus flow cytometer using the ROS dye H_2DCF-DA in conjunction with the necrosis-indicator dye propidium iodide. 10000 cells per sample were analysed. Data are means ± SEM of three biological replicates.

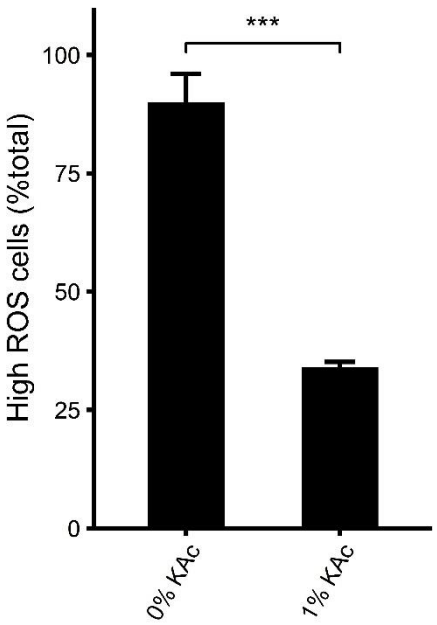

Fig. 3.21. ROS accumulation (% of total cells showing high ROS levels; calculated according to section 2.6 and Fig. 2.1) in Δ*cox4* cells after 41 h of growth in YPD (0% KAc) and after an additional 2 h of growth proceeding supplementation with potassium acetate (final concentration 1% w/v; 1% KAc). ROS accumulation was measured in live cells using a BD Accuri™ C6 Plus flow cytometer using the ROS dye H_2DCF-DA in conjunction with the necrosis-indicator dye propidium iodide. 10000 cells per sample were analysed. Data are means ± SEM of three paired biological replicates. Annotations represent the results of a paired t-test; ***, $P < 0.001$.

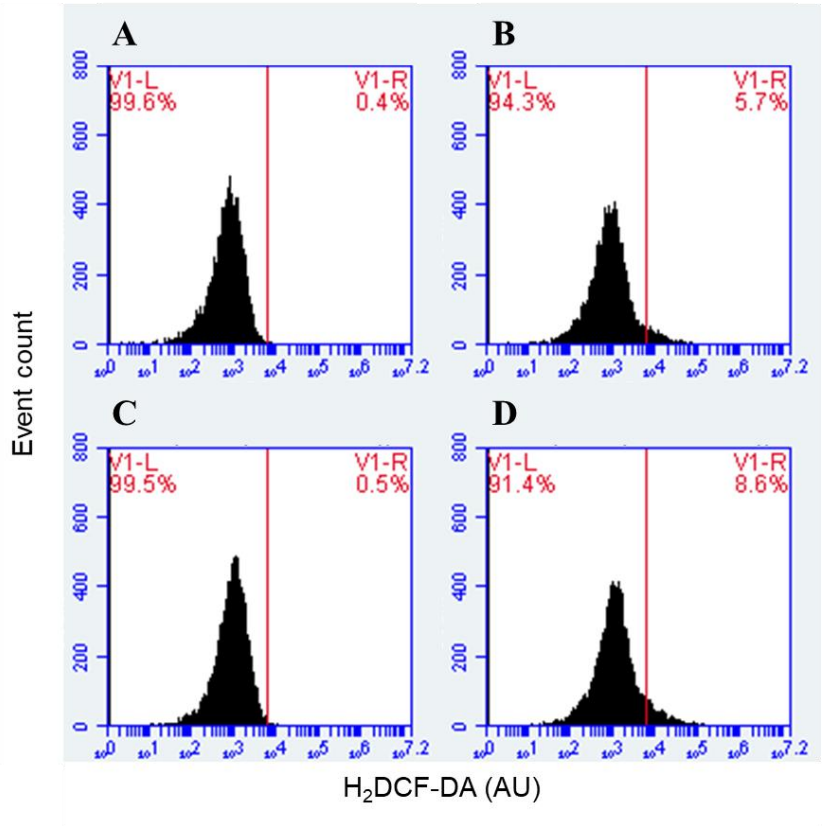

Fig. 3.22. A, B, Representative histograms of ROS accumulation (H_2DCF-DA signal; arbitrary units) in WT cells incubated in YPD media for 41h before (**A**) and after (**B**) treatment with antimycin A (final concentration 50 nM). **C, D,** Representative histograms of ROS accumulation in WT cells incubated in YPD + 1% KAc media for 41h before (**C**) and after (**D**) treatment with antimycin A (final concentration 50 nM). ROS accumulation was measured using a BD Accuri™ C6 Plus flow cytometer with the ROS dye H_2DCF-DA. 10000 cells per sample were analysed. The vertical line was placed after the maximum H_2DCF-DA signals observed in samples **A** and **B**. The annotations to the left and right of the vertical line represent the percentage of cells falling in that area.

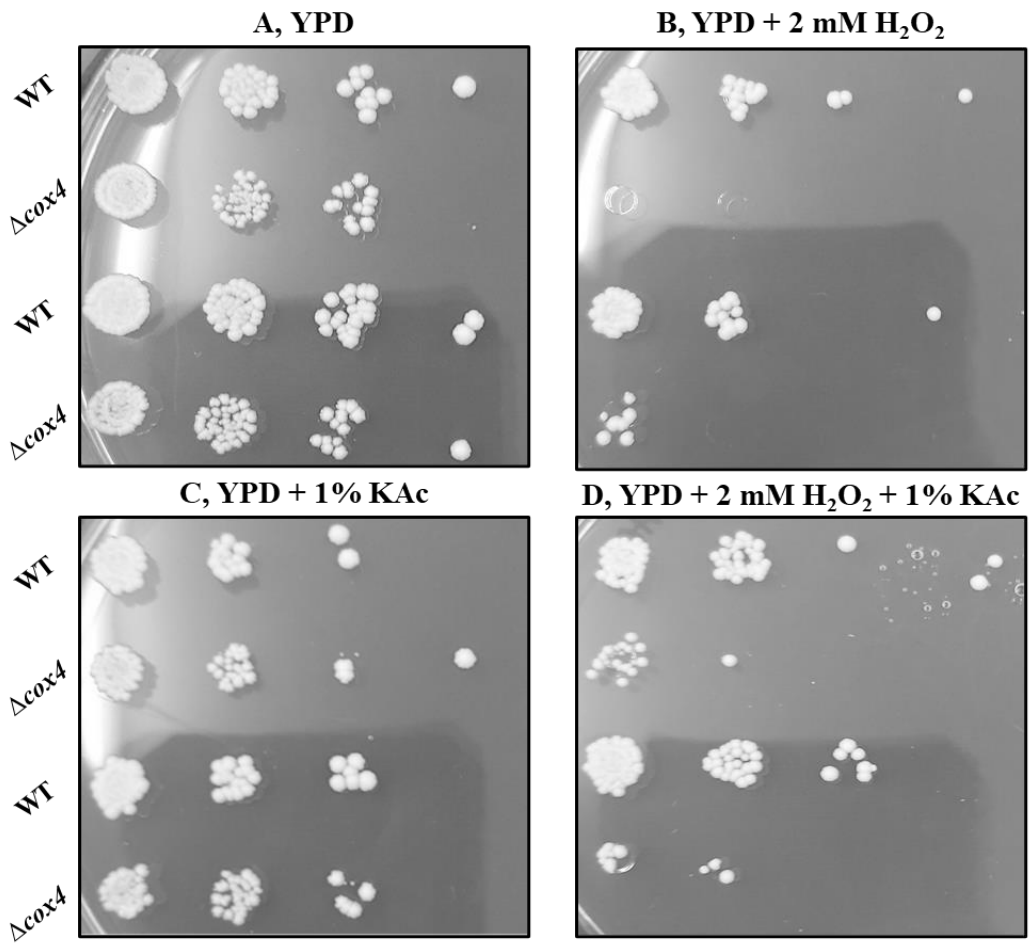

Fig. 3.23. Growth of WT and Δ*cox4* cultures on YPD (**A**), YPD + 2 mM H_2O_2 (**B**), YPD + 1 % potassium acetate (KAc; **C**) and YPD + 2 mM H_2O_2 + 1 % KAc (**D**) plates. Cultures were inoculated to $OD_{600} \approx 0.1$ in sterile water and spotted in serial ten-fold dilutions onto YPD plates +/- KAc and +/- H_2O_2. 1, no dilution (starting $OD_{600} \approx 0.1$); 0.1, ten-fold dilution; 0.01, 100-fold dilution; 0.001, 1000-fold dilution. The plates were incubated in a 30°C stationary incubator for 72 h prior to imaging with a Samsung Galaxy A70 smart phone. Spotting assays were conducted in biological (shown here) and technical duplicates; the data presented here are representative of those technical duplicates. See section 2.9 for further methodological details.

4. Discussion

4.1. The loss of Cox4p is associated with downregulated acetyl-CoA biosynthesis

The data from section 3.1 clearly demonstrate altered acetyl-CoA biosynthesis in Δ*cox4* cells. While it is important to note that the method employed here for the measurement of cellular acetyl-CoA levels was able to detect a moderate, but nevertheless non-significant, reduction in acetyl-CoA levels between Δ*cox4* and WT cells, this is very likely due to the variability in the detection method, as certain contaminants such as free CoA and succinyl-CoA, for example, can interfere with the PicoProbe™ fluorophore. More precise measurements such as Liquid chromatography-tandem mass spectrometry, for example, have shown that respiratory-incompetent p^0 cells show undetectable levels of acetyl-CoA when deprived of glucose (Friis et al., 2014). Considering many studies have demonstrated the strong compartmentalisation of acetyl-CoA metabolism in *S. cerevisiae*, the requirement of the ATP-dependent PDH bypass (requiring *ACS1*/*ACS2*) for nucleocytosolic acetyl-CoA production, and the cruciality of the ETC for ATP production during SP, it is highly likely that a similar degree of acetyl-CoA depletion occurs Δ*cox4* cells (Takahashi et al., 2006). With regards to p^0 cells, the acetyl-CoA depletion observed following glucose deprivation was accompanied by a drastically reduced ATP pool (Friis et al., 2014). However, in the case of Δ*cox4* cells, whether a similar ATP deficit occurs during SP is unknown, though their lack of respiratory capacity makes it highly likely. Therefore, future experiments should aim to re-examine acetyl-CoA levels in Δ*cox4* cells using a more robust method and should attempt to couple these measurements to measurements of cellular ATP levels. Furthermore, these measurements need to be tied to the histone acetylation state, so experiments must be conducted to probe the levels of acetylated histone lysine residues in Δ*cox4* cells during SP.

Interestingly, the data of Gibney et al. (2019) show that even if Δ*cox4* cells phenocopy p^0 cells with respect to acetyl-CoA depletion, ATP is unlikely to be the only causal factor. *ACS2* underwent a marked downregulation in Δ*cox4* upon their entry into SP relative to WT cells, and, similarly, the expression of *ACS1*, which is derepressed upon glucose exhaustion, did not reach the same level as it did in WT cells.

Downregulation of *ACS2* during diauxic shift has been documented previously in WT cells growing under normal conditions (CM + 2% glucose), so the downregulation of *ACS2* in Δ*cox4* cells is not altogether surprising. As such, it is interesting that Gibney et al. (2019) uncovered constitutive *ACS2* expression throughout SP in WT cells, which also occurs under conditions of caloric restriction (Wierman et al., 2017). However, the striking differences in the expression of the Cat8p targets *ACS1*, *ACH1* and *ADY2*, between Δ*cox4* cells and WT cells, are likely much more important with regards to acetyl-CoA depletion. The activity of Cat8p is controlled by the SNF1 complex, a master regulator of metabolism in *S. cerevisiae* and a homolog of the mammalian AMPK complex. The SNF1 complex mediates the transcriptional and metabolic changes that occur during the diauxic shift, when glucose is depleted and cells begin to favour the catabolism of acetate and ethanol. Therefore, aberrant SNF1 signalling in Δ*cox4* cells could be implicated in the absence of Cat8p-target induction during SP in these cells. An inactive SNF1 complex could contribute to acetyl-CoA depletion via this mechanism, but it could also further deplete acetyl-CoA in other ways such as failing to inhibit the acetyl-CoA carboxylase Acc1p, which converts acetyl-CoA to malonyl-CoA in the first step of fatty acid synthesis. During the diauxic shift SNF1 is activated by ADP, which binds to the Snf4p subunit and prevents the dephosphorylation of Tyr210 by Glc7p, thereby preventing the inactivation of SNF1. As such, it is interesting to note that *ACS1* and *ACH1* do not completely fail to be induced upon SP entry, but instead undergo what resembles a partial induction. It is possible that this too may be related to defective energy transduction and depletion of adenylate nucleotides in Δ*cox4* cells. With no way to replenish ATP in SP thanks to their defective ETC, Δ*cox4* cells could quickly deplete their stores of ATP and ADP, and thereby fail to properly activate the SNF1 complex. With this in mind it is important to note that the simultaneous activation of the SNF1 complex and the RTG pathway allowed for the full rescue of ATP levels, acetyl-CoA levels and histone acetylation in p^0 cells (Friis et al., 2014). As such, it is clear that an investigation of cellular ATP and ADP levels and the activity of the SNF1 complex in Δ*cox4* cells ought to be conducted in the future.

4.2. Disrupting acetyl-CoA metabolism does not appear to alter ROS accumulation

Despite the observed links between the loss of Cox4p and altered acetyl-CoA metabolism, directly impairing acetyl-CoA metabolism in various ways appeared to have no impact on ROS accumulation. The deletion of *MPC1* or *ACH1* elicited only small increases in ROS accumulation, consistent with the available literature which shows that the production of superoxide in Δ*mpc1* and Δ*ach1* cells only reaches high levels late in chronological ageing (Eisenberg et al., 2014; Orlandi et al., 2014, 2012). Regardless, this is consistent with the hypothesis regarding acetyl-CoA depletion and Yno1p-mediated ROS accumulation in Δ*cox4* cells, as both *MPC1* and *ACH1* deletion mutants accumulate extracellular acetate, show higher ACS activity and display higher levels of histone H3 acetylation (Eisenberg et al., 2014). The most surprising observations were that the deletion of neither *ACS1* nor *ACS2* appeared to have any effect on ROS accumulation. This could indicate that ROS accumulation is not related to acetyl-CoA metabolism in Δ*cox4* cells, and that it instead involves other processes, perhaps alterations in the activities of the KAT and KDAC complexes. A better explanation, however, might relate to the fact that this study utilised complex media for most experiments. Complex media, such as YPD, may not be fully devoid of carnitine, and therefore cells may utilise this carnitine for the transport of acetyl-CoA from the peroxisome to the cytosol. In Δ*acs1* and tet-*ACS2* cells, this transport may provide sufficient levels of acetyl-CoA for histone acetylation, and therefore will not cause the dissociation of Bdf1p from hypoacetylated histones and the consequent processes leading to elevated ROS production by Yno1p. The influence of exogenous carnitine in complex media could also explain the inconsistencies reported in the literature regarding the growth phenotype of Δ*acs1* cells, with some studies such as Chen et al. (2012) appearing to convincingly demonstrate the requirement of *ACS1* for growth on non-fermentable carbon sources, and others showing that Δ*acs1* cells are capable of growth on both fermentable and non-fermentable carbon sources, albeit with a prolonged lag phase (Van Den Berg and Steensma, 1995). Other phenotypes of acetyl-CoA metabolic mutants can also be strongly influenced by exogenous carnitine. For example, in chronological ageing experiments using synthetic minimal media, Δ*mpc1* cells were shown to accumulate high levels of acetate and $O_2^{\bullet -}$ and show a

substantial reduction in lifespan. When supplemented with exogenous carnitine, however, acetate accumulation, $O_2^{\bullet-}$ accumulation and longevity all reverted to WT levels (Eisenberg et al., 2014; Orlandi et al., 2014). Therefore, a straightforward starting point for future experiments will be to re-measure ROS accumulation in Δ*acs1* and tet-*ACS2* cells in synthetic minimal medium. It will also be interesting to examine precisely how the phenotypes of these mutants change upon supplementation with carnitine.

4.3. ROS accumulation is elevated by the deletion of *NGG1* or *HDA2*

Despite the lack of ROS accumulation in Δ*acs1* and tet-*ACS2* cells, the majority of the KAT and KDAC mutants displayed at least a slight elevation in ROS accumulation relative to the WT strain. However, two mutants stood out from the rest: Δ*ngg1* and Δ*hda2*, both in terms of their ROS accumulation and, in the case of Δ*hda2* cells, their respiratory phenotype. Intriguingly, both *NGG1* and *HDA2* encode structural subunits of their respective KAT and KDAC complexes. This study clearly demonstrated that *NGG1* and *HDA2* deletion mutants accumulated higher levels of ROS than mutants lacking the catalytic subunits of their respective KAT and KDAC complexes (Gcn5p and Hda1p, respectively). This appears to suggest that ROS accumulation in Δ*hda2* and Δ*ngg1* cells is not related to the abolition of the activity of their respective KAT and KDAC subunits but is instead related to their roles outside of these complexes.

This is highly likely for Δ*hda2* cells, as the absence of either Hda1p, Hda2p or Hda3p results in negligible Hda1C deacetylase activity (Wu et al., 2001). There has been little research done on the unique roles of these subunits, but Kaluarachchi Duffy et al. (2012) conducted a synthetic-dosage-lethal (SDL) interaction screen to examine how SDL interactions differ between *HDA1*, *HDA2* and *HDA3* deletion mutants. Their research demonstrated that approximately 55% of the interactions were unique to each subunit, suggesting they have widespread roles independent of their association in Hda1C. Furthermore, many of the SDL interactions in Δ*hda2* cells involved peroxisome biogenesis or maintenance, and further investigation of peroxisomal integrity in these cells revealed a strong defect in protein import. Additionally, while there appears to be no literature regarding ROS accumulation in either Δ*hda2* or Δ*ngg1* cells, previous research has demonstrated that the deletion of *HDA2* conferred greater sensitivity to hydrogen peroxide than the deletion of either *HDA1* or *HDA2*, which accords with

the ROS accumulation data produced by this study. Considering the importance of the peroxisomes as a source of ROS (see section 1.4), they may be a promising starting point to investigate ROS accumulation in Δ*hda2* cells.

With regards to Ngg1p, there is no similar research into its roles outside of the Gcn5p-containing KAT complexes. However, ROS accumulation in the *NGG1* deletion mutant may related to the specific effects of Ngg1p on the KAT activity of Gcn5p. Both Ngg1p and Ada2p, another subunit of the Gcn5p-containing KAT complexes, appear to greatly expand the range of lysine acetylations conducted by Gcn5p. Monomeric Gcn5p was shown to acetylate only histone H3 K14, whereas the introduction of Ada2p (Ada2-Gcn5 double complex) expanded the range of lysine acetylation to include H3 K18, and the further introduction of Ngg1p (Ada2-Ngg1-Gcn5 triple complex) expanded the range of lysine acetylation to also include H3 K9 and H3 K23 (Balasubramanian et al., 2002). Furthermore, the loss of Ngg1p may impact nonhistone protein acetylation by Gcn5p as well, as its absence appears to still allow for the association of Ada2p with Gcn5p, producing a less abundant subcomplex which is unable to maintain balanced levels of nonhistone protein acetylation (Rössl et al., 2019). From this work it is clear than an interesting path of research will be to see if the deletion of *NGG1* results in altered, but not absent, patterns of histone acetylation, how these patterns differ from those elicited by the deletion of *GCN5*, and whether these differences underlie the elevated ROS accumulation observed in Δ*ngg1* cells. A relatively straightforward way to investigate the latter question will be to introduce mutations in the differentially-acetylated lysine residues which mimic constitutive acetylation (lysine to glutamate) or prevent acetylation (lysine to arginine), to see how altering the acetylation state of these residues impacts ROS accumulation.

In the future, a better way to screen for KAT and KDAC complexes (or subcomplexes) which may be involved in ROS accumulation in Δ*cox4* cells, may be to screen mutants lacking *COX4* along with various KAT/KDAC complexes. Given that ROS accumulation in Δ*cox4* cells was proposed to be related to acetyl-CoA depletion and concomitant histone hypoacetylation, inhibiting KAT activity in these cells should cause a synthetic growth defect, whereas inhibiting KDAC activity should ameliorate their ROS accumulation and improve their fitness. This could be expanded to include mutants deficient

in more than one KAT/KDAC complex, which, thanks to the redundancy between the KAT/KDAC complexes, will likely prove a more powerful approach to link KAT/KDAC activity to ROS accumulation in Δ*cox4* cells.

4.4. Acetyl-CoA may underlie gene expression changes in Δ*pde2* cells treated with cAMP

As outlined in section 4.1, this study clearly demonstrated that the loss of Cox4p causes the downregulation of many genes associated with acetyl-CoA metabolism. While this should be coupled to direct examination of the histone acetylation state of Δ*cox4* cells in the future, the computational approach employed in this study utilising the YHMI in conjunction with GO-SLIM nevertheless provided a good indication that acetylation is a key regulator of gene expression in cells lacking Cox4p. Though it is important to note that this study had to infer this indirectly using gene expression data from Δ*pde2* cells treated with cAMP, a condition which induces a significant decline in *COX4* transcript number and greatly elevates ROS accumulation (Leadsham and Gourlay, 2010). Therefore, any analysis will be complicated by the fact that cAMP is likely to induce many other cellular changes independent of the loss of Cox4p.

The analysis of gene expression data from Δ*pde2* cells showed that genes downregulated by cAMP treatment were generally enriched for acetylated histone lysine residues in the coding regions and, in the case of genes encoding mitochondrial proteins, the promoters. Since histone acetylation is strongly correlated with active transcription (Pokholok et al., 2005), this indicates that cAMP treatment induces a hypoacetylation phenotype in Δ*pde2* cells, which may be due to the loss of Cox4p downregulating acetyl-CoA biosynthesis as is suggested in section 4.1. The observation that many of these acetylated lysine residues were also binding sites for Bdf1p (H4 K8ac, K12ac and K16ac in particular), provides additional support for the pre-eminence of CIV dysfunction in inducing these changes, since in Δ*cox4* cells Bdf1p is observed to associate with the mitochondria and is essential for Yno1p-mediated ROS production (see section 1.4.2).

The YHMI analysis of gene expression data from Δ*pde2* cells was contrasted with an identical analysis of gene expression data from Δ*bdf1* and Mut-*BDF1* cells. This comparison indicated that Δ*bdf1* cells phenocopy cAMP-treated Δ*pde2* cells with respect to histone hypoacetylation. Both mutants showed similar patterns of acetylation enrichment, especially of the Bdf1p binding sites H4 K5ac, K8ac, K12ac, H3 K14ac and H2A K5ac, in the coding regions of downregulated mitochondrial and non-mitochondrial genes. This again points to the involvement of Bdf1p in the phenotype of cAMP-treated Δ*pde2* cells, indicating that the cause of their elevated ROS accumulation may be the same mechanism of Yno1p-mediated ROS production occurring in Δ*cox4* cells. The observation that genes downregulated by the loss of Bdf1p were enriched for its binding sites also serves as validation of the efficacy of the YHMI for this kind of analysis. Bdf1p is associated with the basal transcription factor TFIID, so one would expect the loss of Bdf1p to downregulate genes enriched for its binding sites. In this regard the fact that lysine acetylation enrichment was observed in the coding regions and not the promoters may seem strange, but, surprisingly, previous studies have indicated that Bdf1p is not localised to the promoters (Matangkasombut and Buratowski, 2003). It could, however, still promote active transcription via its other known functions, such as preventing the spread of heterochromatin to the sub-telomeric regions of chromosomes (Ladurner et al., 2003).

The analysis of gene expression data using the YHMI in conjunction with GO-SLIM also revealed some unexpected insights that were unrelated to acetylation enrichment. Chief among these was the observation that both mitochondrial and non-mitochondrial DR genes from cAMP-treated Δ*pde2* cells were enriched in binding sites for RSC complex subunits. Whether or not this relates to the loss of Cox4p or some other effect brought about by cAMP treatment, this indicates that the gene expression changes and potentially the ROS accumulation observed in cAMP-treated Δ*pde2* cells may be related to the action of the RSC complex. The RSC complex is one of two SWI/SNF-type chromatin remodelling complexes in yeast, with diverse functions including the regulation of transcription, DNA repair, chromosome segregation, and mitochondrial functions, the latter of which it regulates in part via the activation of the HAP complex (Imamura et al., 2015). As such, the role of the RSC complex in cAMP-treated Δ*pde2* cells could prove an interesting future avenue of research.

The GO-SLIM analysis of Δ*bdf1* and Mut-*BDF1* cells also revealed interesting insights into the role of Bdf1p outside of its acetyl-lysine binding capacity. There were slight differences in the enrichment of cellular component terms between Δ*bdf1* and Mut-*BDF1* cells, indicating that Bdf1p may have unique functions which it may be able to fulfil regardless of the acetyl-lysine binding capacity of its bromodomains. This accords with the available literature, as the temperature sensitivity of Δ*bdf1* cells can be reversed by the expression of a mutant Bdf1p lacking acetyl-lysine binding capacity (Matangkasombut and Buratowski, 2003). Moreover, García-Oliver et al. (2017) observed that Δ*bdf1* cells were unable to grow on acetate or glycerol at 30°C, but observed no such respiratory defect in cells expressing Bdf1p with mutated or deleted bromodomains. In general, the functions of Bdf1p independent of its lysine binding capacity has been severely understudied, so in the future these functions should be elucidated in detail. This could begin simply with looking at how the localisation of Bdf1p changes under different growing conditions (fermentative vs. respiratory, for example) and under different stresses.

4.5. Boosting acetyl-CoA biosynthesis reduces ROS accumulation in Δ*cox4* cells

ROS accumulation was diminished in Δ*cox4* cells by two interventions which likely increased the nucleocytosolic pool of acetyl-CoA: 1, the overexpression of *ACS2* in Δ*cox4* cells, and 2, treatment of Δ*cox4* cells with potassium acetate. Both interventions reduced time-dependent ROS accumulation in Δ*cox4* cells, which supports the notion that acetyl-CoA depletion underlies Yno1p-mediated ROS accumulation by eliciting the dissociation of Bdf1p from hypoacetylated histones. While the overexpression of *ACS2* appeared to slightly delay ROS accumulation in Δ*cox4* cells (future experiments should measure this over a longer time period to see if cells overexpressing *ACS2* eventually "catch up" with non-transformed cells), supplementation with potassium acetate appeared completely to restore ROS accumulation to WT levels, with only a slight elevation observed after 41 h of growth. This provides very strong evidence for a link between the histone acetylation state and Yno1p-mediated ROS production in Δ*cox4* cells, as supplementation with potassium acetate at the same concentration utilised in this study allowed respiratory-incompetent p^0 cells to maintain WT-levels of

H4 acetylation following glucose depletion (Friis et al., 2014). Future experiments will need to confirm whether the treatment of Δ*cox4* cells with potassium acetate also boosts H4 acetylation during SP, and given that Bdf1p-bromodomains preferentially bind acetylated lysine residues in histone H3 and H4 (in particular H4 K5, K8, K12 and K16), it is also crucial to investigate how acetate supplementation effects the localisation of Bdf1p. If these experiments reveal that Bdf1p does not associate with the mitochondria in acetate-supplemented Δ*cox4* cells during SP, this will provide very strong evidence that the impaired acetyl-CoA metabolism observed in Δ*cox4* cells causes their elevated accumulation of ROS.

After establishing that potassium acetate supplementation appeared to abolish ROS accumulation in Δ*cox4* cells, it was disappointing to uncover that their peroxide sensitivity was not reduced to the same extent. However, this could be due to acetate supplementation decreasing the viability of Δ*cox4* cells, resulting in a growth defect that masks the antioxidant phenotype effects of potassium acetate. The observation that cells growing on YPD + 1% KAc plates grew slightly worse when compared to cells growing on YPD control plates seems to support this. Similar findings are discussed by Friis et al. (2014), who found that supplementing p^0 cells with 1% potassium acetate after glucose removal results in a sharp decline in their viability. This decline observed in p^0 cells was accompanied by a decline in cellular ATP concentration, likely because respiratory-incompetent cells cannot metabolise acetate and therefore instead utilise it in other metabolic pathways that expend ATP, such as the PDH bypass route of acetyl-CoA biosynthesis. This may also occur in Δ*cox4* cells, so future experiments should investigate how their viability is altered by potassium acetate supplementation.

4.6. Conclusions and future directions

This study investigated a hypothesised metabolic model of ROS accumulation (see section 1.8). The model proposed that the loss of the CIV subunit Cox4p would cause a severe energy deficit during SP, resulting in a reduced nucleocytosolic pool of acetyl-CoA, concomitant histone acetylation, and the consequent dissociation of Bdf1p from the hypoacetylated histones. Bdf1p would then associate with the mitochondria, alongside Ras2p, during SP, thereby inducing a chain of events which would prevent the degradation of Yno1p and greatly elevate ROS production by this enzyme (Fig. 1.2A).

Overall, the results of this study and the literature examined herein lend support to this hypothesis. However, as outlined above, this study requires further refinement before the relationship between acetyl-CoA and Yno1p-mediated ROS accumulation can be firmly established. There are many potential avenues to follow in this regard, such as the use of more sensitive techniques to assess cellular acetyl-CoA levels, the investigation of the histone acetylation state in Δ*cox4* cells, and the examination of KAT/KDAC subunit deletions which cause synthetic growth defects in Δ*cox4* cells. However, two lines of inquiry come to mind which will likely yield far more interesting and conclusive results than any of those previously mentioned. The first would be a relatively simple experiment, and would involve mutating H4 K5, K8, K12 and K16 to glutamate residues, which mimic constitutive acetylation, in Δ*cox4* cells, and examining how this affects the localisation of Bdf1p and ROS accumulation. Mutation of all four lysine residues may not be necessary but would be a more powerful design, as Bdf1p binds with much greater affinity to tetra-acetylated H4 than it does to mono-acetylated forms (Matangkasombut and Buratowski, 2003). This experiment would directly investigate whether the association of Bdf1p with the mitochondria in Δ*cox4* cells requires histone hypoacetylation, and it would do so in such a way as to avoid the numerous other metabolic changes that increasing the cellular level of acetyl-CoA likely produces. The second line of inquiry would be much larger in scale. As mentioned above, Friis et al. (2014) demonstrated that constitutive activation of the SNF1 complex and RTG pathway allowed for the full rescue of ATP levels, acetyl-CoA levels and histone acetylation in p^0 cells. It seems possible that this is accomplished by inducing the expression of *ACS1* (upregulated by SNF1) along with the glyoxylate cycle genes (upregulated by the RTG pathway), thus re-routing metabolism towards the peroxisomes and cytoplasm, perhaps in a way similar to that outlined in Fig. 4.1. Whether simultaneous activation of the SNF1 and RTG pathways can rescue ROS accumulation and improve lifespan in Δ*cox4* cells ought to be determined, especially if future research indicates that ROS accumulation in other organisms is related to acetyl-CoA metabolism. Because if this is the case, then there must be attempts made to identify therapeutic strategies to revert the cellular capacity for acetyl-CoA biosynthesis to normal levels, and such attempts must first elucidate how metabolism needs to be reprogrammed to achieve this.

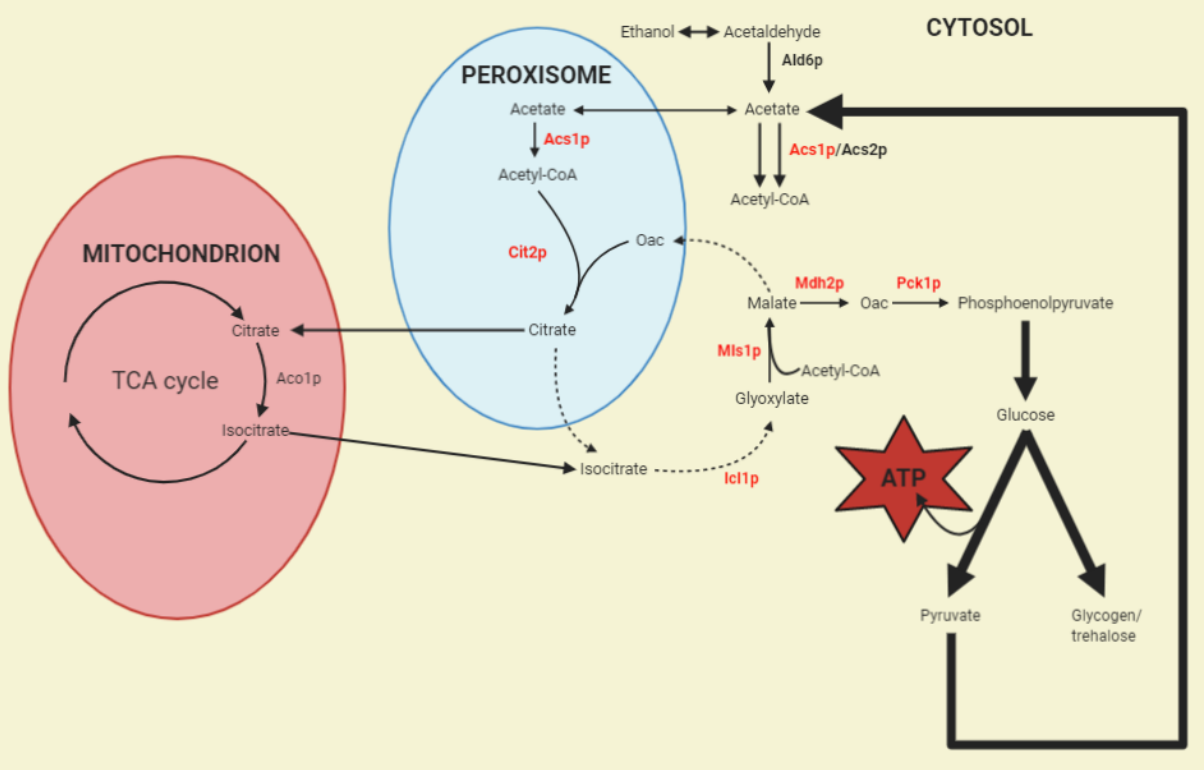

Fig. 4.1. Schematic representation of one possible metabolic route which could allow respiratory-incompetent Δ*cox4* and p^0 cells to utilise non-fermentable carbon sources for growth, the maintenance of histone acetylation, etc. Enzymes coloured red are those expected to be upregulated upon simultaneous activation of the SNF1 and RTG pathways. Figure adapted from Chen et al. (2012). Ald6p, acetaldehyde dehydrogenase; Acs1p, acetyl-CoA synthetase 1; Acs2p, acetyl-CoA synthetase 2; Cit2p, citrate synthase 2; Aco1p, aconitase; Icl1p, isocitrate lyase 1; Mls1p, malate synthase; Mdh2p, malate dehydrogenase; Pck1p, phosphoenolpyruvate carboxykinase. Multi-step metabolic pathways are indicated by bold lines. Dashed lines represent reactions occurring in locations not identified by Chen et al. (2012).

Even if these experiments firmly establish that ROS accumulation in Δ*cox4* cells is regulated metabolically via the levels of acetyl-CoA, there will still be many unanswered questions with regards to Yno1p-mediated ROS accumulation. Nevertheless, establishing a metabolic cause for this process will be a good starting point to further develop our understanding of the conditions which cause cells

to accumulate harmful levels of ROS. Furthermore, if this model proves accurate, it will hopefully spur others to investigate the relationship between metabolic processes, PTMs and ROS accumulation in other organisms.

5. Supplementary Materials

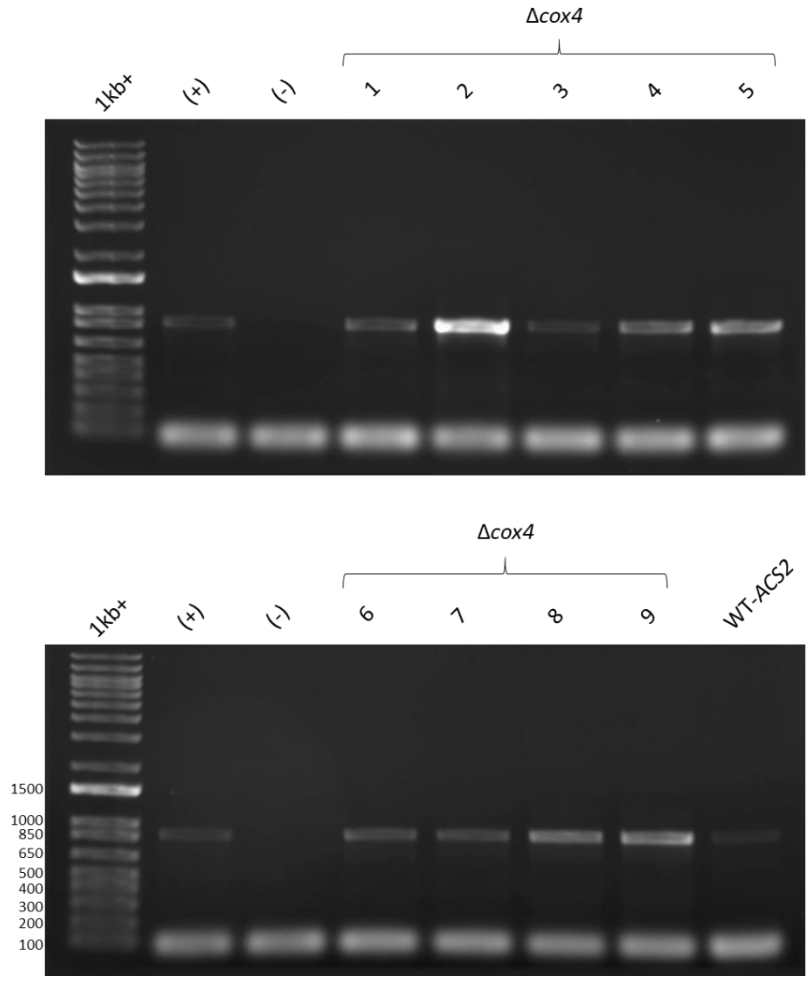

Fig. A.1. Confirmation of pAG306-*ACS2* transformations. Genomic DNA was extracted from WT and Δ*cox4* transformants growing on SD-URA media according to section 2.4. DNA extracts were subject to PCR reactions according to Table 2.4-2.5 using a forward primer specific to the AmpR selection marker in the pAG306 vector backbone and a reverse primer specific to a region of chromosome 1 850 bp downstream of the pAG306 integration site. The PCR reactions were then run on a 0.8% agarose gel at 120 V for 30 min before being visualised using a SynGene GBox XX6 imaging system and captured using GeneSys imaging software.The annotations to the left of the figure represent the size of the DNA ladder in bp (Invitrogen 1kb+ DNA ladder). The annotations above the figure are colony codes: (+), WT cells transformed with the pAG306 empty vector, acting as a positive control; (-), non-transformed WT cells, acting as a negative control; 1-9, Δ*cox4-ACS2* transformants; WT, WT-*ACS2* transformant.

Table A.1. Significantly (P < 0.05) enriched/depleted histone acetylation sites in the promoter regions of downregulated (DR) or upregulated (UR) non-mitochondrial genes in Mut-*BDF1* cells. The data presented here were produced using microarray data from Ladurner et al. (2003), analysed with the Yeast Histone Modification Identifier (YHMI; see section 2.8 and Wu et al. [2018] for further information).

Cell	Dataset	Name	Trend	P-value	Fold Enrichment	Observed Ratio (A/B)	Expected Ratio (C/D)
Mut-*BDF1*	DR	H4ac [H2O2]	Depleted	0.006	0.763	55/211 (26.07%)	2244/6572 (34.14%)
		H3K4ac	Depleted	0.018	0.752	40/211 (18.96%)	1656/6572 (25.20%)
		H3K18ac	Depleted	0.028	0.855	83/211 (39.34%)	3022/6572 (45.98%)
		H3K14ac	Depleted	0.036	0.872	91/211 (43.13%)	3250/6572 (49.45%)
	UR	H4ac	Depleted	< 0.001	0.473	21/82 (25.61%)	3559/6572 (54.15%)
		H3K18ac	Depleted	< 0.001	0.424	16/82 (19.51%)	3022/6572 (45.98%)

Table A.2. Significantly (P < 0.05) enriched/depleted histone acetylation sites in the coding regions of downregulated (DR) or upregulated (UR) non-mitochondrial genes in Mut-*BDF1* cells. The data presented here were produced using microarray data from Ladurner et al. (2003), analysed with the Yeast Histone Modification Identifier (YHMI; see section 2.8 and Wu et al. [2018] for further information).

Cell	Dataset	Name	Trend	P-value	Fold Enrichment	Observed Ratio (A/B)	Expected Ratio (C/D)
Mut-*BDF1*	DR	H4K5ac	Enriched	< 0.001	1.969	28/211 (13.27%)	443/6572 (6.74%)
		H4K12ac	Enriched	0.002	2.023	20/211 (9.48%)	308/6572 (4.69%)
		H4K8ac	Enriched	0.003	1.629	33/211 (15.64%)	631/6572 (9.60%)
		H3K18ac	Enriched	0.003	1.325	74/211 (35.07%)	1740/6572 (26.48%)
		H2AK5ac	Enriched	0.018	1.742	17/211 (8.06%)	304/6572 (4.63%)
		H3K27ac	Enriched	0.045	2.966	4/211 (1.90%)	42/6572 (0.64%)
	UR	H4ac	Depleted	< 0.001	0.574	25/82 (30.49%)	3491/6572 (53.12%)
		H3K14ac	Depleted	< 0.001	0.466	15/82 (18.29%)	2578/6572 (39.23%)

	H3K9ac	Depleted	0.001	0.462	10/82 (12.20%)	1734/6572 (26.38%)
	H3K18ac	Depleted	0.016	0.599	13/82 (15.85%)	1740/6572 (26.48%)
	H4K8ac	Enriched	0.023	1.778	14/82 (17.07%)	631/6572 (9.60%)
	H4K12ac	Enriched	0.037	2.082	8/82 (9.76%)	308/6572 (4.69%)

Table A.3. Significantly ($P < 0.05$) enriched/depleted histone acetylation sites in the promoter regions of downregulated (DR) or upregulated (UR) mitochondrial genes in Mut-*BDF1* cells. The data presented here were produced using microarray data from Ladurner et al. (2003), analysed with the Yeast Histone Modification Identifier (YHMI; see section 2.8 and Wu et al. [2018] for further information).

Cell	Dataset	Name	Trend	P-value	Fold Enrichment	Observed Ratio (A/B)	Expected Ratio (C/D)
Mut-*BDF1*	DR	H3K18ac	Depleted	0.027	0.680	15/48 (31.25%)	3022/6572 (45.98%)
	UR	H2AK5ac	Depleted	0.003	0.000	0/31 (0.00%)	1097/6572 (16.69%)
		H3K18ac	Depleted	0.017	0.561	8/31 (25.81%)	3022/6572 (45.98%)
		H3K9ac	Depleted	0.035	0.498	5/31 (16.13%)	2129/6572 (32.40%)

Table A.4. Significantly (P < 0.05) enriched/depleted histone acetylation sites in the coding regions of downregulated (DR) or upregulated (UR) mitochondrial genes in Mut-*BDF1* cells. The data presented here were produced using microarray data from Ladurner et al. (2003), analysed with the Yeast Histone Modification Identifier (YHMI; see section 2.8 and Wu et al. [2018] for further information).

Cell	Dataset	Name	Trend	P-value	Fold Enrichment	Observed Ratio (A/B)	Expected Ratio (C/D)
Mut-*BDF1*	DR	H3K23ac	Enriched	< 0.001	3.011	17/48 (35.42%)	773/6572 (11.76%)
		H4K8ac	Enriched	< 0.001	2.821	13/48 (27.08%)	631/6572 (9.60%)
		H2AK5ac	Enriched	0.001	3.603	8/48 (16.67%)	304/6572 (4.63%)
		H3K18ac	Enriched	0.003	1.731	22/48 (45.83%)	1740/6572 (26.48%)
		H4K12ac	Enriched	0.007	3.112	7/48 (14.58%)	308/6572 (4.69%)
		H4K5ac	Enriched	0.014	2.473	8/48 (16.67%)	443/6572 (6.74%)
		H4ac [H2O2]	Enriched	0.026	1.375	26/48 (54.17%)	2589/6572 (39.39%)
	UR	H3K14ac	Depleted	0.039	0.576	7/31 (22.58%)	2578/6572 (39.23%)
		H3K14ac [H2O2]	Enriched	0.048	1.343	20/31 (64.52%)	3158/6572 (48.05%)

References

Abrahám, E., Hourton-Cabassa, C., Erdei, L., Szabados, L., 2010. Methods for determination of proline in plants., in: Sunkar, R. (Ed.), Methods in Molecular Biology (Clifton, N.J.). Humana Press, Totowa, NJ, pp. 317–331. https://doi.org/10.1007/978-1-60761-702-0_20

Adachi, H., Fujiwara, Y., Ishii, N., 1998. Effects of oxygen on protein carbonyl and aging in Caenorhabditis elegans mutants with long (age-1) and short (mev-1) life spans. Journals Gerontol. - Ser. A Biol. Sci. Med. Sci. 53, 24–244. https://doi.org/10.1093/gerona/53A.4.B240

Andréasson, C., Ott, M., Büttner, S., 2019. Mitochondria orchestrate proteostatic and metabolic stress responses. EMBO Rep. 20, e47865. https://doi.org/10.15252/embr.201947865

Anisimov, V.N., Bakeeva, L.E., Egormin, P.A., Filenko, O.F., Isakova, E.F., Manskikh, V.N., Mikhelson, V.M., Panteleeva, A.A., Pasyukova, E.G., Pilipenko, D.I., Piskunova, T.S., Popovich, I.G., Roshchina, N. V., Rybina, O.Y., Saprunova, V.B., Samoylova, T.A., Semenchenko, A. V., Skulachev, M. V., Spivak, I.M., Tsybul'Ko, E.A., Tyndyk, M.L., Vyssokikh, M.Y., Yurova, M.N., Zabezhinsky, M.A., Skulachev, V.P., 2008. Mitochondria-targeted plastoquinone derivatives as tools to interrupt execution of the aging program. 5. SkQ1 prolongs lifespan and prevents development of traits of senescence. Biochem. 73, 1329–1342. https://doi.org/10.1134/S0006297908120055

Anisimov, V.N., Egorov, M. V., Krasilshchikova, M.S., Lyamzaev, K.G., Manskikh, V.N., Moshkin, M.P., Novikov, E.A., Popovich, I.G., Rogovin, K.A., Shabalina, I.G., Shekarova, O.N., Skulachev, M. V., Titova, T. V., Vygodin, V.A., Vyssokikh, M.Y., Yurova, M.N., Zabezhinsky, M.A., Skulachev, V.P., 2011. Effects of the mitochondria-targeted antioxidant SkQ1 on lifespan of rodents. Aging (Albany. NY). 3, 1110–1119. https://doi.org/10.18632/aging.100404

Aßkamp, M.R., Klein, M., Nevoigt, E., 2019. Involvement of the external mitochondrial NADH dehydrogenase Nde1 in glycerol metabolism by wild-type and engineered Saccharomyces cerevisiae strains. FEMS Yeast Res. 19, 26. https://doi.org/10.1093/femsyr/foz026

Baccolo, G., Stamerra, G., Damiano Pellegrino, C., Orlandi, I., Vai, M., 2018. Mitochondrial Metabolism and Aging in Yeast. Int. Rev. Cell Mol. Biol. 340, 1–33. https://doi.org/10.1016/bs.ircmb.2018.05.001

Baeza, J., Smallegan, M.J., Denu, J.M., 2016. Mechanisms and Dynamics of Protein Acetylation in Mitochondria. Trends Biochem. Sci. 41, 231–244. https://doi.org/10.1016/j.tibs.2015.12.006

Baile, M.G., Claypool, S.M., 2013. The power of yeast to model diseases of the powerhouse of the cell. Front. Biosci. 18, 241–278. https://doi.org/10.2741/4098

Balaban, R.S., Nemoto, S., Finkel, T., 2005. Mitochondria, oxidants, and aging. Cell 120, 483–495. https://doi.org/10.1016/j.cell.2005.02.001

Balasubramanian, R., Pray-Grant, M.G., Selleck, W., Grant, P.A., Tan, S., 2002. Role of the Ada2 and Ada3 transcriptional coactivators in histone acetylation. J. Biol. Chem. 277, 7989–7995. https://doi.org/10.1074/jbc.M110849200

Barnes, C.E., English, D.M., Cowley, S.M., 2019. Acetylation & Co: an expanding repertoire of histone acylations regulates chromatin and transcription. Essays Biochem. 63, 97–107. https://doi.org/10.1042/EBC20180061

Berdichevsky, A., Viswanathan, M., Horvitz, H.R., Guarente, L., 2006. C. elegans SIR-2.1 Interacts with 14-3-3 Proteins to Activate DAF-16 and Extend Life Span. Cell 125, 1165–1177. https://doi.org/10.1016/j.cell.2006.04.036

Bhaumik, S.R., Green, M.R., 2002. Differential Requirement of SAGA Components for Recruitment of TATA-Box-Binding Protein to Promoters In Vivo. Mol. Cell. Biol. 22, 7365–7371. https://doi.org/10.1128/mcb.22.21.7365-7371.2002

Bleier, L., Dröse, S., 2013. Superoxide generation by complex III: From mechanistic rationales to functional consequences. Biochim. Biophys. Acta - Bioenerg. https://doi.org/10.1016/j.bbabio.2012.12.002

Bouchez, C., Devin, A., 2019. Mitochondrial Biogenesis and Mitochondrial Reactive Oxygen Species

(ROS): A Complex Relationship Regulated by the cAMP/PKA Signaling Pathway. Cells 8, 287. https://doi.org/10.3390/cells8040287

Bouchez, C.L., Yoboue, E.D., De La Rosa Vargas, L.E., Salin, B., Cuvellier, S., Rigoulet, M., Duvezin-Caubet, S., Devin, A., 2020. “labile” heme critically regulates mitochondrial biogenesis through the transcriptional co-activator Hap4p in Saccharomyces cerevisiae. J. Biol. Chem. 295, 5095–5109. https://doi.org/10.1074/jbc.RA120.012739

Boveris, A., Oshino, N., Chance, B., 1972. The cellular production of hydrogen peroxide. Biochem. J. 128, 617–630. https://doi.org/10.1042/bj1280617

Brown, G.C., Borutaite, V., 2012. There is no evidence that mitochondria are the main source of reactive oxygen species in mammalian cells. Mitochondrion. https://doi.org/10.1016/j.mito.2011.02.001

Cai, L., Sutter, B.M., Li, B., Tu, B.P., 2011. Acetyl-CoA Induces Cell Growth and Proliferation by Promoting the Acetylation of Histones at Growth Genes. Mol. Cell 42, 426–437. https://doi.org/10.1016/j.molcel.2011.05.004

Cai, L., Tu, B.P., 2011. On acetyl-CoA as a gauge of cellular metabolic state. Cold Spring Harb. Symp. Quant. Biol. 76, 195–202. https://doi.org/10.1101/sqb.2011.76.010769

Carmo, C., Naia, L., Lopes, C., Rego, A.C., 2018. Mitochondrial Dysfunction in Huntington’s Disease, in: Nóbrega, C., de Almeida, L. (Eds.), Polyglutamine Disorders. Springer International Publishing, Cham, pp. 59–83. https://doi.org/10.1007/978-3-319-71779-1_3

Carrozza, M.J., Florens, L., Swanson, S.K., Shia, W.J., Anderson, S., Yates, J., Washburn, M.P., Workman, J.L., 2005. Stable incorporation of sequence specific repressors Ash1 and Ume6 into the Rpd3L complex. Biochim. Biophys. Acta - Gene Struct. Expr. 1731, 77–87. https://doi.org/10.1016/j.bbaexp.2005.09.005

Chen, C., Turnbull, D.M., Reeve, A.K., 2019. Mitochondrial Dysfunction in Parkinson’s Disease-Cause or Consequence? Biology (Basel). 8, 38. https://doi.org/10.3390/biology8020038

Chen, X.F., Kuryan, B., Kitada, T., Tran, N., Li, J.Y., Kurdistani, S., Grunstein, M., Li, B., Carey, M.,

2012. The Rpd3 core complex is a chromatin stabilization module. Curr. Biol. 22, 56–63. https://doi.org/10.1016/j.cub.2011.11.042

Chen, Y., Siewers, V., Nielsen, J., 2012. Profiling of cytosolic and peroxisomal acetyl-CoA metabolism in Saccharomyces cerevisiae. PLoS One 7, 42475. https://doi.org/10.1371/journal.pone.0042475

Chen, Y., Zhang, Y., Siewers, V., Nielsen, J., 2015. Ach1 is involved in shuttling mitochondrial acetyl units for cytosolic C2 provision in Saccharomyces cerevisiae lacking pyruvate decarboxylase. FEMS Yeast Res. 15, 1–8. https://doi.org/10.1093/femsyr/fov015

Cheng, C., Zhao, X., Zhang, M., Bai, F., 2016. Absence of Rtt109p, a fungal-specific histone acetyltransferase, results in improved acetic acid tolerance of Saccharomyces cerevisiae. FEMS Yeast Res. 16, 10. https://doi.org/10.1093/femsyr/fow010

Choudhary, C., Kumar, C., Gnad, F., Nielsen, M.L., Rehman, M., Walther, T.C., Olsen, J. V., Mann, M., 2009. Lysine acetylation targets protein complexes and co-regulates major cellular functions. Science (80-.). 325, 834–840. https://doi.org/10.1126/science.1175371

Eberharter, A., Sterner, D.E., Schieltz, D., Hassan, A., Yates, J.R., Berger, S.L., Workman, J.L., 1999. The ADA Complex Is a Distinct Histone Acetyltransferase Complex in Saccharomyces cerevisiae. Mol. Cell. Biol. 19, 6621–6631. https://doi.org/10.1128/mcb.19.10.6621

Eisenberg, T., Schroeder, S., Andryushkova, A., Pendl, T., Küttner, V., Bhukel, A., Mariño, G., Pietrocola, F., Harger, A., Zimmermann, A., Moustafa, T., Sprenger, A., Jany, E., Büttner, S., Carmona-Gutierrez, D., Ruckenstuhl, C., Ring, J., Reichelt, W., Schimmel, K., Leeb, T., Moser, C., Schatz, S., Kamolz, L.P., Magnes, C., Sinner, F., Sedej, S., Fröhlich, K.U., Juhasz, G., Pieber, T.R., Dengjel, J., Sigrist, S.J., Kroemer, G., Madeo, F., 2014. Nucleocytosolic depletion of the energy metabolite acetyl-coenzyme A stimulates autophagy and prolongs lifespan. Cell Metab. 19, 431–444. https://doi.org/10.1016/j.cmet.2014.02.010

Enjalbert, B., Parrou, J.L., Vincent, O., Francois, J., 2000. Mitochondrial respiratory mutants of Saccharomyces cerevisiae accumulate glycogen and readily mobilize it in a glucose-depleted

medium. Microbiology 146, 2685–2694. https://doi.org/10.1099/00221287-146-10-2685

Fedoseeva, I. V, Pyatrikas, D. V, Stepanov, A. V, Fedyaeva, A. V, Varakina, N.N., Rusaleva, T.M., Borovskii, G.B., Rikhvanov, E.G., 2017. The role of flavin-containing enzymes in mitochondrial membrane hyperpolarization and ROS production in respiring Saccharomyces cerevisiae cells under heat-shock conditions. Sci. Rep. 7. https://doi.org/10.1038/s41598-017-02736-7

Feng, Y., Li, W., Li, J., Wang, J., Ge, J., Xu, D., Liu, Y., Wu, K., Zeng, Q., Wu, J.W., Tian, C., Zhou, B., Yang, M., 2012. Structural insight into the type-II mitochondrial NADH dehydrogenases. Nature 491, 478–482. https://doi.org/10.1038/nature11541

Fiori, A., Mason, T.L., Fox, T.D., 2003. Evidence that synthesis of the Saccharomyces cerevisiae mitochondrially encoded ribosomal protein Var1p may be membrane localized. Eukaryot. Cell 2, 651–653. https://doi.org/10.1128/EC.2.3.651-653.2003

Friis, R.M.N., Glaves, J.P., Huan, T., Li, L., Sykes, B.D., Schultz, M.C., 2014. Rewiring AMPK and Mitochondrial Retrograde Signaling for Metabolic Control of Aging and Histone Acetylation in Respiratory-Defective Cells. Cell Rep. 7, 565–574. https://doi.org/10.1016/j.celrep.2014.03.029

Galdieri, L., Zhang, T., Rogerson, D., Lleshi, R., Vancura, A., 2014. Protein Acetylation and Acetyl Coenzyme A Metabolism in Budding Yeast. Eukaryot. Cell 13, 1472–1483. https://doi.org/10.1128/EC.00189-14

García-Oliver, E., Ramus, C., Perot, J., Arlotto, M., Champleboux, M., Mietton, F., Battail, C., Boland, A., Deleuze, J.F., Ferro, M., Couté, Y., Govin, J., 2017. Bdf1 Bromodomains Are Essential for Meiosis and the Expression of Meiotic-Specific Genes. PLoS Genet. 13. https://doi.org/10.1371/journal.pgen.1006541

Gaupel, A.C., Begley, T.J., Tenniswood, M., 2015. Gcn5 Modulates the Cellular Response to Oxidative Stress and Histone Deacetylase Inhibition. J. Cell. Biochem. 116, 1982–1992. https://doi.org/10.1002/jcb.25153

Gietz, R.D., Woods, R.A., 2002. Transformation of Yeast by the Liac/SS Carrier DNA/PEG Method.

Methods Enzymol. 350, 87–96.

Gladyshev, V.N., 2014. The free radical theory of aging is dead. Long live the damage theory! Antioxidants Redox Signal. 20, 727–731. https://doi.org/10.1089/ars.2013.5228

Gomes, F., Tahara, E.B., Busso, C., Kowaltowski, A.J., Barros, M.H., 2013. nde1 deletion improves mitochondrial DNA maintenance in Saccharomyces cerevisiae coenzyme Q mutants. Biochem. J 449, 595–603. https://doi.org/10.1042/BJ20121432

Gorman, G.S., Chinnery, P.F., DiMauro, S., Hirano, M., Koga, Y., McFarland, R., Suomalainen, A., Thorburn, D.R., Zeviani, M., Turnbull, D.M., 2016. Mitochondrial diseases. Nat. Rev. Dis. Prim. 2. https://doi.org/10.1038/nrdp.2016.80

Grivennikova, V.G., Kozlovsky, V.S., Vinogradov, A.D., 2017. Respiratory complex II: ROS production and the kinetics of ubiquinone reduction. Biochim. Biophys. Acta - Bioenerg. 1858, 109–117. https://doi.org/10.1016/j.bbabio.2016.10.008

Gruber, J., Fong, S., Chen, C.B., Yoong, S., Pastorin, G., Schaffer, S., Cheah, I., Halliwell, B., 2013. Mitochondria-targeted antioxidants and metabolic modulators as pharmacological interventions to slow ageing. Biotechnol. Adv. https://doi.org/10.1016/j.biotechadv.2012.09.005

Guaragnella, N., Coyne, L.P., Chen, X.J., Giannattasio, S., 2018. Mitochondria-cytosol-nucleus crosstalk: Learning from Saccharomyces cerevisiae. FEMS Yeast Res. 18, 1–15. https://doi.org/10.1093/femsyr/foy088

Ha, S.D., Ham, S., Kim, M.Y., Kim, J.H., Jang, I., Lee, B.B., Lee, M.K., Hwang, J.T., Roh, T.Y., Kim, T.S., 2019. Transcription-dependent targeting of Hda1C to hyperactive genes mediates H4-specific deacetylation in yeast. Nat. Commun. 10. https://doi.org/10.1038/s41467-019-12077-w

Halliwell, B., Gutteridge, J.M.C., 2015. Free Radicals in Biology and Medicine, 5th ed. Oxford University Press, Oxford. https://doi.org/10.1093/acprof:oso/9780198717478.001.0001

Harman, D., 1972. The Biologic Clock: The Mitochondria? J. Am. Geriatr. Soc. 20, 145–147. https://doi.org/10.1111/j.1532-5415.1972.tb00787.x

Harman, D., 1956. Aging: a theory based on free radical and radiation chemistry. J. Gerontol. 11, 298–300. https://doi.org/10.1093/geronj/11.3.298

Hoke, S.M.T., Genereaux, J., Liang, G., Brandl, C.J., 2008. A Conserved Central Region of Yeast Ada2 Regulates the Histone Acetyltransferase Activity of Gcn5 and Interacts with Phospholipids. J. Mol. Biol. 384, 743–755. https://doi.org/10.1016/j.jmb.2008.09.088

Howe, L., Kusch, T., Muster, N., Chaterji, R., Yates, J.R., Workman, J.L., 2002. Yng1p Modulates the Activity of Sas3p as a Component of the Yeast NuA3 Histone Acetyltransferase Complex. Mol. Cell. Biol. 22, 5047–5053. https://doi.org/10.1128/mcb.22.14.5047-5053.2002

Hughes, A.L., Gottschling, D.E., 2012. An early age increase in vacuolar pH limits mitochondrial function and lifespan in yeast. Nature 492, 261–265. https://doi.org/10.1038/nature11654

Huh, K., Falvo, J. V, Gerke, L.C., Carroll, A.S., Howson, R.W., Weissman, J.S., O'shea, E.K., 2003. Global analysis of protein localization in budding yeast.

Imamura, Y., Yu, F., Nakamura, M., Chihara, Y., Okane, K., Sato, M., Kanai, M., Hamada, R., Ueno, M., Yukawa, M., Tsuchiya, E., 2015. RSC Chromatin-remodeling complex is important for mitochondrial function in Saccharomyces cerevisiae. PLoS One 10. https://doi.org/10.1371/journal.pone.0130397

Jaiswal, D., Turniansky, R., Green, E.M., 2017. Choose Your Own Adventure: The Role of Histone Modifications in Yeast Cell Fate. J. Mol. Biol. 429, 1946–1957. https://doi.org/10.1016/j.jmb.2016.10.018

Jazwinski, S.M., 2013. The retrograde response: When mitochondrial quality control is not enough. Biochim. Biophys. Acta - Mol. Cell Res. 1833, 400–409. https://doi.org/10.1016/j.bbamcr.2012.02.010

John, S., Howe, L.A., Tafrov, S.T., Grant, P.A., Sternglanz, R., Workman, J.L., 2000. The something about silencing protein, Sas3, is the catalytic subunit of NuA3, a yTAF(II)30-containing HAT complex that interacts with the Spt16 subunit of the yeast CP (Cdc68/Pob3)-FACT complex.

Genes Dev. 14, 1196–1208. https://doi.org/10.1101/gad.14.10.1196

Kaluarachchi Duffy, S., Friesen, H., Baryshnikova, A., Lambert, J.P., Chong, Y.T., Figeys, D., Andrews, B., 2012. Exploring the yeast acetylome using functional genomics. Cell 149, 936–948. https://doi.org/10.1016/j.cell.2012.02.064

Kausar, S., Wang, F., Cui, H., 2018. The Role of Mitochondria in Reactive Oxygen Species Generation and Its Implications for Neurodegenerative Diseases. Cells 7, 274. https://doi.org/10.3390/cells7120274

Kelso, G.F., Porteous, C.M., Coulter, C. V, Hughes, G., Porteous, W.K., Ledgerwood, E.C., Smith, R.A.J., Murphy, M.P., 2001. Selective targeting of a redox-active ubiquinone to mitochondria within cells: Antioxidant and antiapoptotic properties. J. Biol. Chem. 276, 4588–4596. https://doi.org/10.1074/jbc.M009093200

Krivoruchko, A., Zhang, Y., Siewers, V., Chen, Y., Nielsen, J., 2015. Microbial acetyl-CoA metabolism and metabolic engineering. Metab. Eng. 28, 28–42. https://doi.org/10.1016/j.ymben.2014.11.009

Kurdistani, S.K., Tavazoie, S., Grunstein, M., 2004. Mapping global histone acetylation patterns to gene expression, Cell. https://doi.org/10.1016/j.cell.2004.05.023

Ladurner, A.G., Inouye, C., Jain, R., Tjian, R., 2003. Bromodomains Mediate an Acetyl-Histone Encoded Antisilencing Function at Heterochromatin Boundaries. Mol. Cell 11, 365–376.

Lambert, A.J., Brand, M.D., 2004. Superoxide production by NADH:ubiquinone oxidoreductase (complex I) depends on the pH gradient across the mitochondrial inner membrane. Biochem. J. 382, 511–517. https://doi.org/10.1042/BJ20040485

Lasserre, J.P., Dautant, A., Aiyar, R.S., Kucharczyk, R., Glatigny, A., Tribouillard-Tanvier, D., Rytka, J., Blondel, M., Skoczen, N., Reynier, P., Pitayu, L., Rötig, A., Delahodde, A., Steinmetz, L.M., Dujardin, G., Procaccio, V., Rago, J.P. Di, 2015. Yeast as a system for modeling mitochondrial disease mechanisms and discovering therapies. Dis. Model. Mech. 8, 509–522. https://doi.org/10.1242/dmm.020438

Leadsham, J.E., Gourlay, C.W., 2010. CAMP/PKA signaling balances respiratory activity with mitochondria dependent apoptosis via transcriptional regulation. BMC Cell Biol. 11. https://doi.org/10.1186/1471-2121-11-92

Leadsham, J.E., Sanders, G., Giannaki, S., Bastow, E.L., Hutton, R., Naeimi, W.R., Breitenbach, M., Gourlay, C.W., 2013. Loss of cytochrome c oxidase promotes ras-dependent ros production from the er resident nadph oxidase, yno1p, in yeast. Cell Metab. 18, 279–286. https://doi.org/10.1016/j.cmet.2013.07.005

Lechner, T., Carrozza, M.J., Yu, Y., Grant, P.A., Eberharter, A., Vannier, D., Brosch, G., Stillman, D.J., Shore, D., Workmana, J.L., 2000. Sds3 (suppressor of defective silencing 3) is an integral component of the yeast Sin3·Rpd3 histone deacetylase complex and is required for histone deacetylase activity. J. Biol. Chem. 275, 40961–40966. https://doi.org/10.1074/jbc.M005730200

Lee, K.K., Sardiu, M.E., Swanson, S.K., Gilmore, J.M., Torok, M., Grant, P.A., Florens, L., Workman, J.L., Washburn, M.P., 2011. Combinatorial depletion analysis to assemble the network architecture of the SAGA and ADA chromatin remodeling complexes. Mol. Syst. Biol. 7. https://doi.org/10.1038/msb.2011.40

Lee, K.K., Swanson, S.K., Florens, L., Washburn, M.P., Workman, J.L., 2009. Yeast Sgf73/Ataxin-7 serves to anchor the deubiquitination module into both SAGA and Slik(SALSA) HAT complexes. Epigenetics Chromatin 2, 2. https://doi.org/10.1186/1756-8935-2-2

Li, W., Sun, L., Liang, Q., Wang, J., Mo, W., Zhou, B., 2006. Yeast AMID homologue Ndi1p displays respiration-restricted apoptotic activity and is involved in chronological aging. Mol. Biol. Cell 17, 1802–1811. https://doi.org/10.1091/mbc.E05-04-0333

Liu, W., Zhang, B., Jiang, R., 2017. Improving acetyl-CoA biosynthesis in Saccharomyces cerevisiae via the overexpression of pantothenate kinase and PDH bypass. Biotechnol. Biofuels 10, 41. https://doi.org/10.1186/s13068-017-0726-z

Liu, Z., Butow, R.A., 2006. Mitochondrial Retrograde Signaling. Annu. Rev. Genet. 40, 159–185.

https://doi.org/10.1146/annurev.genet.40.110405.090613

Magwere, T., West, M., Riyahi, K., Murphy, M.P., Smith, R.A.J., Partridge, L., 2006. The effects of exogenous antioxidants on lifespan and oxidative stress resistance in Drosophila melanogaster. Mech. Ageing Dev. 127, 356–370. https://doi.org/10.1016/j.mad.2005.12.009

Martin, D.G.E., Baetz, K., Shi, X., Walter, K.L., MacDonald, V.E., Wlodarski, M.J., Gozani, O., Hieter, P., Howe, L., 2006. The Yng1p Plant Homeodomain Finger Is a Methyl-Histone Binding Module That Recognizes Lysine 4-Methylated Histone H3. Mol. Cell. Biol. 26, 7871–7879. https://doi.org/10.1128/mcb.00573-06

Matangkasombut, O., Buratowski, S., 2003. Different sensitivities of bromodomain factors 1 and 2 to histone H4 acetylation. Mol. Cell 11, 353–363. https://doi.org/10.1016/S1097-2765(03)00033-9

Mehrotra, S., Galdieri, L., Zhang, T., Zhang, M., Pemberton, L.F., Vancura, A., 2014. Histone hypoacetylation-activated genes are repressed by acetyl-CoA- and chromatin-mediated mechanism. Biochim. Biophys. Acta - Gene Regul. Mech. 1839, 751–763. https://doi.org/10.1016/j.bbagrm.2014.05.029

Morgan, D.O., 2007. The Cell Cycle: Principles of Control. New Science Press Ltd., London. https://doi.org/10.1093/icb/icm066

Mou, Z., Kenny, A.E., Curcio, M.J., 2006. Hos2 and Set3 promote integration of Ty1 retrotransposons at tRNA genes in Saccharomyces cerevisiae. Genetics 172, 2157–2167. https://doi.org/10.1534/genetics.105.054072

Murphy, Michael P., 2009. How mitochondria produce reactive oxygen species. Biochem. J. 417, 1–13. https://doi.org/10.1042/BJ20081386

Murphy, Michael P, 2009. How mitochondria produce reactive oxygen species. Biochem. J. 417, 1–13. https://doi.org/10.1042/BJ20081386

Ojaimi, J., Masters, C.L., Opeskin, K., McKelvie, P., Byrne, E., 1999. Mitochondrial respiratory chain activity in the human brain as a function of age. Mech. Ageing Dev. 111, 39–47.

https://doi.org/10.1016/S0047-6374(99)00071-8

Orlandi, I., Casatta, N., Vai, M., 2012. Lack of Ach1 CoA-transferase triggers apoptosis and decreases chronological lifespan in yeast. Front. Oncol. 2 JUN. https://doi.org/10.3389/fonc.2012.00067

Orlandi, I., Coppola, D.P., Vai, M., 2014. Rewiring yeast acetate metabolism through mpc1 loss of function leads to mitochondrial damage and decreases chronological lifespan. Microb. Cell 1, 393–405. https://doi.org/10.15698/mic2014.12.178

Peng, W., Togawa, C., Zhang, K., Kurdistani, S.K., 2008. Regulators of cellular levels of histone acetylation in Saccharomyces cerevisiae. Genetics 179, 277–289. https://doi.org/10.1534/genetics.107.085068

Pérez-Martínez, M.E., Benet, M., Alepuz, P., Tordera, V., 2020. Nut1/Hos1 and Sas2/Rpd3 control the H3 acetylation of two different sets of osmotic stress-induced genes. Epigenetics 15, 251–271. https://doi.org/10.1080/15592294.2019.1664229

Pérez, V.I., Van Remmen, H., Bokov, A., Epstein, C.J., Vijg, J., Richardson, A., 2009. The overexpression of major antioxidant enzymes does not extend the lifespan of mice. Aging Cell 8, 73–75. https://doi.org/10.1111/j.1474-9726.2008.00449.x

Picone, P., Nuzzo, D., Caruana, L., Scafidi, V., Di Carlo, M.D., 2014. Mitochondrial dysfunction: Different routes to Alzheimer's disease therapy. Oxid. Med. Cell. Longev. 2014. https://doi.org/10.1155/2014/780179

Pokholok, D.K., Harbison, C.T., Levine, S., Cole, M., Hannett, N.M., Tong, I.L., Bell, G.W., Walker, K., Rolfe, P.A., Herbolsheimer, E., Zeitlinger, J., Lewitter, F., Gifford, D.K., Young, R.A., 2005. Genome-wide map of nucleosome acetylation and methylation in yeast. Cell 122, 517–527. https://doi.org/10.1016/j.cell.2005.06.026

Polevoda, B., Hoskins, J., Sherman, F., 2009. Properties of Nat4, an Nα-Acetyltransferase of Saccharomyces cerevisiae That Modifies N Termini of Histones H2A and H4. Mol. Cell. Biol. 29, 2913–2924. https://doi.org/10.1128/mcb.00147-08

Poveda, A., Sendra, R., 2008. Site specificity of yeast histone acetyltransferase B complex in vivo. FEBS J. 275, 2122–2136. https://doi.org/10.1111/j.1742-4658.2008.06367.x

Pray-Grant, M.G., Schieltz, D., McMahon, S.J., Wood, J.M., Kennedy, E.L., Cook, R.G., Workman, J.L., Yates, J.R., Grant, P.A., 2002. The Novel SLIK Histone Acetyltransferase Complex Functions in the Yeast Retrograde Response Pathway. Mol. Cell. Biol. 22, 8774–8786. https://doi.org/10.1128/mcb.22.24.8774-8786.2002

Quinlan, C.L., Orr, A.L., Perevoshchikova, I. V., Treberg, J.R., Ackrell, B.A., Brand, M.D., 2012. Mitochondrial complex II can generate reactive oxygen species at high rates in both the forward and reverse reactions. J. Biol. Chem. 287, 27255–27264. https://doi.org/10.1074/jbc.M112.374629

Quinlan, C.L., Treberg, J.R., Brand, M.D., 2011. Mechanisms of mitochondrial free radical production and their relationship to the aging process, in: Handbook of the Biology of Aging. Elsevier Inc., pp. 47–61. https://doi.org/10.1016/B978-0-12-378638-8.00003-8

Rinnerthaler, M., Büttner, S., Laun, P., Heeren, G., Felder, T.K., Klinger, H., Weinberger, M., Stolze, K., Grousl, T., Hasek, J., Benada, O., Frydlova, I., Klocker, A., Simon-Nobbe, B., Jansko, B., Breitenbach-Koller, H., Eisenberg, T., Gourlay, C.W., Madeo, F., Burhans, W.C., Breitenbach, M., 2012. Yno1p/Aim14p, a NADPH-oxidase ortholog, controls extramitochondrial reactive oxygen species generation, apoptosis, and actin cable formation in yeast. Proc. Natl. Acad. Sci. U. S. A. 109, 8658–8663. https://doi.org/10.1073/pnas.1201629109

Rojo, E.E., Guiard, B., Neupert, W., Stuart, R.A., 1998. Sorting of D-lactate dehydrogenase to the inner membrane of mitochondria. Analysis of topogenic signal and energetic requirements. J. Biol. Chem. 273, 8040–8047. https://doi.org/10.1074/jbc.273.14.8040

Rössl, A., Denoncourt, A., Lin, M.S., Downey, M., 2019. A synthetic non-histone substrate to study substrate targeting by the Gcn5 HAT and sirtuin HDACs. J. Biol. Chem. 294, 6227–6239. https://doi.org/10.1074/jbc.RA118.006051

Sakellariou, G.K., Pearson, T., Lightfoot, A.P., Nye, G.A., Wells, N., Giakoumaki, I.I., Griffiths, R.D., McArdle, A., Jackson, M.J., 2016. Long-Term administration of the mitochondria-Targeted antioxidant mitoquinone mesylate fails to attenuate age-related oxidative damage or rescue the loss of muscle mass and function associated with aging of skeletal muscle. FASEB J. 30, 3771–3785. https://doi.org/10.1096/fj.201600450R

Sampath, V., Liu, B., Tafrov, S., Srinivasan, M., Rieger, R., Chen, E.I., Sternglanz, R., 2013. Biochemical characterization of Hpa2 and Hpa3, two small closely related acetyltransferases from saccharomyces cerevisiae. J. Biol. Chem. 288, 21506–21513. https://doi.org/10.1074/jbc.M113.486274

Sandmeier, J.J., French, S., Osheim, Y., Cheung, W.L., Gallo, C.M., Beyer, A.L., Smith, J.S., 2002. RPD3 is required for the inactivation of yeast ribosomal DNA genes in stationary phase. EMBO J. 21, 4959–4968. https://doi.org/10.1093/emboj/cdf498

Sanz, A., 2016. Mitochondrial reactive oxygen species: Do they extend or shorten animal lifespan? Biochim. Biophys. Acta - Bioenerg. https://doi.org/10.1016/j.bbabio.2016.03.018

Schaar, C.E., Dues, D.J., Spielbauer, K.K., Machiela, E., Cooper, J.F., Senchuk, M., Hekimi, S., Van Raamsdonk, J.M., 2015. Mitochondrial and Cytoplasmic ROS Have Opposing Effects on Lifespan. PLoS Genet. 11, 1–24. https://doi.org/10.1371/journal.pgen.1004972

Schriner, S.E., Linford, N.J., Martin, G.M., Treuting, P., Ogburn, C.E., Emond, M., Coskun, P.E., Ladiges, W., Wolf, N., Van Remmen, H., Wallace, D.C., Rabinovitch, P.S., 2005. Extension of murine life span by overexpression of catalase targeted to mitochondria. Science (80-.). 308, 1909–1911. https://doi.org/10.1126/science.1106653

Senoo-Matsuda, N., Yasuda, K., Tsuda, M., Ohkubo, T., Yoshimura, S., Nakazawa, H., Hartman, P.S., Ishii, N., 2001. A Defect in the Cytochrome b Large Subunit in Complex II Causes Both Superoxide Anion Overproduction and Abnormal Energy Metabolism in Caenorhabditis elegans. J. Biol. Chem. 276, 41553–41558. https://doi.org/10.1074/jbc.M104718200

Shi, L., Tu, B.P., 2015. Acetyl-CoA and the regulation of metabolism: Mechanisms and consequences. Curr. Opin. Cell Biol. 33, 125–131. https://doi.org/10.1016/j.ceb.2015.02.003

Siebels, I., Dröse, S., 2013. Q-site inhibitor induced ROS production of mitochondrial complex II is attenuated by TCA cycle dicarboxylates. Biochim. Biophys. Acta - Bioenerg. 1827, 1156–1164. https://doi.org/10.1016/j.bbabio.2013.06.005

Smith, E.R., Eisen, A., Gu, W., Sattah, M., Pannuti, A., Zhou, J., Cook, R.G., Lucchesi, J.C., Allis, C.D., 1998. ESA1 is a histone acetyltransferase that is essential for growth in yeast. Proc. Natl. Acad. Sci. U. S. A. 95, 3561–3565. https://doi.org/10.1073/pnas.95.7.3561

Sprouffske, K., Wagner, A., 2016. Growthcurver: An R package for obtaining interpretable metrics from microbial growth curves. BMC Bioinformatics 17, 172. https://doi.org/10.1186/s12859-016-1016-7

Starai, V.J., Celic, I., Cole, R.N., Boeke, J.D., Escalante-Semerena, J.C., 2002. Sir2-dependent activation of acetyl-CoA synthetase by deacetylation of active lysine. Science (80-.). 298, 2390–2392. https://doi.org/10.1126/science.1077650

Sternglanz, R., Schindelin, H., 1999. Structure and mechanism of action of the histone acetyltransferase Gcn5 and similarity to other N-acetyltransferases. Proc. Natl. Acad. Sci. U. S. A. 96, 8807–8808. https://doi.org/10.1073/pnas.96.16.8807

Sun, N., Youle, R.J., Finkel, T., 2016. The Mitochondrial Basis of Aging. Mol. Cell. https://doi.org/10.1016/j.molcel.2016.01.028

Sutton, A., Shia, W.J., Band, D., Kaufman, P.D., Osada, S., Workman, J.L., Sternglanz, R., 2003. Sas4 and Sas5 are required for the histone acetyltransferase activity of Sas2 in the SAS complex. J. Biol. Chem. 278, 16887–16892. https://doi.org/10.1074/jbc.M210709200

Takahashi, H., McCaffery, J.M., Irizarry, R.A., Boeke, J.D., 2006. Nucleocytosolic Acetyl-Coenzyme A Synthetase Is Required for Histone Acetylation and Global Transcription. Mol. Cell 23, 207–217. https://doi.org/10.1016/j.molcel.2006.05.040

ThermoFisher, n.d. Gateway Cloning Protocols | Thermo Fisher Scientific - UK [WWW Document]. URL https://www.thermofisher.com/uk/en/home/life-science/cloning/gateway-cloning/protocols.html (accessed 3.30.20).

Treberg, J.R., Quinlan, C.L., Brand, M.D., 2011. Evidence for two sites of superoxide production by mitochondrial NADH-ubiquinone oxidoreductase (complex I). J. Biol. Chem. 286, 27103–27110. https://doi.org/10.1074/jbc.M111.252502

Trendeleva, T.A., Zvyagilskaya, R.A., 2018. Retrograde Signaling as a Mechanism of Yeast Adaptation to Unfavorable Factors. Biochem. 83, 98–106. https://doi.org/10.1134/S0006297918020025

Van Den Berg, M.A., Steensma, H.Y., 1995. ACS2, a Saccharomyces Cerevisiae Gene Encoding Acetyl-Coenzyme A Synthetase, Essential for Growth on Glucose. Eur. J. Biochem. 231, 704–713. https://doi.org/10.1111/j.1432-1033.1995.0704d.x

van Roermund, C.W., Elgersma, Y., Singh, N., Wanders, R.J., Tabak, H.F., 1995. The membrane of peroxisomes in Saccharomyces cerevisiae is impermeable to NAD(H) and acetyl-CoA under in vivo conditions. EMBO J. 14, 3480–3486. https://doi.org/10.1002/j.1460-2075.1995.tb07354.x

van Rossum, H.M., Kozak, B.U., Pronk, J.T., van Maris, A.J.A., 2016. Engineering cytosolic acetyl-coenzyme A supply in Saccharomyces cerevisiae: Pathway stoichiometry, free-energy conservation and redox-cofactor balancing. Metab. Eng. 36, 99–115. https://doi.org/10.1016/j.ymben.2016.03.006

Venters, B.J., Wachi, S., Mavrich, T.N., Andersen, B.E., Jena, P., Sinnamon, A.J., Jain, P., Rolleri, N.S., Jiang, C., Hemeryck-Walsh, C., Pugh, B.F., 2011. A Comprehensive Genomic Binding Map of Gene and Chromatin Regulatory Proteins in Saccharomyces. Mol. Cell 41, 480–492. https://doi.org/10.1016/j.molcel.2011.01.015

Wang, M., Collins, R.N., 2014. A lysine deacetylase Hos3 is targeted to the bud neck and involved in the spindle position checkpoint. https://doi.org/10.1091/mbc.E13-10-0619

Weinert, B.T., Iesmantavicius, V., Moustafa, T., Schölz, C., Wagner, S.A., Magnes, C., Zechner, R.,

Choudhary, C., 2014. Acetylation dynamics and stoichiometry in Saccharomyces cerevisiae. Mol. Syst. Biol. 10, 716. https://doi.org/10.1002/msb.134766

Wierman, M.B., Maqani, N., Strickler, E., Li, M., Smith, J.S., 2017. Caloric Restriction Extends Yeast Chronological Life Span by Optimizing the Snf1 (AMPK) Signaling Pathway. Mol. Cell. Biol. 37. https://doi.org/10.1128/mcb.00562-16

Wierman, M.B., Smith, J.S., 2014. Yeast sirtuins and the regulation of aging. FEMS Yeast Res. 14, 73–88. https://doi.org/10.1111/1567-1364.12115

Wiese, M., Bannister, A.J., 2020. Two genomes, one cell: Mitochondrial-nuclear coordination via epigenetic pathways. Mol. Metab. 38, 100942. https://doi.org/10.1016/j.molmet.2020.01.006

Wu, J., Carmen, A.A., Kobayashi, R., Suka, N., Grunstein, M., 2001. HDA2 and HDA3 are related proteins that interact with and are essential for the activity of the yeast histone deacetylase HDA1. Proc. Natl. Acad. Sci. U. S. A. 98, 4391–4396. https://doi.org/10.1073/pnas.081560698

Wu, W.S., Tu, H.P., Chu, Y.H., Nordling, T.E.M., Tseng, Y.Y., Liaw, H.J., 2018. YHMI: A web tool to identify histone modifications and histone/chromatin regulators from a gene list in yeast. Database 2018, 1–13. https://doi.org/10.1093/database/bay116

Xiong, B., Lu, S., Gerton, J.L., 2010. Hos1 is a lysine deacetylase for the Smc3 subunit of cohesin. Curr. Biol. 20, 1660–1665. https://doi.org/10.1016/j.cub.2010.08.019

Yi, D.G., Hong, S., Huh, W.K., 2018. Mitochondrial dysfunction reduces yeast replicative lifespan by elevating RAS-dependent ROS production by the ER-localized NADPH oxidase Yno1. PLoS One 13, 1–18. https://doi.org/10.1371/journal.pone.0198619

Yu, G., Wu, Q., Gao, Y., Chen, M., Yang, M., 2019. The epigenetics of aging in invertebrates. Int. J. Mol. Sci. 20. https://doi.org/10.3390/ijms20184535

Zhao, R.Z., Jiang, S., Zhang, L., Yu, Z. Bin, 2019. Mitochondrial electron transport chain, ROS generation and uncoupling (Review). Int. J. Mol. Med. 44, 3–15. https://doi.org/10.3892/ijmm.2019.4188